

Productive bond scission processes in polymer mechanochemistry

Citation for published version (APA):

Li, B. (2019). *Productive bond scission processes in polymer mechanochemistry*. [Phd Thesis 1 (Research TU/e / Graduation TU/e), Chemical Engineering and Chemistry]. Technische Universiteit Eindhoven.

Document status and date:

Published: 29/01/2019

Document Version:

Publisher's PDF, also known as Version of Record (includes final page, issue and volume numbers)

Please check the document version of this publication:

- A submitted manuscript is the version of the article upon submission and before peer-review. There can be important differences between the submitted version and the official published version of record. People interested in the research are advised to contact the author for the final version of the publication, or visit the DOI to the publisher's website.
- The final author version and the galley proof are versions of the publication after peer review.
- The final published version features the final layout of the paper including the volume, issue and page numbers.

[Link to publication](#)

General rights

Copyright and moral rights for the publications made accessible in the public portal are retained by the authors and/or other copyright owners and it is a condition of accessing publications that users recognise and abide by the legal requirements associated with these rights.

- Users may download and print one copy of any publication from the public portal for the purpose of private study or research.
- You may not further distribute the material or use it for any profit-making activity or commercial gain
- You may freely distribute the URL identifying the publication in the public portal.

If the publication is distributed under the terms of Article 25fa of the Dutch Copyright Act, indicated by the "Taverne" license above, please follow below link for the End User Agreement:

www.tue.nl/taverne

Take down policy

If you believe that this document breaches copyright please contact us at:

openaccess@tue.nl

providing details and we will investigate your claim.

Productive Bond Scission Processes in Polymer Mechanochemistry

PROEFSCHRIFT

ter verkrijging van de graad van doctor aan de Technische Universiteit
Eindhoven, op gezag van de rector magnificus prof.dr.ir. F.P.T. Baaijens,
voor een commissie aangewezen door het College voor Promoties, in het
openbaar te verdedigen op dinsdag 29 Januari 2019 om 13:30 uur

door

Bao Li

geboren te Sanyuan, China

Dit proefschrift is goedgekeurd door de promotoren en de samenstelling van de promotiecommissie is als volgt:

voorzitter:	prof. dr. ir. E. J. M. Hensen
1e promotor:	prof. dr. R. P. Sijbesma
2e promotor:	dr. ir. J. P. A. Heuts
leden:	prof. dr. J. H. Van Esch (Technische Universiteit Delft)
	prof. N. A. J. M. Sommerdijk
	prof. dr. A. P. H. J. Schenning

Het onderzoek of ontwerp dat in dit proefschrift wordt beschreven is uitgevoerd in overeenstemming met de TU/e Gedragscode Wetenschapsbeoefening.

致父亲，

春蚕到死丝方尽，蜡炬成灰泪始干。

Bao Li

Productive Bond Scission Processes in Polymer Mechanochemistry
Eindhoven University of Technology, 2019

Cover design: Bao Li

Front cover:

End: Productive Bond Scission Processes in Polymer Mechanochemistry

Back Cover:

This is a new beginning...

《岁寒三友讼》

云集九霄起霓裳，竹出青冥松傲霜，
夺魂寻骨几轮回，雪中红梅暗浮香。

Printed by Gildeprint, the Netherlands

A catalogue record is available from the Eindhoven University of Technology Library
ISBN: 978-90-386-4691-6

This work has been financially supported by the Ministry of Education, Culture and
Science of the Netherlands (Gravitation program 024.001.035).

Copyright © 2019 by Bao Li

Productive Bond Scission Processes in Polymer Mechanochemistry

Table of Content

Chapter I

Introduction: Mechanochemistry -- from destructive to constructive.....	- 1 -
1.1 Mechanochemistry: from destructive to constructive.....	- 2 -
1.2 Techniques used for mechanically induced chemical reactions.....	- 5 -
1.2.1 Techniques for solution mechanochemistry.....	- 5 -
1.2.2 Techniques for solid-state mechanochemistry.....	- 7 -
1.2.3 Single molecule force spectroscopy for mechanochemistry at the molecular level.....	- 9 -
1.3 Design of mechanophores.....	- 10 -
1.3.1 Spiropyran-based mechanophore.....	- 11 -
1.3.2 <i>Gem</i> -dihalorocyclopropane (<i>gDHC</i>)-based mechanophore...-	14 -
1.3.3 Bisadamantyl 1,2-dioxetane-based mechanophore.....	- 19 -
1.3.4 Coordination complex-based and other mechanophores.....	- 21 -
1.4 Heterolytic scission induced by mechanical force.....	- 22 -
1.5 Outline of this thesis.....	- 23 -
References.....	- 25 -

Chapter II

Mechanically induced chemiluminescence in a poly (hexyl methacrylate) network.....	- 31 -
2.1 Introduction.....	- 32 -
2.1.1 Mechanochemiluminescence.....	- 32 -
2.1.2 Scientific cameras for image recording.....	- 32 -
2.2 Results and Discussion.....	- 34 -
2.2.1 Synthesis.....	- 34 -
2.2.2 Mechanical properties of the mechanophore-contained PHMA network.....	- 35 -
2.2.3 Mechanically induced chemiluminescence of the PHMA network.....	- 38 -
2.2.4 Quantitative analysis of light emission.....	- 40 -
2.3 Conclusions.....	- 42 -
2.4 Experimental.....	- 43 -

2.4.1 Materials and instrumentation.....	- 43 -
2.4.2 Mechanical testing.....	- 44 -
2.4.3 Synthesis.....	- 44 -
References.....	- 48 -

Chapter III

Optical sensing of covalent bond scission for the observation of mechanical damage in a PNIPAm hydrogel network.....	- 51 -
3.1 Introduction.....	- 52 -
3.2 Results and Discussion.....	- 54 -
3.2.1 Synthesis.....	- 54 -
3.2.2 Mechanical properties in uniaxial compression determined by micro indentation.....	- 55 -
3.2.3 Mechanically induced fluorescence.....	- 57 -
3.3 Conclusions.....	- 63 -
3.4 Experimental.....	- 64 -
3.4.1 Materials and instrumentation.....	- 64 -
3.4.2 Synthesis.....	- 66 -
References.....	- 71 -

Chapter IV

Study on mechanochemistry of <i>N</i> -heterocyclic salts polymeric materials.....	- 73 -
4.1 Introduction to mechanically induced heterolytic bond cleavage.....	- 74 -
4.2 Sonication of imidazolium-centered linear polyTHF.....	- 77 -
4.2.1 Synthesis.....	- 77 -
4.2.2 Chain scission in Imi- <i>c</i> -pTHF with sonication.....	- 78 -
4.3 Study on mechanochemistry of linear bis(phenyl)fluorene-centered poly(methyl acrylate).....	- 80 -
4.3.1 Synthesis.....	- 81 -
4.3.2 Chain scission in bPF- <i>c</i> -PMA with sonication.....	- 82 -
4.4 Study on mechanochemistry of an <i>N</i> -benzyl pyridinium-based network.....	- 85 -
4.4.1 Synthesis.....	- 85 -
4.4.2 Cationic ring opening polymerization of epoxide initiated with model pyridinium initiator.....	- 87 -
4.4.3 Kinetics.....	- 89 -
4.4.4 Temperature-dependent reactivity of BpySbF6 for	

polymerization.....	- 90 -
4.4.5 Thermally initiated polymerization and mechanically induced polymerization with <i>N</i> -benzyl pyridinium-based network.....	- 92 -
4.5 Conclusions.....	- 93 -
4.6 Experimental.....	- 94 -
4.6.1 Materials and instrumentation.....	- 94 -
4.6.2 Sonication experiments.....	- 95 -
4.6.3 General procedure for epoxide polymerization with pyridinium salts as initiators.....	- 96 -
4.6.4 Synthetic procedures and characterization.....	- 96 -
References.....	- 103 -
Chapter V	
Electrochemistry of mono and bifunctional viologen derivatives.....	- 105 -
5.1 Introduction.....	- 106 -
5.2 Electrochemistry of viologen and its derivatives.....	- 109 -
5.3 ESR dimerization studies of (bis)(viologen)s.....	- 116 -
5.4 Mechanical activation of diamagnetic bis(viologen).....	- 118 -
5.5 Conclusions.....	- 120 -
5.6 Experimental.....	- 120 -
5.6.1 Materials and instrumentation.....	- 120 -
5.6.2 Synthetic procedure and characterization.....	- 121 -
References.....	- 129 -
Summary.....	- 131 -
Curriculum Vitae.....	- 135 -
Acknowledgement.....	- 137 -

Chapter I

Introduction: Mechanochemistry -- from destructive to constructive

ABSTRACT

Polymer mechanochemistry has attracted much interest over the past decade. With the design of new mechanophores, mechanochemistry has changed from a destructive to a constructive process. Upon application of mechanical force, the mechanophores undergo productive chemical reactions to provide functionality to materials or to give feedback to understand the state of the materials. This chapter focuses on the techniques usually employed in polymer mechanochemistry and discusses four recently developed mechanophores in detail.

1.1 Mechanochemistry: from destructive to constructive

The presence of highly developed sensory and nervous systems provides creatures with a favorable position in the hierarchically organized ecological pyramid because such complicated system gives the subject a clear view of the surroundings to avoid danger or at least make preparations to face it. Among sensory neurons, mechanoreceptors (Figure 1.1 (a))¹, responding to mechanical forces such as pressure or distortion, play irreplaceable roles for creatures during their lifetime. The response to mechanical force by mechanoreceptors is a biochemical or electrical signal, as is shown in Figure 1.1 (b).² Chemical reactions initiated by direct absorption of mechanical energy are defined as mechanochemical reactions and establish the realm of mechanochemistry. Mechanochemistry is sometimes referred to as the fourth sub-discipline of chemistry in a classification based on the specific mode of supplying energy to promote chemical reactions - alongside thermochemistry, electrochemistry, and photochemistry.³ Mechanochemical reactions do not only occur in living systems, since many mechanically induced chemical reactions have been found or invented by researchers and are used in practical applications. Examples include milling and grinding of crystals, metals, and alloys, molecular weight reduction of polymers, and breaking of individual chemical bonds in single molecule force spectroscopy. The first documented example of a mechanochemical reaction was reported in 315 B.C. by Theophrastus of Ephesus, the successor of Aristotle, who demonstrated that the grinding of cinnabar (mercury(II) sulphide) in a brass mortar in the presence of vinegar resulted in reduction to form liquid mercury. Modern mechanochemistry is employed in many applications, such as fabrication of nanoparticles⁴, inorganic/organic synthesis⁵, treatment of waste⁶, and preparation of catalysts⁷.

Since Bakelite, the first entirely man-made polymer, was invented by Leo Hendrik Baekeland in 1907,⁸ a multitude of synthetic polymer materials has been developed and used in a wide range of daily applications such as coatings, packaging, engineering composites, and electronic materials, because polymers combine strength and toughness with a high processability. During use, polymer materials may lose part of their strength due to mechanochemical reactions from erosion. Therefore, it is of great importance to understand the influence of mechanical stress on the mechanical properties and stability of polymeric materials. Traditional study methods can only provide the relationship between stress and mechanical properties on a macroscopic scale (usually shown as a stress-strain curve, see Figure 1.1 (c)), from which it is difficult to obtain detailed information at the molecular level. The

development of mechanochemistry, however, allows scientists to understand this relation in more detail, and to give a view on how to reduce such stress to extend the service life of the materials. Polymers present a particular convenient platform for the study of mechanical effects on molecular chemical bonds: the macroscopic forces applied to a polymer can be transferred along the polymer chain on the molecular level and accumulate to an extent that they are sufficient to break covalent bonds.

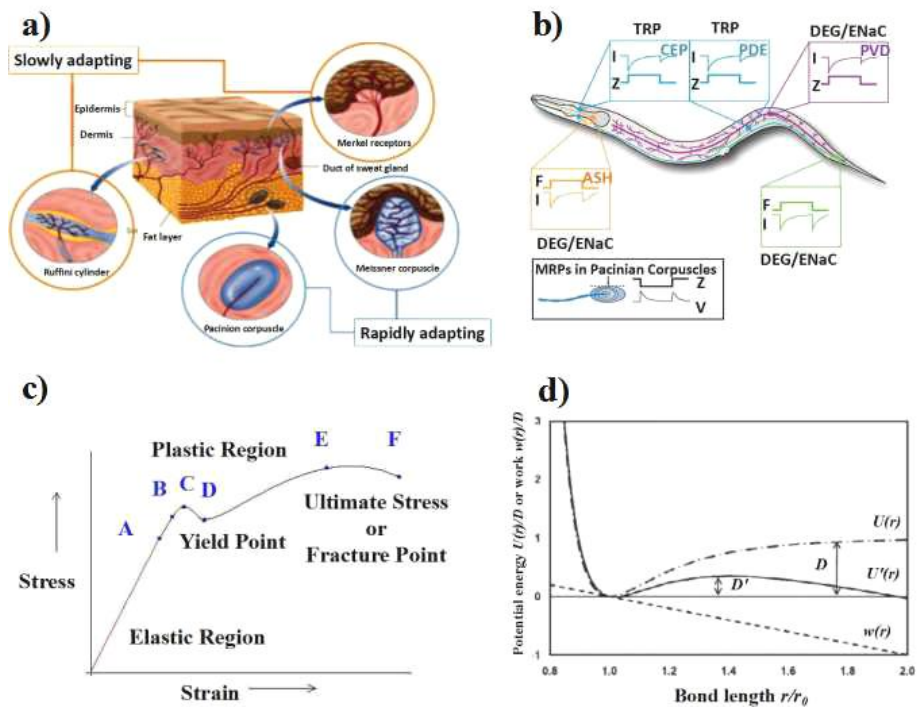


Figure 1.1. a) A schematic of the mechanoreceptors embedded in the skin. Reprinted with permission from Ref. [1]. b) Mechanoreceptor currents in *C. elegans* mechanoreceptor neurons activate in response to the application and removal of mechanical stimulation. Reprinted with permission from Ref. [2]. c) A typical stress-strain curve for polymer materials. d) Morse energy potentials of a covalent bond at rest (dot-dashed line) and under force (solid line). The activation energy to decomposition is reduced from D to D' by the mechanical work (dashed line). Reprinted with permission from ref. [10].

It is obvious that in its early stage, polymer mechanochemistry focused on the degradation of polymer materials and mechanochemistry was regarded as a

destructive process. In the 1930s, Staudinger was the first to describe polymer mechanochemistry when he interpreted the decrease in molecular weight upon mastication of polymers.⁹ Later on in 1940, Kauzmann and Eyring¹⁰ studied the activation of chemical bonds in large molecules within fluids and developed a theoretical framework for the enhanced scission of covalent bonds under force. In the absence of an external force, the potential energy of a chemical bond with a dissociation energy D , is described by a Morse potential, $U(r)$, as depicted in Figure 1.1(d) (Eq. 1.1). If the bond is stretched with an external force of F from its equilibrium position r_0 to a new position r' , the potential energy will be lowered by an amount equal to the work by the external force, $W(r) = F(r' - r_0)$, and the Morse potential for the stretched bond ($U'(r)$) will be expressed with a new activation barrier D' where the relation between D and D' is expressed by Eq. 1.2.

$$U(r) = D(1 - e^{-a(r-r_0)})^2 \quad \text{Eq. 1.1}$$

$$D'/D = x \log\left(\frac{1-x-\sqrt{1-2x}}{x}\right) + \sqrt{1-2x} \quad \text{Eq. 1.2}$$

In these equations r is the length of the bond, r_0 is the equilibrium separation of the atoms, D is the dissociation energy, and $a = \sqrt{k/2D}$, k being the force constant of the bond in the neighborhood of the equilibrium separation, $x = F/Da$.

It can be inferred with the Thermally Activated Barrier to Scission (TABS) model¹¹ that if D is lowered by a mechanical force to reach to a level that is sufficiently low, the barrier to dissociation may be overcome through thermal fluctuations ($RT \sim 2.5$ kJ/mol at 25°C), that is, the bond is activated mechanically. The fundamental work of Kauzmann and Eyring opened the door towards the realm of polymer mechanochemistry and based on their work, more refined theoretical approaches¹² have been developed and tailor-made mechanoresponsive systems¹³ have been designed for use in experimental studies. Such systems have been coining mechanophores. Since Moore introduced the term mechanophore¹⁴ in the context of functional groups that change color under force, scientists have begun to design new mechanophores for specific functions in mechanochemistry. As an example, the incorporation of novel functions in mechanophores, such as mechanically activated catalysts (mechanocatalysts), turns mechanochemistry into a productive process rather than just a destructive one. However, there is still a long way to go to extend

mechanochemistry to practical applications.

1.2 Techniques used for mechanically induced chemical reactions

In order to investigate mechanochemical reactions, external mechanical forces have to be applied, but the preferred technique depends on the specific reaction. Ultrasound sonication is often used for mechanochemistry studies in dilute solutions, while tensile and compression tests are utilized in the solid state. To investigate the effect of swelling stress on materials, continuous swelling is also employed in mechanochemistry, while single molecule force spectroscopy (SMFS) is a suitable method to study the reaction within one polymer chain at the molecular level. In addition, less well defined techniques such as grinding and ball milling, and some other techniques are also used in polymer mechanochemistry, including elongational flow and laser-induced acoustic waves. All these techniques differ significantly in the maximum attainable strain rates and forces (Figure 1.2),¹³ therefore it is of great importance to make appropriate choices for particular reactions.

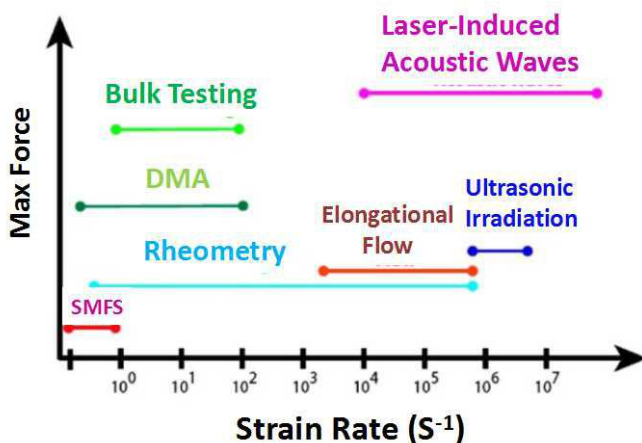


Figure 1.2. Common techniques to study mechanical reactivity in polymers, with their accessible ranges in strain rate and applied force. Reprinted with permission from ref. [13].

1.2.1 Techniques for solution mechanochemistry

As a first screening for new mechanophores, ultrasound sonication of dilute polymer solutions is usually employed in more fundamental investigations of mechanoreactivity. Because higher strain rates of 10⁶-10⁷ s⁻¹ are accessible than with other solution techniques^{15,16}, ultrasound allows mechanical activation to be obtained

in polymers of lower molecular weight and with high scission rates. As shown in Figure 1.3, sonication of solutions creates high-frequency pressure oscillations, leading to the nucleation and growth of gas bubbles¹⁷. At a certain size, the generated bubbles becomes unstable and collapses violently, resulting in the formation of local hotspots within the bubbles in which the temperature and pressure increase drastically. Polymer chains outside collapsing bubbles experience a velocity gradient, with the part of the chain closest to the center of the cavitation being pulled in at a greater velocity than the far end of the chain. This velocity gradient creates stress along the polymer backbone. The large elongational stresses cause the polymer to uncoil, and the stresses are accumulated through the polymer backbone, after which the covalent bonds along the polymer chain begin to deform, ultimately leading to chain scission. Because the flow field is centrosymmetric with respect to the molecule, the stress reaches a maximum at the center of the polymer chain, and as a consequence chain scission preferentially takes place around its midpoint.¹⁸ Further study demonstrated that under the extreme conditions close to the hotspots created by the collapse of the cavitation bubbles, the volatile content pyrolyzes and this results in reactive species such as radicals, protic secondary byproducts *etc.*¹⁹

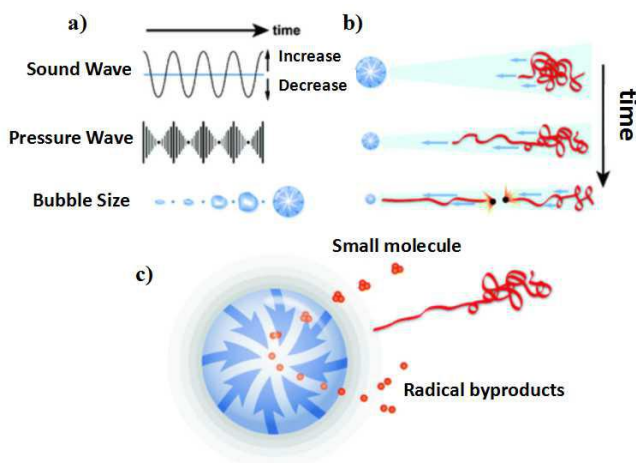


Figure 1.3. Schematic of mechanism of sonication-induced mechanoactivation of polymer chain scission: a) formation and growth of cavitation bubbles from pressure variations; b) collapse of bubbles generates solvodynamic shear force; c) molecules with different lengths respond to the shear force. Reprinted with permission of Ref. [13].

The first report of cavitation in liquid media dates back to 1895 by Thornycroft and Barnaby²⁰ when they observed that their torpedo boats suffered from erosion and

vibration coming from the consequence of collapsing bubbles due to hydrodynamic cavitation that generated intense pressure and temperature gradients in the local vicinity. Later on, the investigation of this phenomenon by Lord Rayleigh²¹ was launched and his pioneering work on the problem of the collapse of an empty cavity inside a liquid provides the theoretical foundation for cavitation studies. It was not until 1927 with the appearance of the first report²² on the effects of ultrasound on chemical and biological processes that cavitation became a useful tool in chemistry, and one of the first applications²³ reported the ultrasound-induced degradation of biological polymers. Price and Smith^{18 (c)} found that a lower solubility of saturating gas results in a lower limiting molecular weight and higher degradation rate for degradation of polystyrene, and recent studies in Sijbesma's group²⁴ also demonstrated that the heat capacity of the dissolved gases affects the formation of the products. The use of methane instead of argon for instance, significantly decreases the production of radicals because the increased degrees of freedom in methane result in a higher heat capacity, which in turn decreases the temperature in the hotspots and suppresses the formation of the reactive byproducts. Both examples illustrate that dissolved gasses play a significant role in sonication-activated mechanochemical reactions.

1.2.2 Techniques for solid-state mechanochemistry

Polymer mechanochemistry studies how molecules react directly to forces, so mechanical forces should be transferred to polymer chains and activate the reactions. Solution-based mechanochemical reactions are usually activated by ultrasound sonication, cross slots and contraction flow, while mechanoactivation in solid state polymeric materials is achieved predominantly in compression, shear or tension. In some cases grinding or ball-milling²⁵, mastication⁹, squeezing²⁶, compression from the touch of a pen²⁷ or other non-standard loading techniques can also be used, but it is difficult to control the applied force with those techniques. In this introduction we therefore focus on well-controlled compression and tension tests.

A tension test, also known as tensile test, is probably the most fundamental type of mechanical test performed on a material to quickly determine its response to tensile forces. As the sample is being pulled (Figure 1.4), it will be stretched and the strength along with its elongation (known as strain) can be determined. The external loading, F , is distributed over the cross section, A , resulting in a stress $\sigma = F/A$.²⁸ Therefore, in a homogeneous and isotropic sample, microscopic stress is controlled by the macroscopic force. Strain rate is also an important parameter that needs to be

carefully controlled in materials testing. Many mechanochemical reactions in the solid state have been studied by compression rather than by tension because compression produces less stress concentration (resulting in necking); in a compression test, the specimen usually remains homogeneous until higher strains. Upon necking, the deformation is limited to a very small part of the sample and results in less overall activation. Hence, the activation by compression is much more efficient than that by tension. An example of compression-induced mechanoactivation is the activation of a ruthenium complex that results in polymerization and cross-linking reactions of the monomers *in situ*²⁹ upon compression

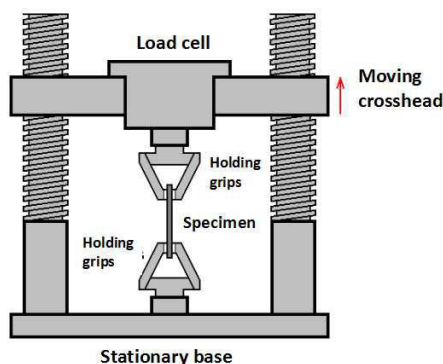


Figure 1.4. A schematic of tensile testing.[28]

The effects of solvent swelling in bulky polymers on bond scission has also been studied in mechanochemical reactions. It is difficult to control and measure the swelling stress, but because since swelling is very common in certain applications, especially for hydrogels, it is necessary and important to study the mechanical behavior of materials during swelling. The different concentrations of absorbed water during the first stage of diffusion induces non-uniform swelling. The swelling stress field comes from the mutual constraint between swollen and un-swollen zones in the sample, and is conveniently detected by photoelasticity experiment.³⁰ Usually the swelling stress is not large enough to break covalent bonds, but in specific cases, large enough for some mechanochemical reactions to take place. For example, spiropyran in Moore's group³¹ and 1,2-dioxetane in Sijbesma's group³² were successfully activated by swelling stress. Furthermore, Ma's group³³ found that swelling stress can trigger a retro Diels-Alder reaction at the surface of polyelectrolyte-carboxylated poly(OEGMA-*r*-HEMA) as well.

1.2.3 Single molecule force spectroscopy for mechanochemistry at the molecular level

Characterization of the mechanoactivity at the molecular level can be achieved with single molecule force spectroscopy (SMFS) techniques, such as atomic force microscopy (AFM), which can provide the force threshold for unbinding or activation of chemical bonds within a single molecule. Since the invention of AFM by Binnig³⁴ in 1986, AFM has been used in many experimental studies on nano-scale phenomena for imaging the atomic topography and measuring interacting forces in a variety of research fields, including physics, chemistry, biology and engineering; especially during last two decades, it has emerged as a powerful approach for investigating the mechanical processes involving proteins³⁵ and recently for studying how single molecules react to mechanical force³⁶ (Figure 1.5³⁷). The example shown in Figure 1.5(b) with SMFS demonstrates a cycloreversion of triazole into azide and alkyne by mechanical force. Although the initial report of this reaction (a so-called retro-click reaction of triazole) was retracted³⁸, the AFM experiments and quantum chemical calculations clearly showed the activation of the cycloreversion of triazole; furthermore, the computational work from Stauch and Dreuw³⁹ also offered its support on the possibility of a mechanically induced retro-click reaction.

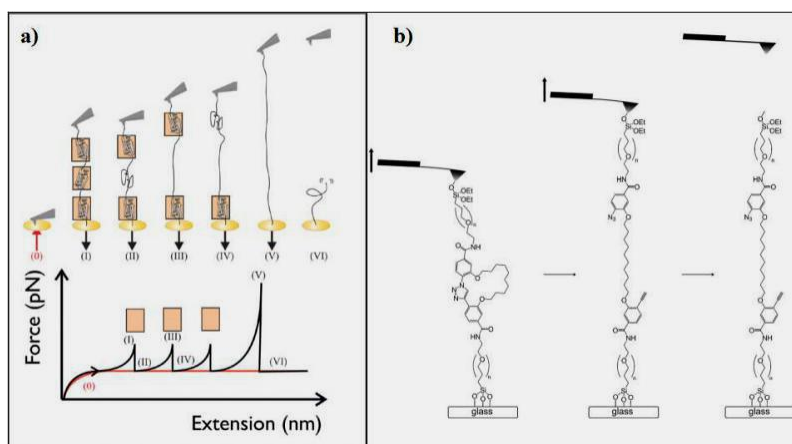


Figure 1.5. a) Schematic diagram showing the steps involved in obtaining a force-extension trace; Reprinted with permission of Ref. [37]. b) Upon stretching of the molecule, a double rupture event is observed if bond rupture occurs first in the triazole branch. Reprinted with permission of Ref. [36]

As shown in Figure 1.5, AFM uses a sharp tip mounted at the end of a flexible cantilever whose position is controlled by a piezo-electric device to probe the properties of the sample, including its topological features and mechanical characteristics. In SMFS experiments, a molecular spring is attached to an anchored molecule or molecular assembly.⁴⁰ Pulling transfers mechanical stress within the molecular system and, eventually, forces a molecular transition such as the unfolding of a nucleic acid or protein or the dissociation of a chemical bond. Figure 1.5(a) schematically shows the steps involved in obtaining a force-extension trace.

1.3 Design of mechanophores

Regardless of use or processing method of a material, mechanically induced degradation, deformation or damage is unwanted, harmful and/or destructive. However, it is inevitable and often occurs unpredictably and randomly within the material. A need for understanding these processes has spurred chemists and materials scientists to search for functional groups that report the force-induced chemical events leading to degradation. Mechanophores are usually designed as relatively weak chemical bonds or unstable units, such as metal-ligand coordination bonds⁴¹, covalent peroxide and azo linkages⁴², which can undergo a chemical reaction induced by mechanical force. In 2005, azo-functionalized poly(ethylene glycol) underwent a homolytic scission under sonication in Moore's group^{42(b)} and produced two nitriles; by then, polymer mechanochemistry started to enjoy a renaissance. In a poly ladderene example⁴³, the unstable four-membered rings along the polymer chain are the mechanophores. Upon ultrasound sonication, poly ladderene rearranges dramatically, converting the strained σ bonds to π bonds with continuous extended conjugation; the stress from the cavitation collapse results in an increased ring strain and transforms the insulating non-conjugated structure into a semiconducting conjugated structure. Similarly, the mechanochemical cycloelimination⁴⁴ of a β -lactam generates a ketene and an imine, demonstrating that mechanical force can lead to a retro-Staudinger cycloaddition reaction. In 2012, Moore's group triggered a mechanochemical transduction: a *gem*-dichlorocyclopropane (gDCC)-based crosslinked network is activated by compression and the mechanophore rearranges and spontaneously releases H^+ ,⁴⁵ .i.e. a mechanoacid.

Although many mechanophores have been developed, to date only four mechanophores have been systematically and thoroughly studied: spiropyran-, bisadamantyl 1,2-dioxetane-, *gem*-dihalocyclopropane (gDHC)-, and coordination

complex-based mechanophores. In the following part of this section these four mechanophores will be discussed in more detail.

1.3.1 Spiropyran-based mechanophore

Spiropyran belongs to a family of compounds with a structure of (substituted) 2 *H*-pyran having a second ring system attached to the 2-carbon atom of the pyran in a spiro manner.⁴⁶ This compound has been known since the beginning of the twentieth century⁴⁷ and evoked wide interest in the middle of the 1920s when its thermochromic and photochromic properties were discovered⁴⁸. The isomeration of spiropyran is shown in Figure 1.6(a)⁴⁹; of the two isomers, spiropyran is colorless while merocyanine is strongly colored, and the reversible switch between these two isomers is usually triggered by light or heating, *i.e.*, the aforementioned thermochromic and photochromic properties.

Inspired by the mechanochromic systems developed by Huck *et al.*⁵⁰, in 2009, the work with a tension or compression loading upon a spiropyran-based mechanophore-crosslinked poly(methyl methacrylate) (PMMA) network from Moore's group⁵¹ opened a door to the exploration of mechanochromic properties of spiropyran. In this work, spiropyran was incorporated into PMMA network as mechanophore crosslinker, when applying tensile loading, the colorless elastomeric network becomes strongly colored (Figure 1.6(b)), indicating that the isomerization from spiropyran to merocyanine occurs upon stress loading. This work is further evidence that macroscopic mechanical loading can trigger the activation of molecular scale events, and has become one of the pioneering investigations of modern polymer mechanochemistry. To this date studies on mechanochemistry with spiropyran are still continuing.

In 2010, a polyurethane (PU) was synthesized via step-growth polymerization and employed to study the bulk mechanical activation of the spiropyran mechanophore. It was found that the absorbance in visible spectroscopy increased linearly with strain and under a constant strain, the merocyanine did not switch back to the thermodynamically preferred spiropyran form, providing evidence of the strain-induced change in the energy landscape of the system.⁵² In 2011, two papers on mechanoactivation of spiropyran⁵³ were published in *Journal of Materials Chemistry*. One focused on environmental effects on the mechanoactivation of spiropyran in linear PMMA with a T_g of 127°C. This work demonstrated that the activation of spiropyran in linear PMMA occurred post-yield within a temperature

window of 90 to 105 °C; it was found that the activation was localized in the drawing regions and that the addition of plasticizer reduces the activation temperature to room temperature and lowers the onset strain for activation to 10%. The other paper tried to activate the spiropyran-crosslinked PMMA by torsional testing to investigate influence of shear rate on activation of spiropyran, illustrating that the activation strain increased slightly with increasing shear rate.

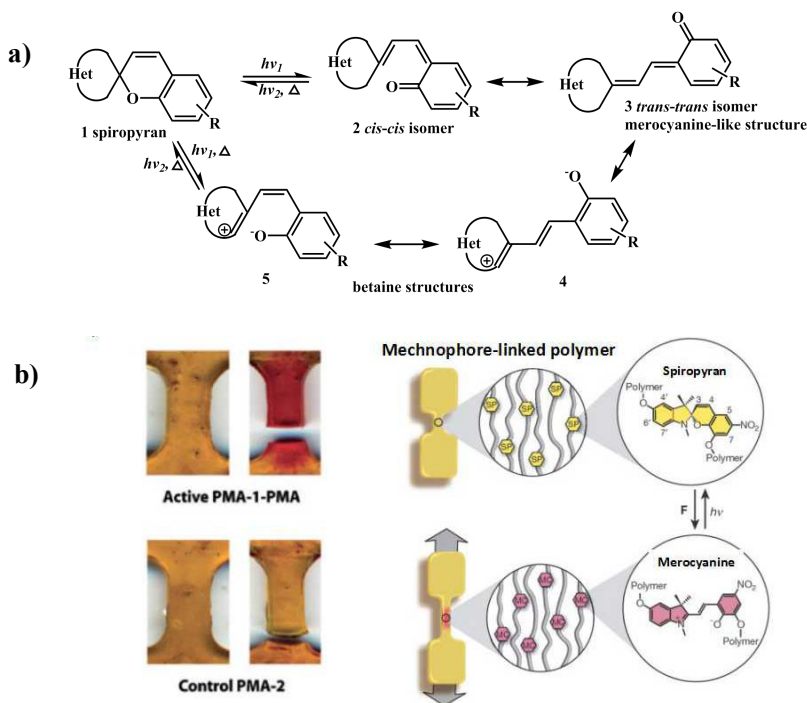


Figure 1.6. a) Schematic of isomerization of spiropyran; Reprinted with permission of Ref. [49]. b) mechanically induced switch of spiropyran to merocyanine within PMMA. Reprinted with permission of Ref. [51].

Moreover, the observation of a strong correlation of cross-sectional fluorescence intensity and location of the elastic-plastic interface provided strong evidence that the activation is induced by mechanical transduction after yielding and upon large scale plastic flow. Further work with spiropyran-crosslinked PMMA was performed in 2013⁵⁴, studying the mechanoactivation in a time scale. It was found that the time required for the onset of activation decreased with increasing the creep stress level, but the strain corresponding to the activation increased. The results confirm that

reaching a large-scale polymer deformation, the onset of flow, and stress-induced mobility are necessary to achieve mechanoactivation. The role of the orientation of mechanophore was also studied later on⁵⁵, concluding that mechanophores in the direction of loading force promotes activation, and are preferentially activated. A spiropyran mechanophore was also used as force probe providing insight into the force distribution in each local environment of segmented materials containing microphase separated hard and soft domains.⁵⁶ In the material with a high percentage of hard domains, the mechanically induced activation shows different behavior in each domain: the level of orientation is higher in the soft domains, while the fluorescence in the direction perpendicular to the force is higher in hard domains. In the parallel direction, the levels of the fluorescence in both domains are similar. It was concluded that mechanoactivation of spiropyran in the hard segments occurs at a lower level of alignment. Spiropyran was also used to study fracture-induced mechanoactivation in rubber toughened PMMA⁵⁷ and the effect of polymer chain alignment and relaxation on the mechanochemical response in an elastomer.⁵⁸ The mechanics of mechanoresponsive elastomers containing spiropyran as mechanophore were also studied in Craig's group in collaboration with Zhao's group.⁵⁹

Many techniques can be used to trigger a mechanochemical reaction. Shockwave as the external mechanical loading was used in a spiropyran incorporated into glassy polystyrene (PS) thin films, showing a stress threshold of approximately 180 MPa to achieve the activation with a corresponding strain of 7%. With increasing stress levels, the activation approached a saturation level.⁶⁰ However, at low strain rates, there was no evidence of activation, even at the failure strains. Besides using shockwaves, solvent swelling was also employed to activate the spiropyran-crosslinked network, as an example mentioned above reported in ref. [31]. Because swelling is slow or even absent with highly polar or apolar solvents, they do not activate the mechanophore; only a few solvents with intermediate polarity could successfully trigger the activation. However, some solvents, such as THF in this case, interact with the mechanophore and influence the equilibrium between spiropyran and merocyanine, indicating that not all solvents are suitable for the study of swelling-induced mechanoactivation.

It is well known that ultrasound sonication is an efficient technique to activate mechanochemical reactions. However, calculation shows that below a certain chain length, the activation is impossible to reach to a detectable extent as the strain rates

required for chain scission are higher than those provided by sonication⁶¹. In 1980, Encina and co-author found that in ultrasound-induced degradation there is a limiting length of each type of polymer chain - denoted as M_{lim} - which can be obtained empirically by plotting rate constants of scission vs molecular weight and extrapolating to a rate constant of zero.⁶² However, not until 2015 when spiropyran was incorporated into a series of acrylate polymers by Moore's group⁶³ it was realized that one should not use the concept of limiting molecular weight, but that of limiting degree of polymerization. Upon sonication, the mechanoactivation behavior of these polymers with different repeating unit compositions and side-chain branching showed a degree of polymerization dependence rather than a molecular weight dependence as commonly reported in the literature.

The work on mechanochemistry with spiropyran as mechanophore mentioned above was done in Moore's group. The group of Craig's also did a lot of work on spiropyran either alone or in collaboration with other groups, and in recent years published mostly on the practical applications, such as repeatable macroscopic shape recovery materials⁶⁴, on-demand fluorescent patterning⁶⁵, mechanochemically active soft robots⁶⁶, 3D printing of complex structures⁶⁷, force-sensitive mechanochromic touch screen⁶⁸, *etc.* Besides, SMFS was employed by Craig and coworkers to quantify the magnitude of the force necessary for activation of spiropyran-based mechanophore, finding that a force of ~240 pN is enough for the ring-opening of spiropyran on the time scale of tens of milliseconds.⁶⁹

1.3.2 *Gem*-dihalorocyclopropane (gDHC)-based mechanophore

Craig's group also pioneered the mechanochemistry of gDHC, including *gem*-difluorocyclopropane (gDFC), *gem*-dichlorocyclopropane (gDCC), and *gem*-dibromocyclopropane (gDBC). In 2009, they reported that under sonication, a gDCC-contained polymer underwent mechanically assisted ring-opening reactions when coupled to elongational shear flows⁷⁰, and the final products were characterized by ¹H NMR. The results confirmed that a polymer with a molecular weight of 310 kDa underwent an average of one scission per polymer after ~4.5 min of sonication, and after 4 hours, over 80% of the gDCC rings opened with a decay of molecular weight from 310 to 39 kDa. Since then, a series of follow-up studies on gDHCs have been published. In these studies, hundreds of gDHCs as mechanophores were introduced into a single polymer chain so that multiple ring-opening reactions occur within the time scale of chain scission, providing a mechanochemical map of the stress distribution.

As noted above, the application of a mechanical force effectively reduces the activation barrier of a reaction. This activation barrier difference (ΔE_{act}) can be described by the mechanical work, given by $\Delta E_{\text{act}} = F \Delta x$, where F is the applied force and Δx is the distance over which that force is applied as the reactant goes from its ground state to an excited transition state. By learning the force curve from SMFS, it is easy to determine the magnitude of the threshold force for mechanoactivation of a reaction. Most work on gDHCs performed in Craig's group was investigated by SMFS. For instance, in 2010 the magnitude of the threshold force for the irreversible extension of gDBC on the time scale of 10^{-2} s was determined to be 1.2 nN with the aid of SMFS.⁷¹ All the experimental and computational studies provide a view of mechanophore activity as a function of: (1) force-free reactivity, 2) the geometry of attachment, and 3) the polymer backbone through which force is transferred to the mechanophore.

With the nearly identical mechanisms that gDHCs undergo disrotatory ring opening reactions with concomitant halide migration to form corresponding 2,3-dihaloalkene, SMFS showed that the forces required to activate gDBC and gDCC fixed along the backbone of poly(butadiene) on the time scale of ~ 0.1 s are 1210 ± 100 pN and 1330 ± 70 pN, respectively.⁷² It demonstrates that in a reaction coupled to a tension from tensile load through the same attachment points and proceeding via the same mechanism, the Δx is expected to be similar. This principle is also observed in solid state mechanochemistry with gDHCs in extrusion⁷³ or compression⁷⁴. The work with extrusion and compression delivered additional information that extrusion of gDBC, embedded along a polybutadiene scaffold, in the presence of benzyltriethylammonium chloride salt does not only lead to ring opening but also subsequent bond formation, which was shown to be over 25 times more prevalent than cleavage in response to the applied stress. Tension from tensile load, however, did not result in measurable activation even till the point of failure, in contrast to the behavior in extrusion and compression experiments.

The dependence of the activity of a mechanophore on geometry changes associated with going from ground state to an excited transition state, was studied for two possible effects: 1) the direction of pulling changes Δx and 2) the direction of pulling changes the reaction mechanism. In 2014, SMFS was employed to study the effect of stereochemistry on mechanically induced electrocyclic ring opening of gDCC, demonstrating that the force required to open the *E*-alkene-substituted gDCC is 0.4 nN lower than that required in the corresponding *Z*-alkene isomer on a time scale of

ca. 0.1 s.⁷⁵ Moreover, in 2015, the study of mechanically induced reactions along both their symmetry-allowed and symmetry-forbidden pathways with SMFS enabled to quantify how forbidden each reaction is.⁷⁶ On a time scale of 0.1 s, the force for the forbidden ring opening reactions of gDFC and gDCC are quantified as approximately 560 pN more and 1000 pN more, respectively than their corresponding allowed analogues (Figure 1.7); this is the first study providing quantitative data for the mechanical acceleration of symmetry-forbidden reactions. It can be explained that because the *cis*-isomer is initially more compact than the *trans*-isomer, Δx is changed by the direction of pulling changes (disrotatory pulling or conrotatory pulling or different sequential combination of two ways), so the *cis*-isomer will have a greater activation length if the two proceed through a common (or structurally very similar) transition state. The underlying reaction mechanism can be changed by the direction of pulling so that the activation energy barrier is affected significantly. As for the ring opening of gDHCs, *cis* stereochemistry pulling triggers a disrotatory ring-opening that is symmetry allowed; however, *trans* stereochemistry pulling triggers a conrotatory ring opening that is symmetry forbidden. In 2010, work with *trans*-gDFC proved that the thermally forbidden conrotatory pathway could be driven by sonication⁷⁷, offering its solid support to the conclusion of previous work⁷⁸ that Woodward-Hoffman orbital symmetry rules could be overridden by mechanical activation. It was revealed by SMFS that the transition to *s-trans/s-trans* 1,3-diradicaloid, which is a minimum on the force-modified potential energy surface, occurs at $f^* \sim 1290$ pN and $f^* \sim 1820$ pN for *cis*-gDFC and *trans*-gDFC respectively.⁷²

The lever-arm effect was suggested by Craig's group⁷² to express how the polymer backbone transfers the force into the reaction points when they tried to quantify and compare the forces associated with the ring opening of gDBC and gDCC incorporated along the backbone of *cis*-polynorbornene and *cis*-polybutadiene: the critical force for isomerization drops by about one-third in the polynorbornene scaffold relative to polybutadiene, for polynorbornene acts as a phenomenological lever with greater mechanical advantage than polybutadiene. The lever-arm effect illustrates that the backbone of the polymer chain has significant influences on the mechanoactivity of the mechanophores.

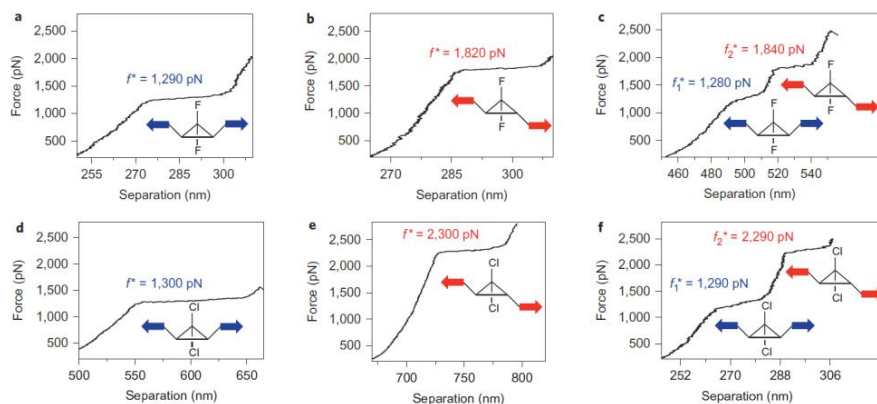


Figure 1.7. Force-separation curves of gDHC-based polymers. Reprinted with permission of Ref. [76]

SMFS studies also demonstrate that tension along a polymer main chain can trap species that are at or very near the transition state from the mechanically induced ring opening of gDFCs, and this trapping results in a new disproportionation reaction between two simultaneously trapped diradicals taking place⁷⁹. And two transitions are observed in the force vs. extension curves of polymers.⁸⁰ The first transition occurs at the force of ~ 1300 pN, attributed to the conversion from *cis*-gDFC to fully opened 1,3-diyl undergoing competing reactions between irreversible diyl consumption to a ring-opened diradicaloid intermediate and isomerization of about 5% of *cis*-gDFC to its *trans* isomer⁸¹. A second transition is observed at forces of ~ 1800 pN and reveal the partial formation of the *trans*-gDFC isomer which is further converted to 1,3-diradicaloid till fully consumed (Figure 1.8).

Further study⁸² on gDHC polybutadiene with pulsed ultrasound provides insights into a smooth and monotonic force distribution from the midchain peak toward the polymer ends. However, the mechanically induced ring opening of gDHC and chain scission always takes place simultaneously. The study on structure-activity relationships of gDCC-based polymer solutions demonstrates that the competition is invariant to sonication power, temperature, polymer concentration, and solvent but is sensitive to initial polymer molecular weight.⁸³ The distribution of peak forces that are experienced by the polymer chain upon sonication is less dependent on the conditions involved, but instead limited by the force at which the polymer chain breaks. The competition between ring opening of gDCC and chain scission is

sensitive to initial molecular weight because both secondary chain scission and chain relaxation have significant molecular weight dependencies.

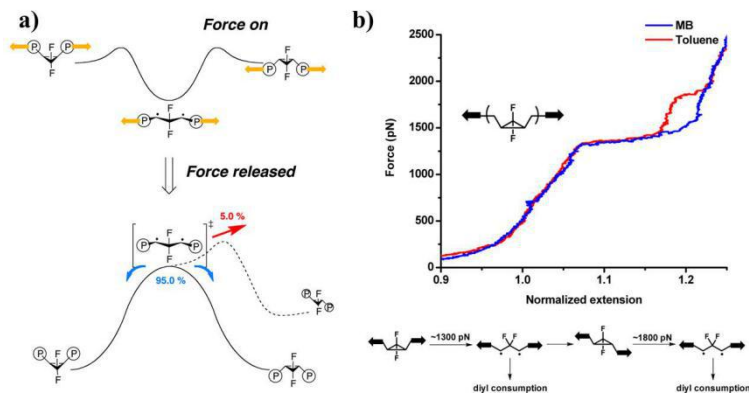


Figure 1.8. Force-induced activation of gDFCs: a) Ring-closing dynamics of a freed tension trapped transition state, and *ca.* 5.0% of the released structures close to the *trans*-isomer. Reprinted with permission of Ref. [81]. b) Representative SMFS force curves of *cis*-gDFC polymer obtained in methyl benzoate (MB in blue line) and toluene (red line). The plateau at 1800 pN evidences that the 5.0% of the in situ formed *trans*-gDFC is pulled open to 1,3-diradicaloid and fully consumed. Reprinted with permission of Ref. [80]

The mechanical properties and mechanochemical responses of an SBS-based triblock thermoplastic elastomer were improved by the incorporation of gDHCs-rich polybutadiene as the central block. When the triblocks are aligned to fiber mats by electrospinning, however, a much greater improvement by a factor of seven in the films was observed.⁸⁴ Within the triblocks, the glassy styrene domains provide weak points for fracture, and the fracture might dissipate energy that might otherwise be channeled into mechanophore activation. Additionally, when gDHC was activated mechanically, two active bromides would be formed and form a crosslinked network in the presence of sebacic acid salts as crosslinker, strengthening the initial polymers (Figure 1.9).⁸⁵

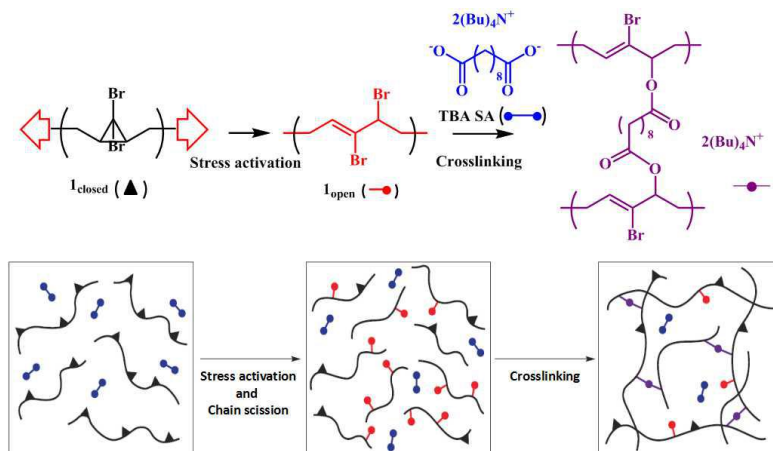


Figure 1.9. A mechanically induced self-strengthening via crosslinking with sebacic acid salts as crosslinker. Reprinted with permission of Ref. [85]

1.3.3 Bisadamantyl 1,2-dioxetane-based mechanophore

1,2-Dioxetane, the cyclic four-membered ring peroxide, and its derivatives are widely known for their application in chemiluminescence, but because of the instability of the ring, most dioxetanes decompose upon moderate heating (40-80°C) to form a mixture of ground state, triplet and a small amount of excited singlet state carbonyl products.⁸⁶ In 1971, however, adamantylideneadamantane peroxide (known as bis(adamantyl)-1,2-dioxetane) was synthesized and has showed remarkable thermal stability, providing opportunities for practical application.⁸⁷ Bis(adamantyl)-1,2-dioxetane decomposes in a first order chemiluminescent process with an activation energy of 35 kcal/mol and a half-life of less than a few minutes when heated up to 200°C⁸⁸ to form singlet and triplet products in a ratio of 1:7.5 and a total chemiexcitation yield of 17%, as determined via chemical titration.⁸⁹ It is interesting that crystallography⁹⁰ showed that the four-membered ring is non-planar with one oxygen atom being lifted about 20° from the plane defined by the two carbons and the remaining oxygen of the four-membered ring. Stretching of the O-O bond causes a compression of adamantyl substituents, and the alternative twisting motion does not appear to be sterically restricted.

Sijbesma's group introduced the use of 1,2-dioxetane in mechanochemistry. In order to incorporate 1,2-dioxetane into polymer chains, the exceptionally stable derivative, bis(adamantyl)-1,2-dioxetane, was chosen so that it would be stable before it was

activated by mechanical force. In 2012, pioneering work of using dioxetane as mechanophore was reported.⁹¹ Bis(adamantyl)-1,2-dioxetane was introduced into a rubber-like poly(methyl methacrylate) (PMMA) network. Upon application of stress, bright blue luminescent light was produced by activation of the dioxetane, allowing real-time monitoring of chain-scission events with high resolution. Later, Clough⁹² investigated the mechanoactivation products of dioxetane in detail and found that the ratio of singlet/triplet products is similar to the ratio of thermoactivation products. This provides a platform to study the stress distribution in polymers by varying both the dioxetane spacing and the network topology. The work on elastomers in collaboration with Creton's group⁹³ clearly showed that the chemiluminescence induced from decomposition of dioxetane mechanically maps of the bond breaking during propagation, providing a view of stress distribution within the network. Furthermore, Chen⁹⁴ studied the mechanoactivation of dioxetane based on polyurethane thermoplastic elastomers, concluding that the mechanoluminescence is influenced by the strength of hydrogen bonding of polymer chains within the matrix, the molecular weight, the concentration of mechanophore and the strain rate. The bond scission is determined by the balance between strain rate and disentanglement rate, and the disentanglement rates decrease continuously when chains are longer than *ca.* 50 hard segments. Dioxetane as force probe was employed to study the Mullins effect of silica-filled elastomer by providing a real-time visualization of stress-induced covalent bond scission (Figure 1.10).⁹⁵ It was unambiguously observed that covalent bond scission is brought about in an anisotropic fashion and is highly sensitive to the direction of the applied strain. The amount of light increases with hysteresis energy in a power law of exponent 2.0, demonstrating that covalent bond scission becomes increasingly important in the strain regime studied. Covalent bond scission contributes significantly to irreversible stress-softening upon the initial extension (*i.e.*, the Mullins effect). Swelling stress-induced activation of dioxetane was also investigated in a glassy polymer network PMMA.⁹⁶ Localized cascades of covalent bond-breaking, which were probably initiated at a sharp, relaxation-controlled diffusion front, was observed upon application of osmotic pressure. The proportion of bonds involved in fracture was observed for the first time by eye through mechanoluminescence.

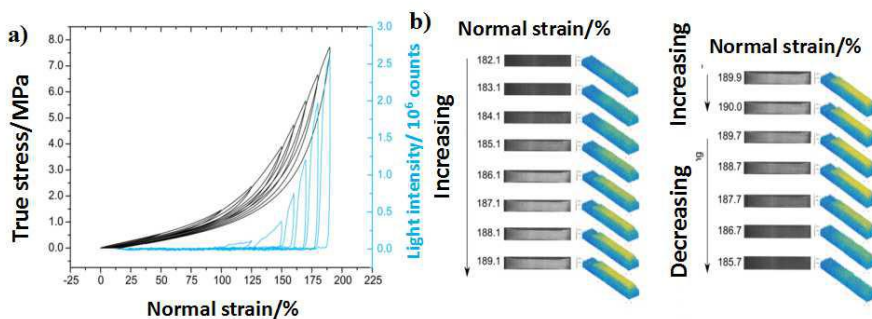


Figure 1.10. Study of Mullins effect with aid of mechanically induced chemiluminescence of dioxetane: a) true stress (black) and light emission (blue) on straining dioxetane-functionalized silica-filled PDMS; b) Image stills from camera recording of mechanoluminescence over the tensile cycle. Reprinted with permission of Ref. [95]

1.3.4 Coordination complex-based and other mechanophores

Strictly speaking, coordination complex-based mechanophores are totally different from aforementioned covalent mechanophores which usually involve cleavage of covalent chemical bonds in mechanochemical reactions, but these coordination complex-based mechanophores, incorporated into polymer chains, usually undergo heterolytic scission of coordination bonds.

Coordination complex-based mechanophores are usually used as mechanocatalyst activated by external mechanical force. The work on mechanochemistry of coordination polymers has been pioneered in Sijbesma's group since 2004.⁹⁷ With a Pd complex polymer in dilute solution, mechanically induced ligand dissociation from complexes was realized by ultrasound. With special design, two long macromolecules were attached to transition metal-organic complexes which acted as mechanophores to yield the dormant catalyst with undetectable catalytic activity. Upon sonication, cleavage of the metal-ligand coordination bond took place, resulting in an active metal site and a ligand, which can further catalyze chemical reactions. Palladium (Pd), platinum (Pt), silver (Ag) and ruthenium (Ru) *N*-heterocyclic carbene (NHC) complex-based mechanophores were studied in depth and were used for transesterification and ring-opening metathesis polymerization, respectively, upon mechanoactivation by sonication.⁹⁸ Recently, a Pd-NHC complex was used to trigger chemiluminescence of dioxetane derivatives upon sonication.⁹⁹ Free carbene, generated mechanochemically, acted as a base and deprotonated the

phenol group from dioxetane to afford an unstable intermediate dioxetane species which decomposes within minutes with the concomitant emission of blue light. Later, other groups also stepped into mechanochemistry of coordination complexes. Binder's group triggered a copper(I)-NHC catalyst for click reaction by sonication and compression¹⁰⁰, and Craig's group activated a Pd complex by SMFS¹⁰¹ and increased the maximum achievable strain of a covalent polymer by combination of coordination complex and dioxetane mechanophores in collaboration with Sijbesma's group¹⁰².

Spiropyran, cyclohalopropane, 1,2-dioxetane, and coordination complexes perform well in mechanochemistry, while with the rapid development of this area and increasing number of groups starting work on it, more and more mechanophores with certain functionality have been and will be created for special functions and studied in depth. A coumarin dimer was developed by Craig's group as a force probe of mechanochemical scission¹⁰³, a mechanogenerated aid was achieved by proton-coupled mechanochemical transduction in Moore's group in 2012¹⁰⁴, and upon activation, the designed mechanophore incorporated in an elastomeric material will release a free furan molecule¹⁰⁵. Much pioneering work was done in the last decade, but more work on mechanochemistry will be done in the future, and the methods employed in mechanochemistry will become more systematic and sophisticated.

1.4 Heterolytic scission induced by mechanical force

Bond cleavage proceeds either in a homolytic fashion to produce two radicals or in a heterolytic fashion to produce a cation - anion pair, and the mode of bond scission depends critically on the chemical environment. In a non-polar system, the formation of radicals via homolysis is favorable while a polar environment will promote the formation of ions by heterolysis. Thermal organic chemical bond scission can be either homolytic or heterolytic¹⁰⁶, but mechanochemical reactions are most often homolytic, with just a few exceptions reported in literature. Mechanically induced heterolytic scission has been observed a long time ago in the mechanical fracture of bulk polymer, such as poly(vinylidene fluoride)¹⁰⁷, but the design of mechanophores that break heterolytically moves forward at a slow pace. Up to date, there are only two reports on mechanophores that break heterolytically, both from Moore's group. Inspired by the photolysis of triarylsulfonium salts¹⁰⁸, PMMA polymer containing a triarylsulfonium salt at the center of the chain was used for mechanoactivation, and upon sonication, phenyl cation was generated via a

heterolytic scission of C-S bond which further reacted with its counter-anion (trifluoromethanesulfonate) to form a trifluoromethyl benzene-terminated polymer. The second example is based on the sonication-induced zwitterionic depolymerization of poly(*o*-phthalaldehyde) (PPA).¹⁰⁹ Both linear and cyclic PPA undergo heterolytic scission and revert the material to monomer. The scarcity of reports on mechanically induced heterolytic scission demonstrates that there is a long way to go to obtain deeper insight in mechanically induced heterolytic scission, requiring the development of new mechanophores.

1.5 Outline of this thesis

The aim of this thesis is to further explore the potential of mechanochemistry to uncover new modes of chemical activation, and to help shed light on failure mechanisms in polymeric materials.

In **Chapter 2** of this thesis, a study of the influence of strain loading rates on mechanoactivation of this mechanophore is reported. The bis(adamantyl)-1,2-dioxetane-based mechanophore was incorporated into a poly(hexyl methacrylate) network, and the mechanoresponsive behavior of the network upon tensile testing with different strain rates was studied.

In **Chapter 3**, The mechanochemistry of a poly(*N*-isopropyl acrylamide) (PNIPAm)-network, crosslinked with a Diels–Alder adduct-based mechanophore is reported. With different degrees of swelling with water, the compression-induced mechanoactivation of the mechanophore was studied and the generated highly fluorescent product was used to map the damage of the materials to give a detailed view of the strain on the microscale.

Up to date, few studies in polymer mechanochemistry have focused on heterolytic scission. In **Chapter 4**, an exploration of mechanophore candidates, including an imidazolium-based mechanophore, an *N*-benzylpyridinium-based mechanophore and a triphenylmethyl ether-based mechanophore is reported. In each case, the targeted scission mode did not appear to occur as expected, but the reason was surveyed in detail.

Further exploration of mechanochemical themes was performed with bis(viologen) and is reported in **Chapter 5**. Inspired by the reversible switch of monomeric and dimeric states with different electromagnetic properties of the reduced form of

bis(viologen), several polymerizable (a)symmetric viologens or bis(viologen)s were prepared, and the redox properties and electromagnetic properties were investigated with cyclic voltammetry and electron paramagnetic resonance spectroscopy respectively, demonstrating a good reversibility of the two reduced states and temperature-dependent electromagnetic properties. However, due to technical limitations on the characterization of the bis(viologen) containing hydrogels under tension in an inert atmosphere, conclusive results on the mechanoactivation were difficult to achieve.

References

- 1 a) E. Amaied, R. Vargiolu, J. M. Bergheau, H. Zahouani, *Wear*, **2015**, 332-333: 715–724; b) R. Winter, V. Harrar, M. Gozdzik, L. R. Harris, *Brain Res*, **2008**, 1242: 54-58;
- 2 S. L. Geffeney, and M. B. Goodman, *Neuron*, **2012**, 74(4): 609-619;
- 3 a) S. L. James, C. J. Adams, C. Bolm, et al., *Chem. Soc. Rev.* **2012**, 41: 413-477; b) M. K. Beyer, H. Clausen-Schaumann, *Chem. Rev.* **2005**, 105(8): 2921-2947;
- 4 P. Baláž, M. Achimovičová, M. Baláž, et al., *Chem. Soc. Rev.* **2013**, **42**: 7571-7637;
- 5 a) S. L. James, C. J. Adams, C. Bolm, et al., *Chem. Soc. Rev.*, **2012**, **41**: 413-447; b) J. L. Do and T. Frisčić, *ACS Cent. Sci.* **2017**, 3: 13–19; c) G.-W. Wang, *Chem. Soc. Rev.*, **2013**, 42: 7668—7700; d) V. Šepelák, A. Düvel, M. Wilkening, K. D. Becker and P. Heitjans, *Chem. Soc. Rev.*, **2013**, **42**: 7507-7520;
- 6 X. Guo, D. Xiang, G. Duan, P. Mou, *Waste Manag.* **2010**, 30: 4–10;
- 7 K. Ralphs, C. Hardacre and S. L. James, *Chem. Soc. Rev.*, **2013**, **42**: 7701-7718;
- 8 a) *National Historic Chemical Landmarks*. American Chemical Society. Retrieved June 25, **2012**; b) L. H. Baekeland. *J. Ind. Eng. Chem.* **1909**, 1: 149-161;
- 9 H. Staudinger, W. Heuer, *Ber. Dtsch. Chem. Ges. A/B* **1934**, 67: 1159-1164;
- 10 W. Kauzmann, H. Eyring, *J. Am. Chem. Soc.* **1940**, 62: 3113–3125;
- 11 T. Q. Nguyen, H.-H. Kausch, *Flexible Polymer Chains in Elongational Flow Theory and Experiment*, Springer-Verlag Berlin Heidelberg **1999**, Springer, Berlin, Heidelberg;
- 12 J. Ribas-Arino, M. Shiga, D. Marx, *Angew. Chem. Int. Ed.* **2009**, **48**, 4190–4193.
- 13 M. M. Caruso, D. A. Davis, Q. Shen, S. A. Odom, N. R. Sottos, S. R. White, J. S. Moore, *Chem. Rev.* **2009**, **109**: 5755-5798;
- 14 C. R. Hickenboth, J. S. Moore, S. R. White, N. R. Sottos, J. Baudry, S. R. Wilson, *Nature* **2007**, 446: 423-427;
- 15 T. Q. Nguyen, H.-H. Kausch, in *Macromol. Synth. Order Adv. Prop.*, Springer Berlin Heidelberg, **1992**, 73–182;
- 16 J. A. Odell, A. Keller, *J. Polym. Sci. Part B Polym. Phys.* **1986**, 24: 1889–1916;
- 17 G. Cravotto, E. C. Gaudino, P. Cintas, *Chem. Soc. Rev.* **2013**, 42: 7521;
- 18 a) M. W. A. Kuijpers, P. D. Iedema, M. F. Kemmere, J. T. F. Keurentjes, *Polymer* **2004**, 45: 6461–6467; b) G. J. Price and P. F. Smith, *Polym. Int.*, **1991**, 24: 159–164; c) G. J. Price and P. F. Smith, *Polymer*, **1993**, 34: 4111–4117; d) G. J. Price and P. F. Smith, *Eur. Polym. J.*, **1993**, 29: 419–424;
- 19 J. Rooze, R. Groote, R. T. M. Jakobs, R. P. Sijbesma, M. M., Iersel, et al., *J. Phys. Chem. B*, **2011**, 115(38): 11038-11043;
- 20 J. Thorneycroft and S.W. Barnaby, *Inst. Civil Eng.* **1895**, 7(4): 711–736;
- 21 L. Rayleigh, *Philos. Mag.* **1917**, 34: 94–98;
- 22 W.T. Richards and A.L. Loomis, *J. Am. Chem.Soc.* **1927**, 49: 3086-3100;
- 23 S. Brohult, *Nature* **1937**, 140: 805;
- 24 R. Groote, R. T. M. Jakobs, R. P. Sijbesma, *ACS Macro Lett.* **2012**, 1: 1012–1015;
- 25 a) W. F. Watson, *Makromol. Chem.* 1959, 34: 240-252; b) C. Liu, Q. Wang, *J. Appl. Polym. Sci.*, **2000**, 78: 2191–2197(); c) G. Janke and G. Schmidt-Naake, *Chem. Eng. Technol.* 2001, 24, 7: 711-715;
- 26 J. N. Brantley, K. M. Wiggins, and C. W. Bielawski, *Angew. Chem. Int. Ed.* **2013**, 52: 3806 – 3808;
- 27 a) G. R. Gossweiler, G. B. Hewage, G. Soriano, Q. Wang, G. W. Welshofer, X. Zhao, S. L. Craig, *ACS MacroLett.* **2014**, 3: 216–219; b) Z. Wang, Z. Ma, Y. Wang, Z. Xu, Y. Luo, Y. Wei, X. Jia, *Adv. Mater.* **2015**, 27: 6469–6474;
- 28 D. Gross, W. Hauger, J. Schröder, W. Wall, J. Bonet, *Engineering Mechanics 2: Mechanics of*

Materials, Springer-Verlag Berlin Heidelberg, **2011**, Springer, Berlin, Heidelberg;

29 R. T. M. Jakobs, S. Ma, and R.P. Sijbesma, *ACS Macro Lett.* **2013**, 2: 613–616

30 a) G. Pitarresi, M. Scafidi, S. Alessi, M. Di Filippo, C. Billaud, G. Spadaro, *Polym. Degrad. Stab.* **2015**, 111: 55-63; b) A. Toscano, G. Pitarresi, M. Scafidi, M. Di Filippo, G. Spadaro, S. Alessi, *Polym. Degrad. Stab.* **2016**, 133: 255-263; c) S. Alessi, M. Di Filippo, G. Pitarresi, M. Scafidi, A. Toscano, *Procedia Eng.* 2015, 109: 507- 516; d) G. Spadaro, G. Pitarresi, S. Alessi, M. Scafidi, A. Toscano, & M. Di Filippo, *Frattura ed Integrità Strutturale*, **2014**, 30: 127-137;

31 C. K. Lee, C. E. Diesendruck, E. Lu, A. N. Pickett, P. A. May, J. S. Moore, and P. V. Braun, *Macromolecules* **2014**, 47: 2690–2694;

32 J. M. Clough, J. van der Gucht and R. P. Sijbesma, *Macromolecules* **2017**, 50: 2043–2053;

33 B. Lyu, W. Cha, T. Mao, Y. Wu, H. Qian, et al., *ACS Appl. Mater. Interfaces* **2015**, 7: 6254–6259;

34 G. Binnig, C. F. Quate and C. Gerber, *Phys. Rev. Lett.* **1986**, 56(9): 930-933;

35 a) K. Mitsui, M. Hara and A. Ikai *FEBS Lett.* **1996**, 385: 29–33; b) J. Zlatanova, S. M. Lindsay and S. H. Leuba *Prog. Biophys. Mol. Biol.* **2000**, 74: 37–61; c) H. Clausen-Schaumann, M. Seitz, R. Krautbauer and H. E. Gaub *Curr. Opin. Cell Biol.* **2000**, 4: 524–530; d) V. Barsegov, D. K. Klimov and D. Thirumalai, *Biophys. J.* **2006**, 90: 3827–3841; e) T. Hoffmann and L. Dougan, *Chem. Soc. Rev.* **2012**, 41: 4781–4796;

36 D. Schutze, K. Holz, J. Muller, M. K. Beyer, U. Luning, and B Hartke, *Angew. Chem. Int. Ed.* **2015**, 54: 2556–2559;

37 M. L Hughes and L. Dougan, *Rep. Prog. Phys.* **2016**, 79: 076601

38 M. McNutt, *Science*, **2015**, 347, 834.

39 T. Stauch and A. Dreuw, *Chem. Sci.*, **2017**, 8: 5567–5575;

40 a) G. Hummer and A. Szabo, *Acc. Chem. Res.* **2005**, 38: 504-513; b) A. Janschoff, M. Neitzert, Y. Oberdorfer, and H. Fuchs, *Angew. Chem. Int. Ed.* **2000**, 39(18): 3212-3237;

41 a) J. M. J. Paulusse, J. P. J. Huijbers, R. P. Sijbesma. *Chem. Eur. J.* **2006**, 12(18): 4928-4934; b) J. M. J. Paulusse, R. P. Sijbesma. *Chem. Commun.* **2008**, 37:4416-44188, c) F. R. Kersey, W. C. Yount, S. L. Craig. *J. Am. Chem. Soc.*, **2006**, 128(12): 3886-3887;

42 a) M. V. Encina, E. Lissi, M. Sarasúa, L. Gargallo, D. Radic. *J. Polym. Sci.: Polym. Lett. Ed.* **1980**, 18(12): 757-760, b) K. L. Berkowski, S. L. Potisek, C. R. Hickenboth, J. S. Moore. *Macromolecules* **2005**, 38(22): 8975-8978;

43 Z. Chen, J. A. M. Mereer, X. Zhu, J. A. H. Romaniuk, R. Pfattner, L. Cegelski, T. J. Martinez, N. Z. Burns, Y. Xia, *science*, **2017**, 357: 475-479

44 M. J. Robb and J. S. Moore, *J. Am. Chem. Soc.*, **2015**, 137 (34): 10946–10949;

45 C. E. Diesendruck, B. D. Steinberg, N. Sugai, M. N. Silberstein, N. R. Sottos, S. R. White, P. V. Braun, and J. S. Moore, *J. Am. Chem. Soc.*, **2012**, 134 (30): 12446–12449;

46 J. C. Crano and R. J. Gugliemetti, *Organic Photochromic and Thermochromic compounds: Volume I: Main Photochromic Families*, Kluwer Academic Publishers, **2002**, NY, United States;

47 H. Decker and T. Fellenberg, *Liebigs Ann. Chem.*, **1909**, 364 (1): 1-44;

48 a) A. Löwenbein and W. Katz, *Ber. Dtsch. Chem. Ges.*, **1926**, 59 (7): 1377-1383; b) W. Diltthey, C. Berres, E. Hölterhoff and H. Wübken, *J. prakt. Chem.*, **1926**, 114: 179-198; c) W. Diltthey and R. Wizinger, *Ber. Dtsch. Chem. Ges.*, **1926**, 59 (8): 1856-1858; d) E. Fischer and Y. Hirshberg, *J. Chem. Soc.*, **1952**, 4522;

49 B. S. Lukyanov and M. B. Lukyanova, *Chem. Heterocycl. Compd.*, **2005**, 41(3): 281-311

50 a) R. A. Nallicheri, M. F. Rubner, *Macromolecules* **1991**, 24: 517–525; b) S.-J. Kim, D. H. Reneker, *Polym. Bull.* **1993**, 31: 367–374; c) S. H. Foulger, P. Jiang, A. C. Lattam, D. W. Smith and J. Ballato, *Langmuir* **2001**, 17: 6023–6026; d) C. Löwe, C. Weder, *Adv. Mater.* **2002**, 14: 1625–1629; d) S.

H. Foulger, P. Jiang, A. Lattam, D. W. Smith, et al., *Adv. Mater.* **2003**, 15: 685–689; e) O. Azzaroni, B. Trappmann, P. van Rijn, F. Zhou, B. Kong, and W. T. S. Huck, *Angew. Chem. Int. Ed.* **2006**, 45: 7440–7443; f) J. E. Comrie, W. T. S. Huck, *Macromol. Rapid Commun.* **2008**, 29: 539–546;

51 D. A. Davis, A. Hamilton, J. Yang, L. D. Cremar, D. Van Gough, et al., *Nature* **2009**, 459: 68–72;

52 C.K. Lee, D.A. Davis, S.R. White, J.S. Moore, N.R. Sottos, P.V. Braun, *J. Am. Chem. Soc.* **2010**, 132: 16107–16111.

53 a) C. M. Kingsbury, P. A. May, D. A. Douglas, S. R. White, J. S. Moore, and N. R. Sottos, *J. Mater. Chem.*, **2011**, 21: 8381–8388; b) B. A. Beiermann, D. A. Davis, S. L. B. Kramer, J. S. Moore, N. R. Sottos, S. R. White, *J. Mater. Chem.*, **2011**, 21: 8443–8447;

54 C. M. Degen, P. A. May, J. S. Moore, S. R. White, N. R. Sottos, *Macromolecules*, **2013**, 46: 8917–8921;

55 B. A. Beiermann, S. L. B. Kramer, J. S. Moore, S. R. White, N. R. Sottos, *ACS Macro Lett.* **2012**, 1: 163–166;

56 C. K. Lee, B. A. Beiermann, M. N. Silberstein, J. Wang, J. S. Moore, N. R. Sottos, P. V. Braun, *Macromolecules*, **2013**, 46: 3746–3752;

57 A.-D. N. Celestine, B. A. Beiermann, P. A. May, J. S. Moore, N. R. Sottos, S. R. White, *Polymer*; **2014**, 55: 4164–4171;

58 B. A. Beiermann, S. L. B. Kramer, P. A. May, J. S. Moore, S. R. White, and N. R. Sottos, *Adv. Funct. Mater.*, **2014**, 24: 1529–1537;

59 Q. Wang, G. R. Gossweiler, S. L. Craig, X. Zhao, *J. Mech. Phys. Solids* **2015**, 82: 320–344

60 M. E. Grady, B. A. Beiermann, J. S. Moore, N. R. Sottos, *ACS Appl. Mater. Inter.*, **2014**, 6: 5350–5355;

61 J. Ribas-Arino, M. Shiga, D. Marx, *Chem. – Eur. J.* **2009**, 15(48): 13331–13335;

62 M. V. Encina, E. Lissi, M. Sarasúa, L. Gargallo, D. Radic, *J. Polym. Sci. Polym. Lett. Ed.* **1980**, 18 (12): 757–760;

63 P. A. May, N. F. Munaretto, M. B. Hamoy, M. J. Robb, J. S. Moore, *ACS Macro Letters*, **2016**, 5: 177–180;

64 G. R. Gossweiler, G. B. Hewage, G. Soriano, Q. Wang, G. W. Welshofer, X. Zhao, and S. L. Craig, *ACS Macro Lett.* **2014**, 3: 216–219;

65 Q. Wang, G. R. Gossweiler, S. L. Craig & X. Zhao, *Nat. Commun.* **2014**, 5: 4899;

66 G. R. Gossweiler, C. L. Brown, G. B. Hewage, E. Sapiro-Gheiler, W. J. Trautman, G. W. Welshofer, and S. L. Craig, *ACS Appl. Mater. Interfaces* **2015**, 7: 22431–22435;

67 G. I. Peterson, M. Yurtoglu, M. B. Larsen, S.L. Craig, M. A. Ganter D. W. Storti, A. J. Boydston, *Rapid Prototyping J.* **2015**, 21(5): 520–527;

68 S. Cho, S. Kang, A. Pandya, R. Shanker, Z. Khan, Y. Lee, J. Park, S. L. Craig, and H. Ko, *ACS Nano* **2017**, 11: 4346–4357;

69 G. R. Gossweiler, T. B. Kouznetsova, and S. L. Craig, *J. Am. Chem. Soc.* **2015**, 137: 6148–6151;

70 J. M. Lenhardt, A. L. Black, and S. L. Craig, *J. Am. Chem. Soc.* **2009**, 131: 10818–10819

71 D. Wu, J. M. Lenhardt, A. L. Black, B. B. Akhremitchev, and S. L. Craig, *J. Am. Chem. Soc.* **2010**, 132: 15936–15938;

72 H. M. Klukovich, T. B. Kouznetsova, Z. S. Kean, J. M. Lenhardt and S. L. Craig, *Nat. Chem.* **2013**, 5: 110–114;

73 A. L. Black, J. A. Orlicki and S. L. Craig, *J. Mater. Chem.*, **2011**, 21: 8460–8465;

74 J. M. Lenhardt, A.L. Black, B. A. Beiermann, B.D. Steinberg, F. Rahman, *J. Mater. Chem.*, **2011**, 21: 8454–8459;

- 75 J. Wang, T. B. Kouznetsova, Z. S. Kean, L. Fan, B. D. Mar, T. J. Martinez, and S. L. Craig, *J. Am. Chem. Soc.* **2014**, 136: 15162–15165;
- 76 J. Wang, T. B. Kouznetsova, Z. Niu, M. T. Ong, H. M. Klukovich, A. L. Rheingold, T. J. Martinez and S. L. Craig, *Nat. Chem.* **2015**, 7: 323-327;
- 77 J. M. Lenhardt, M. T. Ong, R. Choe, C. R. Evenhuis, T. J. Martinez, S. L. Craig, *Science* **2010**, 329 (5995): 1057-1060;
- 78 C. R. Hickenboth, J. S. Moore, S. R. White, N. R. Sottos, J. Baudry & S. R. Wilson *Nature* **2007**, 446: 423-427 ;
- 79 J. M. Lenhardt, J. W. Ogle, M. T. Ong, R. Choe, T. J. Martinez, and S. L. Craig, *J. Am. Chem. Soc.* **2011**, 133: 3222–3225;
- 80 J. Wang, T. B. Kouznetsova, and S. L. Craig, *J. Am. Chem. Soc.* **2016**, 138: 10410–10412;
- 81 J. Wang, M. T. Ong, T. B. Kouznetsova, J. M. Lenhardt, T. J. Martinez, S. L. Craig, *J. Org. Chem.* **2015**, 80: 11773–11778
- 82 A. L. Black Ramirez, J. W. Ogle, A. L. Schmitt, J. M. Lenhardt, M. P. Cashion, M. K. Mahanthappa, and S. L. Craig, *ACS Macro Lett.* **2012**, 1: 23–27;
- 83 J. M. Lenhardt, A. L. Black Ramirez, B. Lee, T. B. Kouznetsova, and S. L. Craig, *Macromolecules* **2015**, 48: 6396–6403;
- 84 A. L. Black Ramirez, A. K. Schmitt, M. K. Mahanthappa and S. L. Craig, *Faraday Discuss.*, **2014**, 170: 337–344;
- 85 A. L. Black Ramirez, Z. S. Kean, J. A. Orlicki, M. Champhekar, S. M. Elsagr, W. E. Krause and S. L. Craig, *Nat. Chem.* **2013**, 5: 757-761;
- 86 a) N. J. Turro, P. Lechtken, G. Schuster, J. Orell, H.-C. Steinmetzer, W. Adam, *J. Am. Chem. Soc.* , **1974**, 96(5): 1627-1629; b) K. R. Kopecky, J. E. Filby, C. Mumford, P. A. Lockwood, J. Ding, *Can. J. Chem.* **1975**, 53: 1103-1122; c) W. Adam, W. J. Baader, *Angew. Chem. Int. Ed.* **1984**, 23(2): 166-167; d) S. Wilsey, F. Bernardi, Massimo Olivucci, M. A. Robb, S. Murphy, and W. Adam, *J. Phys. Chem. A* **1999**, 103: 1669-1677; e) L. De Vico, Y. Liu, J. W. Krogh, and R. Lindh, *J. Phys. Chem. A* **2007**, 111: 8013-8019;
- 87 J. H. Wieringa, J. Strating and H. Wynberg, W. Adam, *Tetrahedron Lett.* **1972**, 2: 169 – 172;
- 88 J. C. Hummelen, T. M. Luider, H. Wynberg, *Pure Appl. Chem.* **2009**, 59: 639–650;
- 89 G. B. Schuster, N. J. Turro, H. C. Steinmetzer, A. P. Schaap, G. Faler, W. Adam, J. C. Liu, *J. Am. Chem. Soc.* **1975**, 97: 7110–7118;
- 90 H. Numan , J. H. Wieringa , H. Wynberg, J. Hess, and A. Vos, *J. Chem. Soc., Chem. Commun.*, **1977**: 591-592;
- 91 Y. Chen, A. J. H. Spiering, S. Karthikeyan, G. W. M. Peters, E. W. Meijer, and R. P. Sijbesma, *Nat. Chem.* **2012**: 559-562;
- 92 J. M. Clough and R. P. Sijbesma, *Chem Phys Chem* **2014**, 15: 3565 – 3571;
- 93 E. Ducrot, Y. Chen, M. Bulters, R. P. Sijbesma, C. Creton, *Science*, **2014**, 344(6180): 186-189;
- 94 Y. Chen and R. P. Sijbesma, *Macromolecules* **2014**, 47: 3797–3805;
- 95 J. M. Clough, C. Creton, S. L. Craig, and R.P. Sijbesma, *Adv. Funct. Mater.* **2016**, 26: 9063–9074;
- 96 J. M. Clough, J. van der Gucht, and R. P. Sijbesma, *Macromolecules* **2017**, 50: 2043–2053
- 97 J. M. J. Paulusse, R. P. Sijbesma, *Angew. Chem., Int. Ed.* **2004**, 43: 4460-4462;
- 98 a) J. M. J. Paulusse, R. P. Sijbesma, *Chem. Commun.* **2008**: 4416-4418; b) S. Karthikeyan, S. L. Potisek, A. Piermattei, R. P. Sijbesma, *J. Am. Chem. Soc.* **2008**, 130: 14968-14969; c) A. Piermattei, S. Karthikeyan and R. P. Sijbesma, *Nat. Chem.* **2009**, 1: 133-137;
- 99 J. M. Clough, A. Balan, T. L. J. van Daal, and R. P. Sijbesma, *Angew. Chem. Int. Ed.* **2016**, 55: 1445

-1449;

- 100 P. Micheal, W. H. Binder, *Angew. Chem. Int. Ed.* **2015**, 54(47): 13918-13922;
- 101 F. R. Kersey, W. C. Yount, and S. L. Craig, *J. Am. Chem. Soc.* **2006**, 128: 3886-3887.
- 102 Z. S. Kean, J. L. Hawk, S. Lin, X. Zhao, R. P. Sijbesma, and S. L. Craig, *Adv. Mater.* **2014**, 26, 6013-6018;
- 103 Z. S. Kean, G. R. Gossweiler, T. B. Kouznetsova, G. B. Hewage and S. L. Craig, *Chem. Commun.*, **2015**, 51, 9157-9160;
- 104 C. E. Diesendruck, B. D. Steinberg, N. Sugai, M. N. Silberstein, N. R. Sottos, S. R. White, P. V. Braun, and J. S. Moore, *J. Am. Chem. Soc.* **2012**, 134, 12446-12449;
- 105 M. B. Larsen and A. J. Boydston, *J. Am. Chem. Soc.* 2014, 136, 1276-1279;
- 106 a) C. A. Grob, P. W. Schiess, *Angew. Chem. Int. Ed.* **1967**, 6 (1): 1-106; b) C. A. Grob, *Angew. Chem. Int. Ed.* **1969**, 8 (8): 535-622;
- 107 a) M. Sakaguchi, H. Kinpara, Y. Hori, S. Shimada, H. Kashiwabara, *J. Polym. Sci. Part B Polym. Phys.* **1988**, 26: 1307-1312; b) M. Sakaguchi, H. Kinpara, Y. Hori, S. Shimada, H. Kashiwabara, *J. Polym. Sci. Part B Polym. Phys.* **1987**, 25: 1431-1437; c) M. Sakaguchi, S. Shimada, H. Kashiwabara, *Macromolecules*, **1990**, 23: 5038-5040; d) M. Sakaguchi, H. Kinpara, Y. Hori, S. Shimada, H. Kashiwabara, *Macromolecules*, **1989**, 22: 1277-1280;
- 108 J. L. Dektar, N. P. Hacker, *J. Am. Chem. Soc.*, **1990**, 112: 6004-6015;
- 109 C. E. Diesendruck, G. I. Peterson, H. J. Kulik, J. A. Kaitz, B. D. Mar, et al., *Nat. Chem.* **2014**, 6: 623-628.

Chapter II

Mechanically induced chemiluminescence in a poly (hexyl methacrylate) network

ABSTRACT

The influence of strain loading rate on mechanochemical response in a poly (hexyl methacrylate) network was studied with bis(adamantyl)-1,2-dioxetane units as the mechanophore. The scission of the dioxetane as the force probe maps the strain loading during the tensile tests, demonstrating a strong localisation at low strain rate. The effect of the strain loading rate on the total intensity of generated light shows that there is a maximum emission at mediate strain rate as a dynamic glass transition.

2.1 Introduction

2.1.1 Mechanochemiluminescence

Mechanochemical transduction plays irreplaceable roles in the mediation of a diverse array of natural processes such as hearing, touching, tissue growth and bioluminescence.¹ To fully understand the principles of those mechanically induced natural processes and mimic them with synthetic polymer materials to fabricate functional materials for practical applications, the concept of polymer mechanochemistry was introduced in late 1980s.² Polymer mechanochemistry aims at understanding and exploiting the principles and practical applications of mechanically induced chemical transduction within macromolecular chains. With the development of polymer mechanochemistry, many mechanoresponsive systems have been developed: for example Moore's group³ mainly focuses on spiropyran-based mechanochromic material which can change its color under external force through isomerization of spiropyran to merocyanine, and Craig's group⁴ has done much research on *Gem*-dihalocyclopropanes (gDHC)- which produce functionalities for further reaction upon application of mechanical force, with potential applications in self-healing materials. In Sijbesma's group, mechanically induced chemiluminescence based on bis(adamantyl)-1,2-dioxetane (Figure 2.1) was reported in 2012.⁵ The four-membered 1,2-dioxetane ring incorporated either as a crosslinker or in the main chain of a linear polymer opens upon mechanical activation, and generates an excited state ketone in the singlet or triplet excited state. When the singlet excited state reverts to the ground state, the excess energy is released as a photon. Initial research focused mostly on the spatiotemporal resolution of the luminescence, and the feasibility to incorporate dioxetane mechanophore into other polymers either well below T_g or in the rubbery state.⁶ However, the effect of strain rate on the intensity and distribution of mechanoluminescence upon straining a polymer network close to T_g has not been studied yet and sparked our interest. To study the effect of strain rate, bis(adamantyl)-1,2-dioxetane was incorporated into a hexyl methacrylate-based network, and tensile tests were employed as the source of the external force, an electron-multiplying charge-coupled device (EMCCD) camera was employed to record the light emission during the tensile experiments, and MATLAB and ImageJ were employed to do the analysis..

2.1.2 Scientific cameras for image recording

When mechanically induced chemiluminescence was first recorded by Chen⁵, a

Canon EOS 5D Mark II digital SLR camera (a scientific Complementary Metal Oxide Semiconductors (sCMOS) camera) was used, and Clough⁶ studied the Mullins effect of a filled elastomer with mechanoluminescence, using the same sCMOS camera, but osmotic stress induced mechanoluminescence⁶ was studied in our group with an Andor iXon Ultra 888 EMCCD camera. In recent years, both sCMOS and EMCCD cameras have widely been used in scientific research.

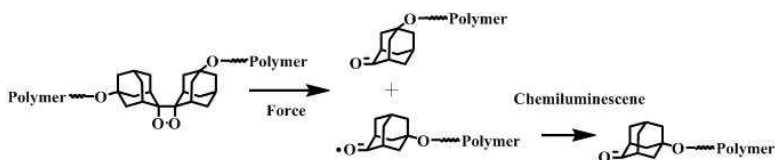


Figure 2.1. Mechanically induced chemiluminescence based on bis(adamantyl)-1,2-dioxetane

The sCMOS and CCD are the two image sensors for digital imaging constituted by many square "pixels". When recording images, the targeted image is projected through a lens onto the capacitor array (a photoactive region in those pixels), and the hit of photons on the photoactive region results in the conversion of incoming photons into electric charge at the interface and the electric charge is accumulated in each capacitor; the sCMOS or CCD reads out these charges and stores it as information. The sCMOS and CCD are similar in many ways, but the different readout modes, global shutter and rolling shutter, respectively (Figure 2.2), affect illumination synchronization, exposure timing, spatial distortions and noise levels in different ways. Popular CCD cameras usually employ interline transfer CCDs in a global shutter mode in which each pixel is exposed at the same instant in time. However, because the signals from all of the pixels are serially moved to an

analog-to-digital (A/D) converter when the exposure is complete, the more pixels there are to transfer, the slower the total frame rate of the camera is. This disadvantage is eliminated with the CMOS by utilizing an A/D for all of the columns of pixels, which can be in the thousands, allowing shorter readout times and ensuring faster frame rates. But for quick capture and switching between several excitation channels, common rolling shutter acquisitions employed usually by CMOS camera can lead to channel bending caused the overlapping of rolling shutter readout, results in artifacts under certain conditions. In all applications, a wise choice of specific camera is necessary to achieve optimal images.

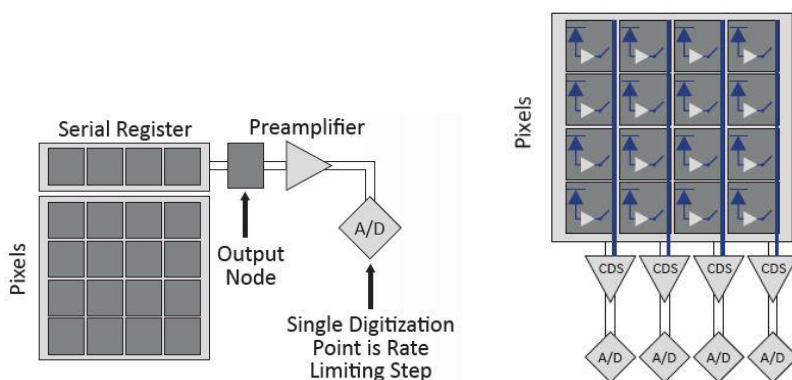


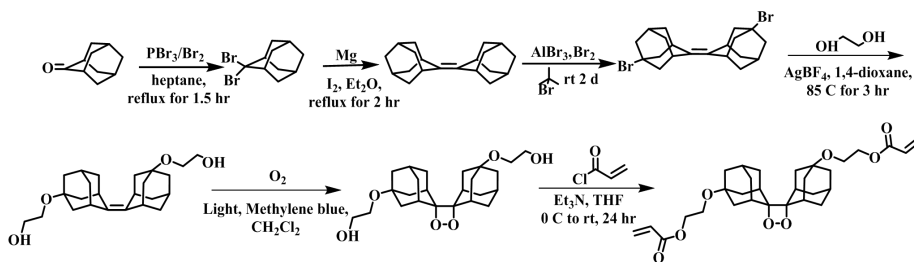
Figure 2.2. Schematics of CCD (left) and sCMOS (right) sensor architectures

2.2 Results and Discussion

2.2.1 Synthesis

The bisacrylate-functionalized 1,2-dioxetane-based mechanophore crosslinker was synthesized according to previous work by Chen and Clough in our group (Scheme 2.1).^{5,6} The bromination of adamantane yields 2,2'-dibromoadamantane which was homocoupled through Grignard reaction to generate adamantylideneadamantane. Another bromination reaction was used to introduce two bromine atoms that allowed reaction with ethylene glycol to introduce hydroxyl functionalities for further derivatization. The photo-activation of hydroxyl-functionalized adamantylideneadamantane catalyzed by methylene blue formed the dioxetane units, and esterification with acryloyl chloride to obtain the polymerizable functionalities produced the final bisacrylate crosslinker. The mechanophore-containing PHMA network was prepared by thermopolymerization of hexyl methacrylate saturated

with the energy acceptor diphenylanthracene (DPA), with tetraethylene glycol dimethacrylate as crosslinker and bisacrylate-functionalized 1,2-dioxetane as co-crosslinker (total crosslinker content 4.5 mol.%, including 0.9 mol.% of dioxetane crosslinker). The reaction was performed under N₂ atmosphere at 65 °C for 24 h with AIBN as thermoinitiator. The resulting PHMA network films were cut into 5 mm × 25 mm slices for tensile experiments.



Scheme 2.1. Synthetic routine towards bisacrylate-functionalized 1,2-dioxetane-based mechanophore crosslinker

2.2.2 Mechanical properties of the mechanophore-contained PHMA network.

The glass transition⁷, or T_g is a key characteristic of amorphous polymer materials or semi-crystalline materials, describing the change of the mobility of the polymer chains -- below T_g the polymer chains are frozen in a glassy state with little mobility while above this temperature, the mobility of the polymer chains increases significantly and the polymer becomes rubbery. T_g is one of the most important properties both in fundamental research on understanding the motion of polymer chains and in practical applications, such as determination of the processing temperature. Around T_g , the mechanical properties change dramatically. Chen's work⁵ demonstrated that in dioxetane-based mechanochemistry, the emission of light in rubbery materials can readily be detected but in glassy materials the signal is weak. In this study, poly(hexyl methacrylate) (PHMA) was selected as the backbone of the network because the glass transition of PHMA is slightly below room temperature, and was determined by DSC as 2.5 °C, within the range of -20 °C to 3 °C from literature values⁸.

The tensile behavior and ultimate mechanical properties are of great importance for the application of polymer materials, and the macroscopic properties are known to highly depend on the strain loading rate, so an understanding of the strain rate dependence of their mechanical properties is a priority before investigating other behavior and applications⁹. The tensile experiments in this work were conducted on

a rheometer equipped with two rotating drums (Figure 2.3) with strain loading rates from 0.001 to 10 s^{-1} . The results are plotted in Figure 2.4. The tensile strength increases from 3.5 MPa to 120 MPa when the strain rate increases from 0.001 s^{-1} to 10 s^{-1} , illustrating that the tensile properties of the PHMA networks are strain rate dependent. In amorphous polymers near T_g , yield stresses are usually observed to be a linear function of $\log(\text{strain rate})$.¹⁰ In this work, the tensile strength has a similar trend with change of strain rate: Figure 2.4 (b) shows two different ranges tensile strength in dependence on strain rate -- the tensile strength displayed a slow increase from 0.001 s^{-1} to 0.1 s^{-1} , while from 0.1 s^{-1} to 10 s^{-1} , the tensile strength increases more strongly, with a transition between 0.1 s^{-1} and 1 s^{-1} . The failure strains, however, for all experiments are in the range of $1.2 - 2.5$.



Figure 2.3. The rheometer used in tensile tests

The strong increase in tensile strength with increasing strain rates is ascribed to the vicinity of the glass transition at $2.5\text{ }^{\circ}\text{C}$, just $20\text{ }^{\circ}\text{C}$ below the temperature of the experiment. It has been reported¹¹ for polyurethanes that its behavior gradually changes from rubbery to leathery to glassy with increasing strain rate, suggesting that physical properties of materials are dependent on strain rate. At lower strain rates, the material is above T_g and behaves as a rubber with a relatively low modulus that is determined by the crosslinking density, while at higher strain rates, chain dynamics in the material are too slow to respond to the strain, and the material behaves more like a glass with a much higher modulus. Strain at break is only weakly dependent on strain rate and varies between $\epsilon_{\text{break}} = 1.2 - 2.5$.

In Figure 2.4 (b), it can be seen that the error bars for the tensile strength are not very large except at a strain rate of 10 s^{-1} , while the error bars for the failure strain are very large except at the intermediate strain rate of 0.1 s^{-1} . The reason for large error bars for the failure strain can be that at low strain rates, defects play an important role, resulting in large error bars for the failure strain, and the microscopic distribution of stresses in the rubbery material is inhomogeneous, leading to overall failure at much lower global stress because the sample fails at a point of stress concentration while, at higher strain rates the poor reproducibility of the data is resulted from that at high strain rate, rupture takes place so quickly that the delay of the computer leads to artifacts in the real-time tensile strength and failure strain measurements although the material is more glass-like, and the crosslinking inhomogeneities play a much smaller role.

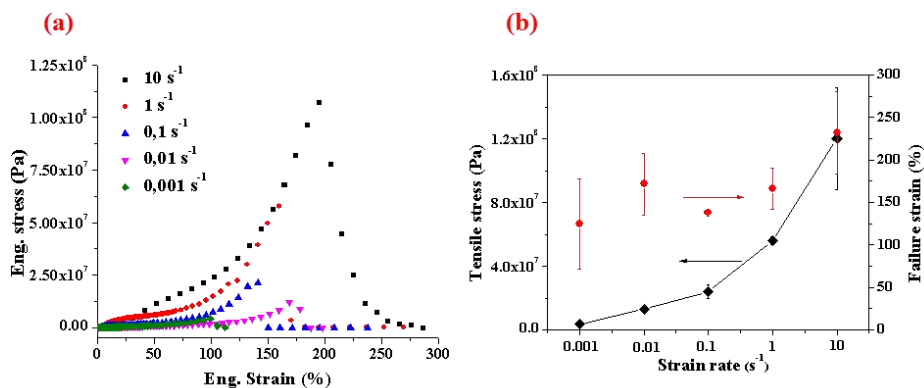


Figure 2.4. (a) Typical stress-strain curves for the tensile experiments with different strain loading rates and (b) the changing trend of the recorded tensile strength and failure strain with changing of strain rates

According to Figure 2.5, it can be seen that the strain energy (here based on the engineering stress and strain, the area till failure under the stress-strain curve) to failure strongly increases from 0.12 to $4.5 \text{ GJ} \cdot \text{m}^{-3}$ over the same range, and the strain energy changes with a similar trend to the tensile strength with increasing strain rate; moreover, upon increasing the strain rate, the modulus changes strongly from 5.81 Mpa to 31.3 Mpa , but its value ($<40 \text{ MPa}$) is still well below the modulus of a glassy polymer (a few GPa , Table 2.1). The change from low strain rate to 1 s^{-1} is dramatic while from 1 s^{-1} to 10 s^{-1} , the modulus slightly increases a bit, which also indicates that at lower strain rates, the network behaves more like rubber while at

higher strain rates, the network behaves more like glass or leather.

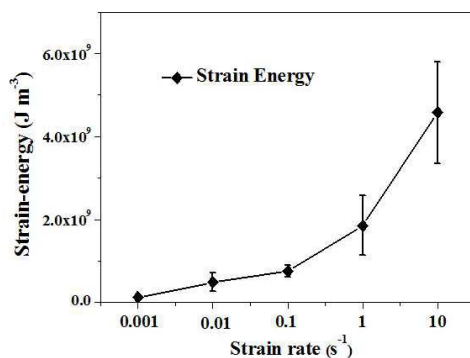


Figure 2.5. The calculated strain-energy density (a) based on the engineering stress and strain with the change of strain rate

Table 2.1 Calculated Young's moduli at different strain rates

Strain rate/s ⁻¹	0.001	0.01	0.1	1	10
E ¹ / MPa	- ²	5.81 ± 4.05	17.9 ± 5.1	29.6 ± 10.9	31.2 ± 6.3 ³

1. E = Young's modulus

2. Not available because no yield point showed in the strain-stress curves.

3. This value is obtained based on several recorded data points due to fast experiments at this high strain rate.

2.2.3 Mechanically induced chemiluminescence of the PHMA network

The incorporation of mechanoresponsive units in polymeric materials provides great opportunities to study how the materials react microscopically to external force in tensile experiments. Previous work on strain-induced dioxetane cleavage in linear acrylate polymers above T_g was carried out by Jakobs¹², and the experiments at different strain rates showed the role of viscoelastic relaxation on amount of bond scission. Research in collaboration with Creton's group¹³ demonstrated that bis(adamantyl)-1,2-dioxetane-based crosslinks can be employed to map bond scission during crack propagation in elastomeric networks. Here, we investigate the effect of strain rate in a PHMA network on overall mechanoluminescence intensity.

Figure 2.6 shows images of mechanically induced chemiluminescence recorded with an Andor iXon Ultra 888 EMCCD camera with a frame rate of 16.8 s^{-1} . In each frame, the camera records light during 19 ms and is inactive during a 40.3 ms ‘dead’ time interval. Figure 2.6 A-D shows second last (A1, B1, C1, and D1) and the last (A2, B2, C2, and D2) frame recorded before the samples failed. The last two frames before failure at strain rates 0.01 and 0.1 s^{-1} only show little light which is strongly localized around the crack, while in the last two images at 1 and 10 s^{-1} , the whole sample emits light. At a strain rate of 0.001 s^{-1} , no light was recorded at all during the entire experiment. The images demonstrate that at relatively low strain rates, bond scission is strongly localized around the final crack while at high strain rates, bond scission is much more homogeneous, and takes place throughout the film. As mentioned above, at lower strain rates, inhomogeneities in the films and defects in the networks play an important role in the failure of materials. The networks are rubbery, and bond scission takes place around defects which are initiation sites for the formation of cracks. At higher strain rates, however, crosslink inhomogeneities have little influence on the initiation of failure, because the material is closer to the glass transition and there is a high barrier to the motion of individual polymer chains or molecular segments. As a result, bonds are broken more homogeneously throughout the sample.

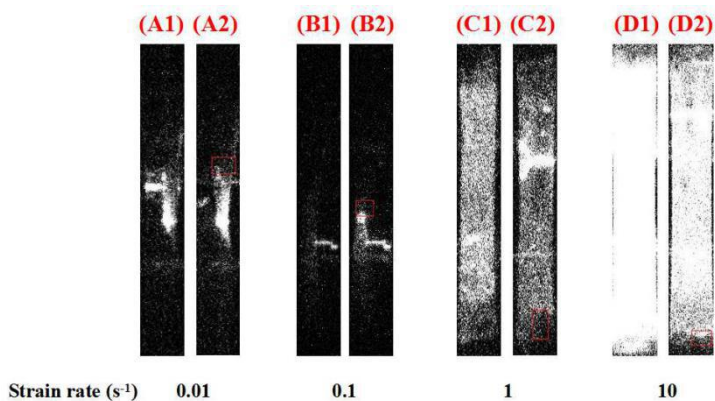


Figure 2.6. Typical full images of mechanically induced chemiluminescence based on bis(adamantyl)-1,2-dioxetane mechanophore before failure during tensile test at different strain rates: A1) second last frame and A2) last frame at strain rate of 0.01 s^{-1} , B1) second last frame and B2) last frame at 0.1 s^{-1} , C1) second last frame and C2) last frame at 1 s^{-1} , D1) second last frame and D2) last frame at 10 s^{-1} .

2.2.4 Quantitative analysis of light emission

Further quantitative analysis was conducted with ImageJ and MATLAB. It has been reported that bias and dark current influence the quality of CCD images significantly.¹⁴ The bias is caused by a constant voltage applied to the CCD detector, and the dark current results from the heat-induced electron motion from CCD itself which is read by CCD when CCD accumulates electrons that will eventually be recorded as light. The effect of the bias and dark current is evident in the frames after time 0 when there is no bond scission yet. Ideally, the artifact from the bias has a constant value and can be subtracted, while artifacts from the dark current can be suppressed almost completely using a professional CCD below -100 °C in a completely dark environment. In the current experiments, the camera was working at -65 °C with exposure time of 19 ms and the environment could not reach completely dark. Therefore artifacts from stray photons were unavoidable, which resulted in an observable gray value of pixels in frames without mechanical activation of the sample. Moreover, there are several other noise sources that affect an EMCCD camera, such as clock-induced noise resulting from spurious electrons created during charge transfers between pixels, and readout noise generated by the readout register.¹⁵ CCD detector artifacts make it more difficult to distinguish isolated activation events from background noise, especially for the smallest events. To remove the artifacts, the raw images were processed using ImageJ and MATLAB and the background was removed by subtracting the mean gray value of the first 50 frames. In Figure 2.7, light intensity vs. recorded frame is plotted along the *x*-axis, and in Figure 2.7 (e) the total amount of light integrated over all frames is plotted as a function of strain rate. The total intensity of generated light varies with strain rate: the highest intensity of total light was obtained with a strain rate of 0.1 s⁻¹, but these experiments also have the highest variation between experiments. No light was recorded at all at a strain rate of 0.001 s⁻¹, so the data is not shown here. As mentioned above, Figure 2.5 shows that the energy to break increases continuously and nonlinearly with strain rate. However, the overall intensity of emitted light (which is proportional to the energy dissipated in bond scission) does not increase monotonously with strain rate, but reaches a maximum at 0.1 s⁻¹, decreases at 1 s⁻¹, and goes up again at the highest strain rate. Although there are not enough data at intermediate strain rates to state with certainty that the intensity at 0.1 s⁻¹ is the actual maximum, the reproducibility of the trend in duplicate experiments strongly suggests that the maximum intensity in this range represents an underlying mechanochemical feature. Because the data in Figure 2.7 are plotted against frame number, the width of the active area - highlighted in yellow - does not reflect the

strain over which light is emitted. Division of the number of active frames by the strain rate indicates that the highlighted regions correspond to delta strain of 0.005, 1.1, 1.3 and 2.3 at strain rates of 0.01, 0.1, 1, and 10 s^{-1} , respectively, suggesting that most of the light was generated in the strain-hardening region. From Figure 2.4(a), it can be seen that in the strain-hardening region, the strength of the material increases with the strain rate. Strong increase strength above 1 s^{-1} suggests that dominant relaxation times in the sample correspond to this rate.

At low strain rates, when the material behaves like a rubber, stresses are distributed over the full length between crosslinkers, and the probability of scission of the weak dioxetane link is maximized at the single chain level, but most of the light is emitted from a small region of the sample, during a short strain interval just before failure. As a result, the total generated light is not much. At high strain rates, when the material has a high modulus like glass or leather, light is emitted from a much larger area, and over a much wider strain interval. However, at the level of the chains, the stress is distributed less effectively and a much lower fraction of dioxetane bonds is broken up to the point of failure, even though the total number of bonds that breaks up to the point of failure is much larger than at low strain rates. Inhomogeneities at the microscopic level dominates the behavior at low strain rates and lead to localisation of stresses, and the material fails at relatively low stress. At high strain rates, the vicinity of the glassy regime homogenizes the material at the microscopic scale and allows straining to much higher stresses. At the intermediate strain rate of 0.1 s^{-1} when the network approaches to its glass transition, the stress is distributed effectively as at high strain rates, and the light is generated over a wide strain interval as at low strain rates, therefore, the total generated light reaches its maximum.

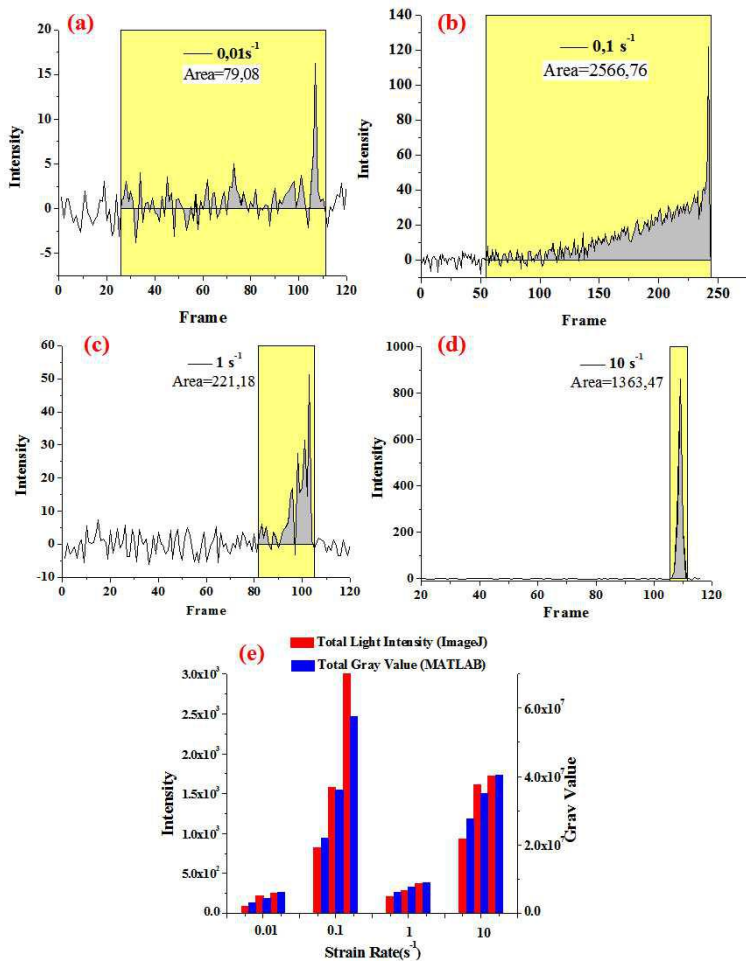


Figure 2.7. Plot of the intensity of generated light along the record frames during tensile tests at different strain rates: a) 0.01, b) 0.1, c) 1, and d) 10 s⁻¹ and e) overall mechanoluminescence light intensity in the tensile experiments as a function of strain rates obtained by ImageJ and MATLAB respectively. Bars indicate individual experiments

2.3 Conclusions

In conclusion, a dioxetane-based mechanoluminescent probe was successfully incorporated in a PHMA network and was investigated successfully with tensile tests at different strain loading rates. The prepared PHMA networks in these experiments have a glass transition temperature which is close to the experimental

temperature, and is strongly strain rate dependent (“dynamic glass transition”)^{11, 16}, that is, T_g shifts with strain rate. The tensile strength and strain energy to failure increase strongly and continuously with strain rate and have a similar trend while the failure strain remains relatively constant in the range of 1.2-2.5.

The dependence of total intensity of emitted light on strain rate behaves neither as the tensile strength nor as the strain energy to failure. At low strain rates, most of the light is generated close to the final crack with a short strain interval before failure, and the intensity of the total generated light is low, while at high strain rates, the light is distributed homogeneously throughout the network film and is generated in a wide strain interval, while the intensity of the total generated light is higher than that at low strain rates; at the intermediate strain rate of 0.1 s^{-1} , however, the total generated light is highest, because at this strain rate, the network film is closer to its glass transition and combines the properties of rubber and glass.

2.4 Experimental

2.4.1 Materials and instrumentation

Unless otherwise specified, reagents and solvents were purchased from Sigma-Aldrich, Merck, or Acros and used without further purification. All reactions were performed under Argon atmosphere unless otherwise specified, and all glassware was oven dried before use. Thin layer chromatography (TLC) was conducted on silica gel 60 F₂₅₄ (Merck, 0.2 mm). Column chromatography was carried out on silica gel, basic alumina, or neutral alumina (0.063-0.2 mm). Deuterated solvents were obtained from Cambridge Isotopes Laboratories.

¹H NMR (400 MHz) and ¹³C NMR (100 MHz) spectra were recorded on a 400 MHz (100 MHz for ¹³C) Varian Mercury VX spectrometer at room temperature using residual protonated solvent signals as internal standards (¹H: $\delta(\text{CDCl}_3) = 7.26 \text{ ppm}$, $\delta(\text{CD}_2\text{Cl}_2) = 5.32 \text{ ppm}$, $\delta((\text{CD}_3)_2\text{SO}) = 2.50 \text{ ppm}$; ¹³C: $\delta(\text{CDCl}_3) = 77.16 \text{ ppm}$, $\delta(\text{CD}_2\text{Cl}_2) = 53.84 \text{ ppm}$, $\delta((\text{CD}_3)_2\text{SO}) = 39.52 \text{ ppm}$).

Matrix assisted laser desorption/ionisation time-of-flight mass spectrometry (MALDI-TOF MS) was performed on a Autoflex Speed MALDI-MS instrument (Bruker, Bremen, Germany) equipped with a 355 nm Nd:YAG smartbeam laser. MALDI-TOF MS experiments were performed by spotting samples on a MTP 384 target ground steel plate using an α -cyano-4-hydroxycinnamic acid (CHCA) (Fluka, Switzerland) matrix. Samples were 1:1 premixed with CHCA in 50/50

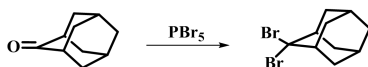
acetonitrile/water supplemented with 0.1% v/v trifluoroacetic acid (TFA). Mass spectra were acquired in reflector positive ion mode by summing spectra from 500 selected laser shots. The MS spectra were calibrated with cesium triiodide of known masses.

2.4.2 Mechanical testing

The sample of crosslinked polymers for tensile tests was prepared by cutting, using a blade, the as-synthesized film into a rectangular shape (5 mm × 25 mm) of thickness *ca.* 0.5 mm. Tensile experiments were performed on a rheometer equipped with two rotating drums. Samples were clamped tightly between the two drums and strained at different rotating rates. A camera was fixed in front of the two drums, in the dark, to record the deformation process.

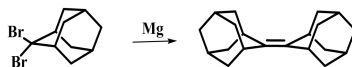
2.4.3 Synthesis

2,2-Dibromoadamantane



Finely divided phosphorus pentabromide was prepared by slowly adding 30 g phosphorus tribromide to a cold, vigorously stirred solution of 17 g bromine in 75 ml n-heptane in a 250-ml round-bottomed flask, with a dropping funnel. When addition was complete (*ca.* 15 min.) 15 g adamantanone was added to the suspension of phosphorus pentabromide in n-heptane and was refluxed for 1.5 h. The cooled mixture was poured into 100 ml ice water, The organic layer was separated and washed twice with 75-ml portions of dilute sodium bisulfite and with water. The organic layer was dried over anhydrous magnesium sulfate and evaporated under reduced pressure. The residue 2,2-dibromoadamantane was crystallized from ethanol to afford colorless needles. (22.65 g, yield : 77%)

Adamantylideneadamantane



The reaction was carried out under anhydrous conditions and the reaction equipment was dried in a drying oven. In a 500-ml round bottomed flask, fitted with

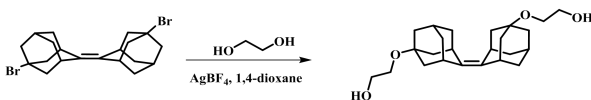
a reflux condenser, dropping funnel. 4 g of activated magnesium ribbons and 25 ml of anhydrous ether. To this suspension was added dropwise a solution of 10 g 2,2-dibromoadamantane in 75 ml anhydrous ether. A small crystal of iodine was added. After addition of ca. 1 g of 2,2-dibromoadamantane, the reaction started, and the remainder of 2,2-dibromoadamantane was added at such a rate that gentle reflux was maintained. The reaction mixture was heated under reflux for 1 hr. Then it was cooled and poured into 100 ml water. The aqueous layer was separated and extracted twice with 50-ml portions of ether. The combined ether layers were washed with 100 ml water and dried over anhydrous magnesium sulfate. After evaporation of the ether under reduced pressure, the adamantylideneadamantane was washed with methanol and allowed to dry. (4.2 g, 91%)

Dibromoadamantylideneadamantane



To a solution of 3.8 g of adamantylideneadamantane and 1.83 ml of tert-butylbromide was added 18.13 g of AlBr_3 . After good mixture 4.35 ml of bromine were added, which gave rise to the evolution of enormous amounts of HBr gas. After 2 days of standing at room temperature, the reaction mixture was poured into ice water and extracted with DCM in a very inconvenient separation (DCM: 1×300 ml, 1×150 ml; H_2O : 2×150 ml). The organic layer was washed with water, dried over MgSO_4 , and evaporated, furnishing a brown-black solid. The solid was washed with warm ethanol (3×150 ml), followed by column chromatography (DCM, neutral Al_2O_3) yielded brown solid (4.1 g, 68%).

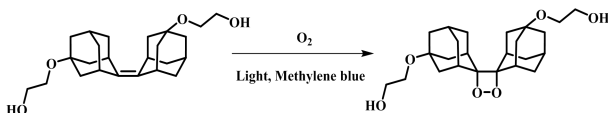
5,5'/7'-Di(2-hydroxyethyloxy) adamantylideneadamantane



To a solution of 5,5'/7'-dibromoadamantylideneadamantane (1.0 g, 2.35 mmol) in 1,4-dioxane (10 ml) was added ethylene glycol (56 mL, 1 mol). The flask was brought under an Ar atmosphere. After the addition of AgBF_4 (2.0 g, 10.27 mmol), the reaction mixture was heated at 85°C for 3 h. Diethyl ether (150 mL) was added

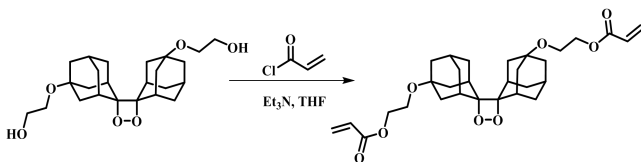
and the mixture was washed with water (2×200 mL). The organic layer was separated, dried over anhydrous Mg₂SO₄, and evaporated to dryness. The crude product was purified by silica gel chromatography eluting with CHCl₃ followed by CHCl₃/MeOH (20/1) to afford 5,5'/7'-di(2-hydroxyethylenoxy) adamantylideneadamantane as a brown solid (0.47 g, 52%). ¹H NMR (CDCl₃, 400 MHz): δ 3.68 (m, 4H), 3.51 (m, 4H), 3.11 (br, 4H), 2.23-1.57 (m, 24H). ¹³C NMR (CDCl₃, 100 MHz): δ 132.21 132.19, 72.38, 72.30, 62.29, 61.12, 42.74, 42.68, 41.18, 41.12, 38.38, 38.34, 33.41, 33.40, 30.82, 30.78. MALDI-TOF (m/z): [M⁺] C₂₄H₃₆O₄ calculated 388.54; found 388.34.

5,5'/7'-Di(2-hydroxyethylenoxy) adamantylideneadamantane 1,2-dioxetane



To a solution of 5,5'/7'-di(2-hydroxyethylenoxy) adamantylideneadamantane (0.3 g, 0.77 mmol) in CH₂Cl₂ (60 mL) was added methylene blue (30 mg). Oxygen was bubbled through the mixture while irradiating with a 600 Watt high pressure sodium lamp. After 4 h, the reaction was complete according to ¹H NMR and the methylene blue was removed with active carbon, followed by filtration. The CH₂Cl₂ was evaporated under reduced pressure to afford 5,5'/7'-di(2-hydroxyethylenoxy) adamantylideneadamantane 1,2-dioxetane as a slight yellow solid (0.29 g, 90%). ¹H NMR (CDCl₃, 400 MHz): δ 3.67 (m, 4H), 3.51 (m, 4H), 2.84 (br, 4H), 2.20-1.44 (m, 24H). ¹³C NMR (CDCl₃, 100 MHz): δ 94.58, 93.93, 72.31, 71.37, 70.75, 62.26, 62.19, 62.14, 61.50, 61.30, 61.18, 46.78, 41.53, 41.25, 41.21, 40.98, 38.50, 38.38, 36.19, 34.06, 34.01, 33.90, 33.76, 33.65, 33.50, 31.62, 29.46, 28.76, 28.57, 28.51. MALDI-TOF (m/z): [M⁺] C₂₄H₃₆O₆ calculated 420.54; found [M+2O] 388.14.

5,5'/7'-bisacrylate-5,5'/7'-dihydroxyethylenoxy-adamantylideneadamantane 1,2-dioxetane



To a solution of 5,5'/7,7'-di(2-hydroxyethylenoxy) adamantylideneadamantane 1,2-dioxetane (0.4 g, 0.95 mmol) and triethylamine (1.5 mL) in dry THF (18 mL) was added dropwise a dry THF solution (20 mL) of acryloyl chloride (0.157 ml, 1.94 mmol) at 0 °C. After stirring at room temperature for 24 h, the solution was poured into water (50 mL) and extracted with diethyl ether (2×30 mL). The combined organic layer was washed with water (50 mL), dried over anhydrous Na₂SO₄ and evaporated under reduced pressure. Crude product was purified by flash chromatography on neutral alumina eluting with CH₂Cl₂ to afford the bisacrylate (0.30 g, 60 %) as a slight yellow oil. ¹H NMR (CDCl₃, 400 MHz): δ 6.41 (m, 2H), 6.14 (m, 2H), 5.83 (m, 2H), 4.25 (m, 4H), 3.63 (m, 4H), 2.83-1.25 (m, 26H). ¹³C NMR (CDCl₃, 100 MHz): δ 166.20, 166.15, 130.99, 130.89, 130.84, 130.79, 128.39, 128.34, 128.29, 94.29, 94.26, 93.93, 72.30, 71.71, 71.60, 71.21, 70.99, 64.40, 64.32, 64.21, 64.13, 59.11, 58.72, 58.55, 58.46, 46.79, 41.55, 41.41, 41.27, 41.14, 41.09, 40.85, 40.47, 40.29, 38.45, 38.37, 38.33, 36.21, 36.16, 36.02, 34.07, 34.02, 33.90, 33.77, 33.65, 33.59, 33.49, 33.39, 31.60, 30.32, 29.57, 29.47, 28.77, 28.71, 28.52.

Preparation of PHMA network

In a glass vial, approximately 10 mg of AIBN, 61 mg of tetraethylene glycol dimethacrylate, 25 mg of 5,5'/7,7'-bisacrylate-5,5'/7,7'-dihydroxyethylenoxy-adamantylideneadamantane 1,2-dioxetane, and 1 mL of hexyl methacrylate saturated with diphenylanthracene (DPA) were homogeneously mixed with each other. The resulting solution was transferred into a Teflon mold (25 mm×45 mm×5 mm), covered with a glass plate, and put in an oven under N₂ atmosphere for 1 hr, and then was heated up to 60 °C, kept for 24 h. The obtained polymer films were taken out and cut into rectangles of 5 mm×25 mm with a cutting blade. The average film thickness was 0.5 mm.

References

- 1 a) P. G. Gillespie, U. Müller, *Cell* **2009**, 139: 33–44; b) D. E. Ingber, *Circ. Res.* **2002**, 91: 877–887; c) S. H. D. Haddock, M. A. Moline, J. F. Case, *Annu. Rev. Mar. Sci.* **2010**, 2: 443–493;
- 2 a) S. L. James, C. J., Adams, C. Bolm, et. al., *Chem. Soc. Rev.* **2012**, 41, 413; b) M. K. Beyer, H. Clausen-Schaumann, *Chem. Rev.* **2005**, 105(8), 2921; c) H. Decker and T. Fellenberg, *Liebigs Ann. Chem.*, **1909**, 364 (1): 1-44;
- 3 a) C. E. Diesendruck, B. D. Steinberg, N. Sugai, M. N. Silberstein, N. R. Sottos, S. R. White, P. V. Braun, and J. S. Moore, *J. Am. Chem. Soc.*, **2012**, 134 (30): 12446–12449; b) C.K. Lee, D.A. Davis, S.R. White, J.S. Moore, N.R. Sottos, P.V. Braun, *J. Am. Chem. Soc.* 2010, 132: 16107–16111; c) C. M. Kingsbury, P. A. May, D. A. Douglas, S. R. White, J. S. Moore, and N. R. Sottos, *J. Mater. Chem.*, **2011**, 21: 8381-8388; d) B. A. Beiermann, D. A. Davis, S. L. B. Kramer, J. S. Moore, N. R. Sottos, S. R. White, *J. Mater. Chem.*, **2011**, 21: 8443-8447; e) B. A. Beiermann, S. L. B. Kramer, J. S. Moore, S. R. White, N. R. Sottos, *ACS Macro Lett.* **2012**, 1: 163-166; f) A.-D. N. Celestine, B. A. Beiermann, P. A. May, J. S. Moore, N. R. Sottos, S. R. White, *Polymer*, **2014**, 55: 4164-4171;
- 4 a) J. M. Lenhardt, A. L. Black, and S. L. Craig, *J. Am. Chem. Soc.* **2009**, 131: 10818–10819; b) D. Wu, J. M. Lenhardt, A. L. Black, B. B. Akhremitchev, and S. L. Craig, *J. Am. Chem. Soc.* **2010**, 132: 15936–15938; c) H. M. Klukovich, T. B. Kouznetsova, Z. S. Kean, J. M. Lenhardt and S. L. Craig, *Nat. Chem.* **2013**, 5: 110-114; d) J. Wang, M. T. Ong, T. B. Kouznetsova, J. M. Lenhardt, T. J. Martínez, S. L. Craig, *J. Org. Chem.* **2015**, 80: 11773–11778; e) A. L. Black Ramirez, J. W. Ogle, A. L. Schmitt, J. M. Lenhardt, M. P. Cashion, M. K. Mahanthappa, and S. L. Craig, *ACS Macro Lett.* **2012**, 1: 23–27;
- 5 Y. Chen, A. J. H. Spiering, S. Karthikeyan, G. W. M. Peters, E. W. Meijer, and R. P. Sijbesma, *Nat. Chem.* **2012**: 559-562;
- 6 a) E. Ducrot, Y. Chen, M. Bulters, R. P. Sijbesma, C. Creton, *Science*, **2014**, 344(6180): 186-189; b) Y. Chen and R. P. Sijbesma, *Macromolecules* **2014**, 47: 3797–3805; c) J. M. Clough, J. van der Gucht, and R. P. Sijbesma, *Macromolecules* **2017**, 50(5): 2043–2053; d) J.M. Clough, C. Creton, S. L. Craig, and R.P. Sijbesma, *Adv. Funct. Mater.* **2016**, 26: 9063–9074; e) J. M. Clough, R. P. Sijbesma, *Chem. Phys. Chem.* **2014**, 15, 3565-3571
- 7 S. Ebnesajjad, **2016**, *Chemical Resistance of Commodity Thermoplastics: Introduction to plastics*, xiii–xxv.
- 8 a) W. C. Child, Jr. and J. D. Ferry, *J. Colloid Sci.*, **1957**, 19: 389-399; b) Y. Hwang G. D. Patterson J. R. Stevens, *J. Polym. Sci. B: Polym. Phys.*, **1996**, 34: 2291-2305; c) S. Kahle, E. Hempel, M. Beiner, R. Unger, K. Schroter, E. Donth, *J. Mol. Struct.* **1999**, 479:149–162; d) F. Garwe, A. SchoInhals, H. Lockwenz, M. Beiner, K. SchroIter, and E. Donth, *Macromolecules* **1996**, 29, 247-253; e) E. Donth, M. Beiner, S. Reissig, J. Korus, F. Garwe, S. Vieweg, S. Kahle, E. Hempel, and K. Schroter, *Macromolecules* **1996**, 29, 6589-6600
- 9 R. Gensler, C.J.G. Plummer, C. Grein, H.-H. Kausch, *Polymer*, **2000**, 41 (10): 3809–3819.
- 10 C. P. Buckley, and D. C. Jones, *Polymer*, **1995**, 36(17): 3301-3312; Eyring H. *J Chem Phys* 1936,4:283.
- 11 S. S. Sarva, S. Deschanel, M. C. Boyce, W. Chen, *Polymer*, **2007**, 48, 2208-2213
- 12 Bob Jakobs: *Catalysis and Luminescence in Mechanically Activated Polymer*, **2013**, PhD thesis
- 13 E. Ducrot, Y. Chen, M. J. H., Bulters, R. P. Sijbesma, C. Creton, *Science*, **2014**, 344: 186-189.
- 14 G. McMullan, S. Chen, R. Henderson, A.R. Faruqi, *Ultramicroscopy* **2009**, 109:1126–1143
- 15 M.P. Edgar, D.S. Tasca, F. Izdebski, R.E. Warburton, J. Leach, M. Agnew, G.S. Buller, R.W. Boyd & M.J. Padgett, *Nat Commun.* **2012**, 3: 984.

16 R. B. Bogoslovov, C. M. Roland, R. M. Gamache, *Appl. Phys. Lett.*, **2007**, *90*, 221910.

Chapter III

Optical sensing of covalent bond scission for the observation of mechanical damage in a PNIPAm hydrogel network

ABSTRACT

The fluorescent anthracene generated by mechanically induced activation of a retro Diels-Alder reaction in a PNIPAm hydrogel network maps the deformation of the material, demonstrating that the compressive deformation was strongly localized close to the center of the sample. The loss of most of the fluorescence by adding a solvent with matching refractive index suggested that mechanically induced dissociation mainly took place at the surface of the material.

3.1 Introduction

“Smart” or “intelligent” materials are designed to have one or more properties that can be significantly changed in a controlled fashion by external stimuli, such as stress, temperature, pH, electric or magnetic fields. Since 1992, when Kasiviswanathan and co-workers¹ gave this definition of “smart”/“intelligent” materials, a wealth of such materials has been developed and used in different areas. Two books from Li *et al.*² and Urban *et al.*³ reviewed intelligent materials and their applications in 2013 and 2016, respectively. In recent years, intelligent systems that report mechanical strain or failure have garnered much interest in the field of smart materials. Incorporation of mechanophores⁴ into the polymer backbone is the most common and straightforward approach for the implementation of this function for a response upon exposure to external mechanical force. Activated by external force, the mechanophore will undergo a chemical reaction—defined as the mechanochemical reaction—and give feedback by changing its physicochemical properties.⁵ The possibility to observe bond-scission or -reconfiguration at the molecular level is an exciting challenge that could lead to fundamental insights into the interplay between the microscopic and macroscopic properties of (bio)materials,⁶ giving a detailed view of damage mechanisms. One of the simplest modes of detection is the change in optical properties, as this method is not only non-invasive and spatiotemporally well resolved but in principle also detectable with the naked eye. Spiropyran, introduced as a mechanophore by Moore’s group⁷, has widely been employed as mechanochromic probe, while the 1,2-dioxetane-based mechanophore from Sijbesma’s group⁸ was established as a highly sensitive chemoluminescent probe to detect the failure of the bulk materials (Figure 3.1). The collaborative work of Sijbesma’s group and Creton’s group⁹ demonstrates that a bis(adamantyl)-1,2-dioxetane-based network can well be employed to map the bonds breaking during crack propagation. The application of the bis(adamantyl)-1,2-dioxetane-based mechanophore in mapping the breaking bonds has also allowed us to study separate scission events in PMMA during solvent swelling. Other mechanochromic moieties have also been successfully activated in polymers, including azobenzene¹⁰, diaryl-bibenzofuranone¹¹ and the coumarin dimer¹². Furthermore, the reorientation of chromophores in polymer blends has been exploited to modulate the absorption spectra of materials.¹³ Mechanically induced formation of anthracene as fluorophore is of interest for the time independent detection of material failure, because its fluorescence quantum yield ($\phi=0.27$) is much higher than that of the widely used merocyanine ($\phi<0.02$) generated

mechanically from spiropyran. Several groups¹⁴ have studied the mechanically induced retro Diels—Alder (DA) reaction releasing anthracene as fluorophore, suggesting potential for practical applications.

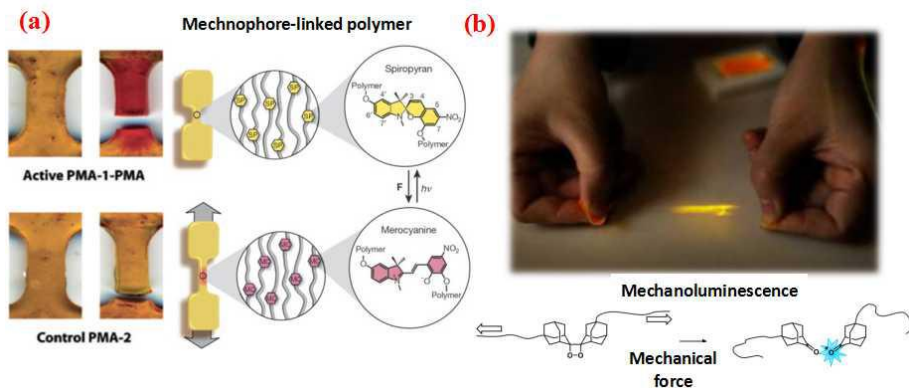


Figure 3.1. Probes for the detection of failure of materials: a) spiropyran as mechanochromic probe and b) 1,2-dioxetane-based mechanophore as chemoluminescent probe

Synthetic biocompatible hydrogels attract much interest because they can be used in a wide range of applications and their properties can be easily engineered; their mechanical properties, however, are dependent not only on the structure of the parent polymers but also on the degree of swelling. Therefore, it is highly desirable to get insight into their macroscopic mechanical properties through the application of molecular level probes. Recently, the work from Moore's group¹⁵ showed that when the mechanophore is incorporated into either the glassy or the rubbery blocks of a polyurethane network, the reaction to the external force depends on the mechanophore's relative orientation with regard to the force vector in uniaxial extension experiments, providing a direction for the investigation of the macroscopic mechanical properties with mechanochemistry.

Previous work¹⁶ has demonstrated that the mechanically induced retro DA reaction of a 9,10- π -extended anthracene and maleimide results in enhanced fluorescence in solution via sonication as well as in the solid state and the spectroscopic and mechanochemical details of the mechanochemical process were unraveled. Under compression, the Diels-Alder adduct-based mechanophore can undergo scission and produce a fluorescent anthracene (Figure 3.2). These satisfying results led us to use this mechanophore to study bond scission in a hydrogel network of crosslinked

poly(*N*-isopropyl acrylamide) (PNIPAm). PNIPAm is interesting in biomaterial hydrogel applications because the mechanical properties can be tuned by swelling with water, and because the gels undergo a reversible Lower Critical Solution Temperature (LCST) transition around 32 °C¹⁷ from a swollen to a dehydrated state. In this work, the sensitive π -extended anthracene mechanophore was incorporated as a crosslinker into gels of PNIPAm networks, with the aim to study the feasibility of using this probe in establishing damage upon compression at different degrees of swelling.

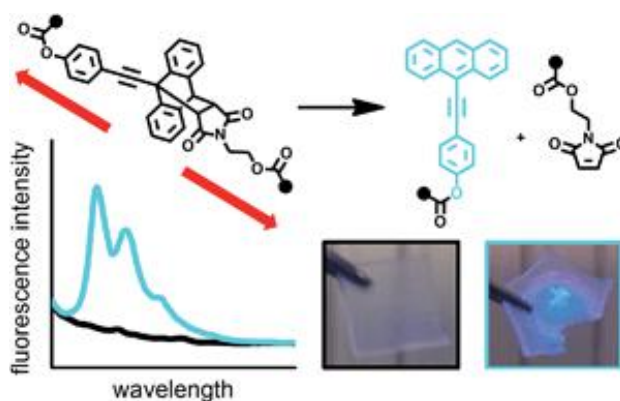


Figure 3.2. The mechanochemistry of the Diels-Alder adduct from a 9,10- π -extended anthracene and maleimide

3.2 Results and Discussion

3.2.1 Synthesis

This study is based on PNIPAM networks containing a π -extended anthracene mechanophore as crosslinker and was initiated by R. Göstl.¹⁸ The bismethacrylate-functionalized Diels-Alder adduct-based mechanophore motif was prepared according to previous work¹⁸ (Scheme 3.1). The synthesis of the mechanophore - a bismethacrylate-functionalized Diels-Alder adduct - started with the Pd-catalyzed Sonogashira-type cross-coupling of TMS-acetylene to commercial 9-bromoanthracene yielding ethynylated derivative (An-TMS) in moderate yields of 38%; subsequently, a Diels-Alder reaction between An-TMS with *N*-(2-hydroxyethyl)maleimide (NHEM)--prepared according to procedure by Haddleton and coworkers¹⁹ -- gave 9,10-adduct (HO-AD-TMS) in quantitative yield. The deprotected product, HO-AD-H, from HO-AD-TMS is coupled with

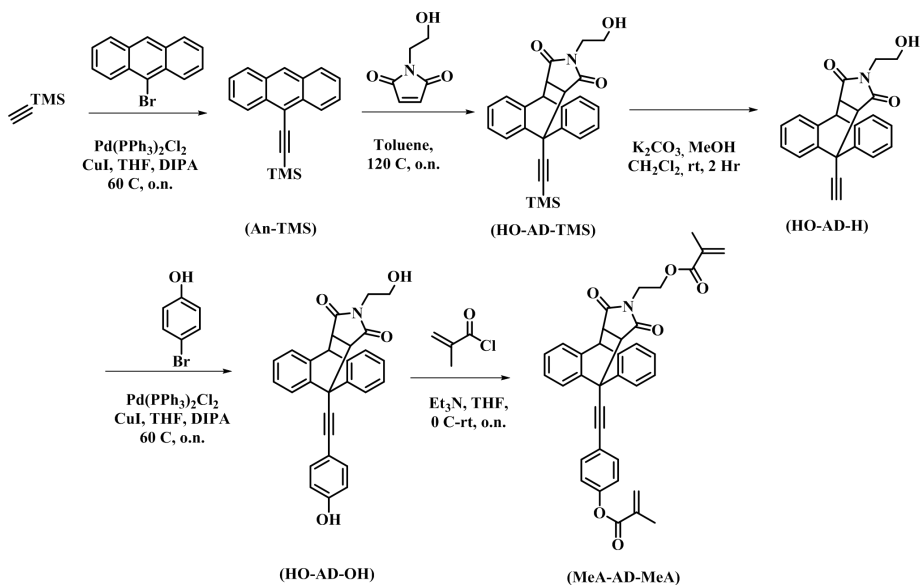
4-bromophenol using a Pd-catalyst to yield a dialcohol, HO-AD-OH. This precursor was further esterified with methacryloyl chloride to give bismethacrylate crosslinker MeA-AD-MeA for further use. The network was obtained by polymerization of *N*-Isopropylacrylamide (NIPAm) with azobisisobutyronitrile (AIBN) as thermoinitiator and the bismethacrylate-functionalized Diels–Alder adduct as crosslinker at 65 °C under N₂ atmosphere for 24 h. The overall crosslink content was 2 mol%, and the mechanophore crosslinker constituted 1% of the total amount of crosslinker; therefore, the overall mechanophore content of the material was 0.02 mol% relative to NIPAm monomer units, highlighting the sensitivity of the employed optical force probe. With different swelling degrees, the network was utilized in the compression experiments. The swelling degree was defined by **Eq. 3.1**.

$$d_s = 100 \cdot \frac{m_{sw} - m_d}{m_d} \quad \text{Eq. 3.1}$$

where d_s is the swelling degree, m_{sw} is the mass of the sample after swollen, m_d is the initial mass of the sample.

3.2.2 Mechanical properties in uniaxial compression determined by micro indentation

The mechanical properties of differently swollen PNIPAm cross-linked networks were determined by uniaxial compression with a micro indenter. Millimeter-sized cylinders of 2% cross-linked PNIPAm network were prepared by thermally initiated polymerization at 65 °C for 24 h in a Teflon mold under N₂ atmosphere. The samples for mechanical testing were polymerized without mechanophore crosslinker. As the optical probe constitutes less than 1 mol% of the overall amount of crosslinker, it can be assumed that the mechanical properties of these networks are virtually identical. The cylinders were cut with a blade into pieces of around 3 mm in height, and then swollen with water to different swelling degrees. The swollen PNIPAm cylinders were compressed with a CSM micro indenter with a maximum applicable load of 10 N using a flat punch indenter of 6 mm in diameter, under constant displacement control. Temperature was controlled with a Peltier device sample stage for experiments at 4 °C.



Scheme 3.1. Synthetic procedure of bismethacrylate-functionalized Diels–Alder adduct-based mechanophore

A homogeneous deformation was applied in the compression experiments in order to obtain a stress-strain curve that displays the intrinsic deformation response even at high deformations. Measurements yielded displacement Δh and force F as parameters which were transformed to compressive strain ε and compressive engineering stress σ_n according to $\varepsilon = \frac{\Delta h}{h_0}$ and $\sigma_n = \frac{F}{A_0}$ where h_0 is the initial

height of the cylinder and A_0 the initial area of the cylinder top contact surface. The elastic modulus E was determined by fitting of the linear region of the loading curve for the non-linear onset of the loading curve is attributed to uneven cylinder height as in this region full contact with the sample surface is established while sudden deviations of the linear loading curve during the experiments are attributed to material failure which was confirmed by optical microscopy after the experiment. Figure 3.3 (a) and (b) show the typical strain-stress curves of the swollen samples with a swelling degree of 20% at 20 °C and 4 °C, respectively, and Figure 3.3 (c) shows the elastic modulus as a function of the swelling degree. As can be seen, the elastic modulus decreases with increasing swelling degree. The reason for the decrease of the elastic modulus is that a) the uptake of water decreases the crosslinking density, and b) water absorption results in the decrease of the glass transition temperature by plasticizing the material and by destroying the secondary

hydrogen bonding.²⁰ Moreover, it has been shown that restricting the magnitude of swelling in other acrylate hydrogels results in improved strain to failure values when compared to their de-swollen or highly swollen counterparts.²¹

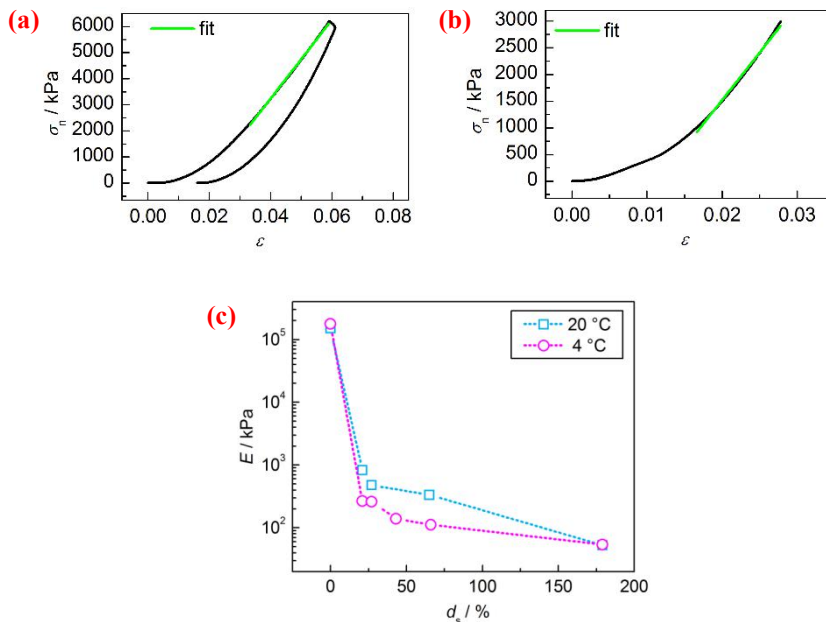


Figure 3.3. Typical stress-strain curves of swollen samples of 2% crosslinked PNIPAm millimeter-sized cylinders without swelling determined at a) 20 °C and b) 4 °C including the linear fit of the elastic region of the loading curve, and c) swelling degree dependence of elastic modulus of differently swollen samples of 2% crosslinked PNIPAm millimeter-sized cylinders at 20 °C and 4 °C as determined by uniaxial compression.

3.2.3 Mechanically induced fluorescence

A PNIPAm network film of *ca.* 2 mm thick, with 0.02 % bismethacrylate crosslinker MeA-AD-MeA as the co-crosslinker was prepared by thermally initiated copolymerization in a Teflon mold at 65 °C under N₂ atmosphere. Prior to compression experiments, samples of approximately 5 mm×5 mm were prepared by cutting with a blade, swollen to targeted swelling degrees between 0 % and 179 % (the equilibrium swelling degree), and stored at either 4 °C or 20 °C for at least 12 h for further testing. Then a force of *ca.* 10⁵ N was applied to the samples using a pellet press for 15 seconds, during which the samples were compressed from a thickness of 2 mm to a final thickness of *ca.* 0.7 mm, and the lateral dimensions

increased to a final diameter of 7 mm although the thickness varied from sample to sample because of the variation in mass. It was difficult to obtain samples with identical dimensions by cutting with a blade for the network is a stiff glass. At swelling degrees higher than 40%, the swollen samples became so brittle that upon compression, they broke into small pieces or even powder. After compression, the samples were collected for fluorescence measurements.

The applied stress changed the samples from transparent to opaque. In general, opacity is caused by inhomogeneities in the refractive index in a sample. When stress is applied to a polymer material, the stress can be released by the polymer chains aligning, resulting in increase of the local density. The difference in density will cause a difference in light reflection and scattering. Furthermore, within the stressed area, the stress can also be relieved through the formation of micro-cracks which can also result in different light reflection and scattering properties. The combination of these effects results in the opacification of the samples.

Location of activation

Bond-scission of the Diels-Alder adduct can conveniently be observed by illumination of the compressed samples with a UV lamp at $\lambda_{\text{exc}} = 365 \text{ nm}$. Non-fragmented samples showed concentrated luminescence in the center of the sample and fading along the radius while the powdered samples were much less luminescent or even non-luminescent (Fig. 3.4).

Since the chemiluminescence of the generated anthracene maps the mechanical activation, the effect that more activation takes place closer to the center of the sample demonstrates that mechanically induced activation under compression is strongly concentrated at the center of the sample.

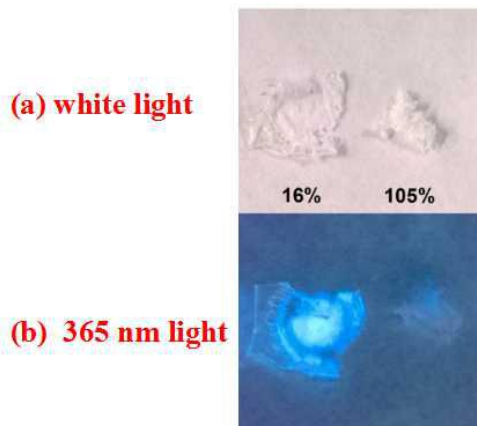


Figure 3.4. Typical images of PNIPAm network samples at two different degrees of swelling compressed at 20 °C exposed to a) white light and b) 365 nm light.

It is reported²² that in a compression experiment, the deformation and failure of a glassy polymer undergoes a cascade of changes from molecular level to macroscale level: at molecular level, the entangled chain segments undergo the rearrangement, slippage, orientation, disentanglement and scission; at a mesoscale level, the crazes are initiated and grow until the breakdown of craze fibrils, and the microcracks start to propagate; at a macroscopic level, the gross failure is induced by microcrack cascades and macrocrack propagations, and the compressive deformation often manifests itself via development of shear bands at the yield point, and it has been observed that in shear bands the deformation is usually localized²⁵. The initiation of shear bands can be well accounted for on the basis of the phenomenological theory of Bowden in which, localisation of shear strain is viewed as an inevitable consequence of the strain softening that is characteristic of yield in glassy polymers.²³ Whenever strain softening occurs, the plastic shear deformation is fundamentally unstable to small perturbations of strain rate produced by surface stress concentrations, particulate inclusions, and ultimately, constitutional heterogeneities, *etc.* Thus, the deformation which starts out will more or less rapidly localize by concentration of the shear deformation inside shear bands, requiring less and less deformation outside the bands.²⁴ Moreover, for brittle materials, the cracking mode is significantly influenced by the contact with the platens (namely the geometry), the size of the specimen on compression tests, and the lateral pressure.²⁵ Because the specimens for compression were much smaller than the indenter, at the beginning of the compression, it can be inferred that the plastic yielding dominated

the deformation, and when the specimens extended to the wall of the pellet press machine, a lateral pressure along the radius of the indenter was received from the wall, resulting in plastic deformation near the edge of the specimen. When Higo and co-workers²⁶ studied the microstructural changes in partially saturated soil during deformation using microfocus X-ray CT, the strain localisation was observed with a similar pattern to as observed with fluorescence in our compression tests. A similar pattern was also observed in compression tests with different materials, and finite element simulations have also shown stress concentration in the center of the specimen.²⁷ When spherical specimens of PMMA were employed by Moore's group²⁸ a similar pattern was observed under compression, showing that the maximum stress develops in the center of the bead and decreases along the radius. Therefore, the localisation of mechanically induced activation is in line with the localisation of compressive deformation within shear bands, a result of the strain softening effect during compression tests.

Quantitation of fluorescence.

To study the mechanically induced activation of bond-scission of the Diels-Alder adduct in PNIPAm network film quantitatively, solid state fluorescence spectroscopy was employed. Figure 3.5 shows fluorescence spectra of the network films activated by compression in the dry state at room temperature (20 °C) and 4 °C, respectively. For each measurement, three points within the most luminescent area (the activation area) of two samples were selected. The results shown in Figure 3.5 are the averages of the six measurements. From Figure 3.5(a), it can be seen that the film is non-fluorescent before compression, while after compression it is strongly fluorescent, suggesting that fluorescent product was generated. Since the fluorescence was not distributed homogeneously in the compressed samples, the measured intensity of the fluorescence has a large error. In line with previous work on the mechanochemistry of the Diels-Alder adduct by Göstl¹⁷ using sonication, the generated fluorescent spectrum matches that of anthracene from a retro Diels-Alder reaction. Therefore it can be concluded that compression activates the retro DA reaction to produce fluorescent anthracene.

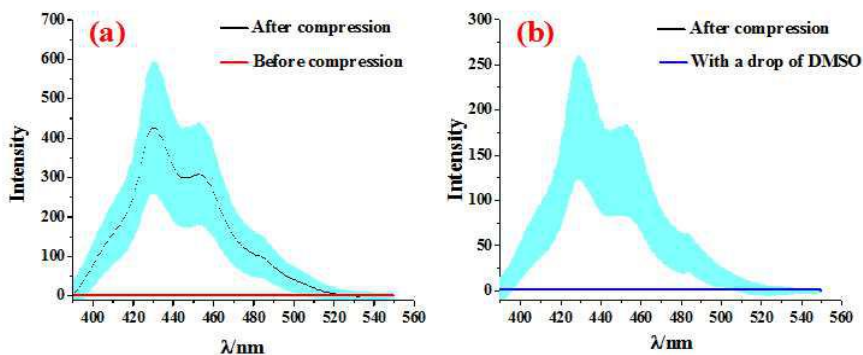


Figure 3.5. Baseline corrected solid state fluorescence spectra of unswollen PNIPAm network compressed to failure with a pellet press at a) 20 °C and b) 4 °C.

Figure 3.5(b) illustrates the fluorescence of the PNIPAm network film compressed in the dry state at 4 °C. Compared with the result of compression at 20 °C, the intensity of the fluorescence decreases slightly. Generally, low temperatures promote brittle fracture,²⁹ and the strain-softening effect becomes weaker. We propose that this effect results in a lower efficiency of mechanoactivation at 4 °C.

In an attempt to assess the fluorescence quantitatively, scattering of the opaque dried samples was suppressed by adding a small amount of DMSO with a refractive index close to that of the network (1.479 for DMSO and 1.47 for PNIPAm¹⁷). By doing this, a transparent sample was obtained. The clear DMSO treated samples no longer showed fluorescence (Figure 3.5(b)). Since the anthracene unit is not quenched by the DMSO,³⁰ the reduction in fluorescence must be related to decreased scattering.

This conclusion was corroborated by experiments in which a compressed sample was swollen with water, a solvent in which the sample scatters light. Dry PNIPAm network was compressed to give a fluorescent material (Fig 3.6a), and subsequently swollen to equilibrium ($d_s = 179\%$). The fluorescence signal became smaller upon swelling, but the decrease in intensity was approximately equal to the increase of volume due to swelling, confirming that after compression the relative optical dilution and a possibly altered fluorescence quantum yield in water are only minor contributions to the observed trend.

In order to rationalize the complete loss of fluorescence in the films upon addition of DMSO, it is proposed that in the compression experiments, nearly all activation is

confined near the surface of the sample, and that the scattering enhances the fluorescence from anthracene units near the surface. Upon addition of DMSO, the enhancement is lost, and the fluorescence intensity is determined by the average concentration of fluorophores.

From Beer's law, in a homogeneous system, the fluorescence-to-excitation reflectance ratio would be proportional to the product of fluorescence quantum yield, path length, and fluorophore absorption coefficient. From Figure 3.4, it also can be seen that the luminescence is scattered dramatically. The scattering effect is a result of inhomogeneities both on the surface and within the body of the film. The formation of crazes and cracks result in the inhomogeneities and changes the trajectory of the light (Figure 3.6). For heterogeneous systems, the fluorescence intensity is significantly influenced by absorption and scattering.³¹ In scattering samples, incident light can only penetrate the top of the film.^{18,32} Reflection (including diffuse reflection and specular reflection on the top layer), and scattering within the bulk of the samples, however, causes amplification of the fluorescent signal (Figure 3.7). In the transparent film with DMSO, light can directly penetrate throughout the film, but there are a few activated anthracene units in the bulk. At the same time, the enhancement at the surface due to scattering and reflection is lost, resulting in a drop of the net fluorescence intensity.

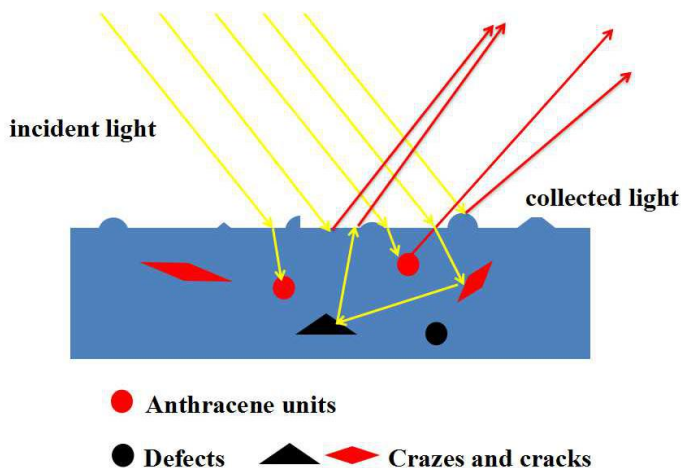


Figure 3.6. Possible light trajectories on and within the top layer of compressed films.

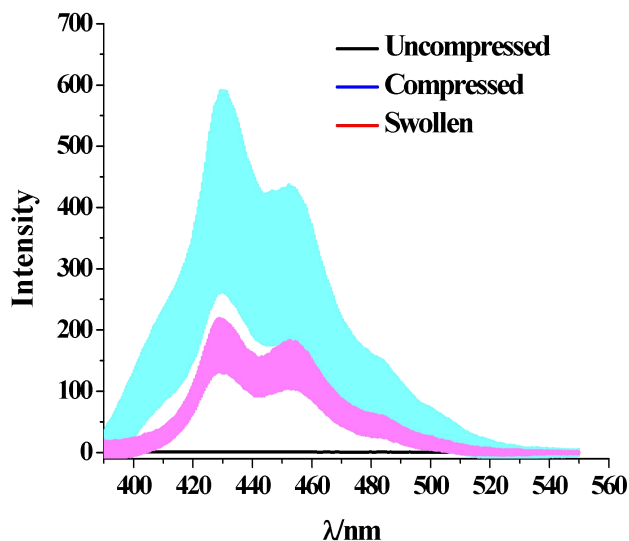


Figure 3.7. Fluorescence spectra recorded a) the uncompressed sample (black), compressed sample (blue with green error bars) and the sample swollen with water after compression (red with pink error bars)

Dependence of activation on degree of swelling

Despite the difficulties to determine the fluorescence intensities accurately, an attempt was made to investigate to establish the dependence of mechanoactivation on swelling degree and temperature during compression. The average fluorescence intensity at the emission maximum ($\lambda_{\text{max}} = 429 \text{ nm}$) of water swollen films after compression and subsequent drying was measured as described above and is plotted against d_s in Figure 3.8. As can be seen, with increasing swelling degree, the intensity of the generated fluorescence at the maximum decreases, which might result from the decrease of the elastic modulus. With a lower elastic modulus, the materials become more flexible and rubbery, and the more supplied mechanical energy is dissipated by the plastic deformation and is not used to activate the mechanochemical reaction.

3.3 Conclusions

In conclusion, from the mechanically induced fluorescence, it is evident that

compressive deformation activates the retro Diels-Alder reaction in glassy bulky material, and with mechanoactivation of the retro Diels-Alder reaction, the generated fluorescent anthracene can be employed to map the deformation of materials. Compressive deformation is localized around the center of the cylindrical sample. Most importantly, much of the observed fluorescence is lost when scattering of the compressed sample is suppressed by adding a solvent with matching refractive index. This phenomenon is tentatively interpreted as a result of scattering enhanced fluorescence close the surface, where most of the mechanoactivation takes place. Furthermore, swelling influences the mechanoactivation, and with higher swelling ratio, the mechanoactivation is less, but because the activation becomes weaker along the radius of the sample, the obtained data have very large error bars, as a result, with the present experiments it is difficult to reach quantitative conclusions about the dependence of the mechanoactivation on degree of swelling of crosslinked PNIPAm films.

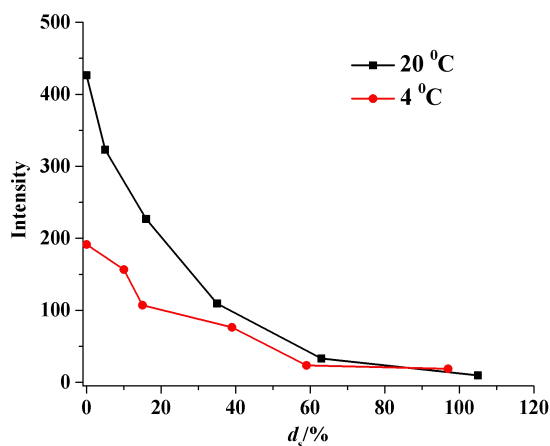


Figure 3.8. Fluorescence intensity ($\lambda_{\text{exc}} = 372 \text{ nm}$) recorded at $\lambda_{\text{max}} = 429 \text{ nm}$ as a function of temperature and degree of swelling.

3.4 Experimental

3.4.1 Materials and instrumentation

Unless otherwise specified, reagent and solvents were purchased from Sigma-Aldrich, Merck, or Acros and used without further purification. NIPAAm was

purified by recrystallization from hexane at 65 °C. TEGDMA was purified by passing over a short column of basic Al₂O₃. AIBN was recrystallized from MeOH at 45 °C. Dioxane was freshly distilled before use. Deuterated solvents were obtained from Cambridge Isotopes Laboratories.

NMR spectra were recorded on a 400 MHz (100 MHz for ¹³C) Varian Mercury VX spectrometer at room temperature using residual protonated solvent signals as internal standards (¹H: δ(CDCl₃) = 7.26 ppm, δ(CD₂Cl₂) = 5.32 ppm, δ((CD₃)₂SO) = 2.50 ppm; ¹³C: δ(CDCl₃) = 77.16 ppm, δ(CD₂Cl₂) = 53.84 ppm, δ((CD₃)₂SO) = 39.52 ppm).

Matrix assisted laser desorption/ionisation time-of-flight mass spectrometry (MALDI-TOF MS) was performed on a Autoflex Speed MALDI-MS instrument (Bruker, Bremen, Germany) equipped with a 355 nm Nd:YAG smartbeam laser. MALDI-TOF MS experiments were performed by spotting samples on a MTP 384 target ground steel plate using an α-cyano-4-hydroxycinnamic acid (CHCA) (Fluka, Switzerland) matrix. Samples were 1:1 premixed with CHCA in 50/50 acetonitrile/water supplemented with 0.1% v/v trifluoroacetic acid (TFA). Mass spectra were acquired in reflector positive ion mode by summing spectra from 500 selected laser shots. The MS spectra were calibrated with cesium triiodide of known masses.

Compression until failure employing a pellet press

Samples of approximately 5 mm×5 mm were cut out from the respective *ca.* 2 mm thick PNIPAm network. Compression with a pellet press exerting a pressure of *ca.* 1.2 GPa on the sample was performed for 30 s either at 20 °C or at 4 °C in a cold room. The sample dimensions decreased in height and increased in area during the compression until the final area of the compression cylinder of 0.785 cm² was covered. The equipment was stored at least for 12 h at the given temperature before use.

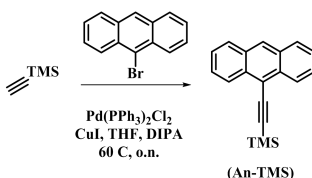
Fluorescence spectroscopy

Fluorescence spectroscopy on compressed and uncompressed samples of differently swollen PNIPAm networks was carried out on a PerkinElmer LS 50B fluorescence spectrometer employing a sample holder for solid samples at room temperature. All analyses were carried out with the same instrument setup (4 nm slit width excitation

beam, 3 nm slit width emission beam, $\lambda_{\text{exc}} = 372 \text{ nm}$, no cut-off filters). Before compression, the background emission of the material was measured by analyzing the uncompressed sample and found to negligible; it was thus omitted in some measurements. Each sample was fixated between two glass object plates for microscopy. For each swelling degree, two samples were prepared and for each sample, several different points of the fluorescent compressed area were measured to account for inhomogeneity of force distribution during compression. Baseline correction to remove the influence of scattering on the solid-state samples was performed using OriginPro 8.5. The mean standard deviation was calculated from these two samples and is depicted as a faded shadow behind the curves.

3.4.2 Synthesis

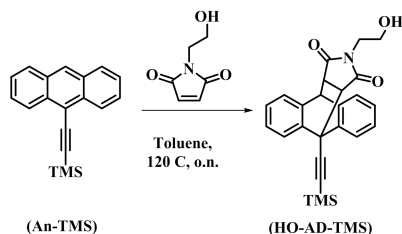
(Anthracen-9-ylethynyl)trimethylsilane (An-TMS)



9-bromoanthracene (1.500 g, 5.830 mmol), $\text{Pd(PPh}_3)_2\text{Cl}_2$ (0.205 g, 0.292 mmol), and CuI (0.056 g, 0.292 mmol) were dissolved in dry THF (10 mL) and degassed with Ar. To this solution were added subsequently TMS-acetylene (0.996 mL, 7,000 mmol) and dry diisopropylamine (10 mL) whereupon the solution turned orange and then black. The whole was stirred at 60 °C under Ar over night. Afterwards, the solution was cooled down and removal of the solvent in vacuo and column chromatography (silica, cyclohexane with 1% toluene) yielded a red oil that was recrystallized from MeCN at -30 °C to give (anthracen-9-ylethynyl)trimethylsilane (An-TMS) (yield: 38%) as orange crystals. $^1\text{H-NMR}$ (400 MHz, CDCl_3): $\delta(\text{ppm}) = 8.59$ (d, 2 H), 8.43 (s, 1 H), 8.01 (d, 2 H), 7.61 (m, 2 H), 7.52 (m, 2 H), 0.45 (s, 9 H). $^{13}\text{C-NMR}$ (100 MHz, CDCl_3): $\delta(\text{ppm}) = 132.9, 131.0, 128.6, 127.9, 126.8, 126.7, 125.6, 106.2, 101.5, 95.4, 0.27$. MALDI-TOF-MS: $m/z = 274.16$ (calcd. 274.12 for $\text{C}_{19}\text{H}_{18}\text{Si}^+$).

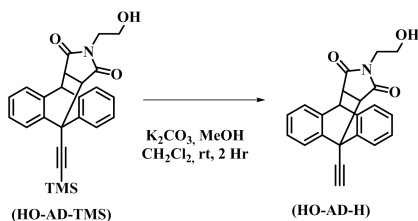
**(Anthracen-9-ylethynyl)trimethylsilane
9,10-Diels-Alder adduct (HO-AD-TMS)**

N-(2-hydroxyethyl)maleimide



(Anthracen-9-ylethynyl)trimethylsilane (An-TMS) (250 mg, 0.911 mmol) and N-(2-hydroxyethyl)maleimide (193 mg, 1.366 mmol) were dissolved in toluene (9 mL) and stirred at 120 °C over night. Evaporation of the solvent in vacuo and column chromatography (silica, cyclohexane : EtOAc = 1 : 1) yielded (anthracen-9-ylethynyl)trimethylsilane N-(2-hydroxyethyl)maleimide 9,10-Diels-Alder adduct (HO-AD-TMS) (yield: 95%) as white foam. ¹H-NMR (400 MHz, CDCl₃): δ(ppm) = 7.81 (d, 1 H), 7.69 (d, 1 H), 7.40 (d, 1 H), 7.31 (m, 3 H), 7.23 (m, 2 H), 4.81 (d, 1 H), 3.34 (m, 2 H), 3.27 (m, 2 H), 3.10 (m, 2 H), 1.20 (t, 1 H), 0.42 (s, 9 H). ¹³C-NMR (100 MHz, CDCl₃): δ(ppm) = 176.6, 174.3, 149.4, 147.1, 140.4, 139.9, 138.2, 137.5, 127.4, 127.3, 127.2, 126.9, 124.9, 124.1, 123.9, 96.6, 60.3, 50.6, 47.5, 47.3, 45.0, 41.3, 0.16. HPLC-MS(ESI⁺): m/z = 416.00 (calcd. 416.16 for C₂₅H₂₆NO₃Si⁺). MALDI-TOFMS:m/z = 438.16 (calcd. 438.15 for C₂₅H₂₅NO₃SiNa⁺).

9-Ethynylanthracene N-(2-hydroxyethyl)maleimide 9,10-Diels-Alder adduct (HO-AD-H)

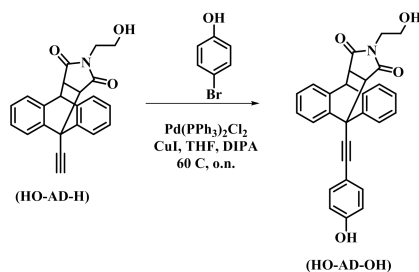


To a degassed solution of K₂CO₃ (80 mg, 0.578 mmol) in MeOH (2 mL) was added a degassed solution of (anthracen-9-ylethynyl)trimethylsilane N-(2-hydroxyethyl)maleimide 9,10-Diels-Alder adduct (HO-AD-TMS) (300 mg, 0.722 mmol) in a mixture of CH₂Cl₂ (2 mL) and MeOH (2 mL) dropwise at rt under Ar and was stirred at that temperature for 2 h. Subsequently, the solution was diluted

with water and extracted with Et₂O. The combined organic layers were dried over anhyd. MgSO₄ and removal of the volatiles in vacuo yielded pure 9-ethynylantracene N-(2-hydroxyethyl)maleimide 9,10-Diels-Alder adduct (OH-An-H) (yield: 92%) as white foam. ¹H-NMR (400 MHz, CDCl₃): δ(ppm) = 7.85 (d, 1 H), 7.74 (d, 1 H), 7.41 (d, 1 H), 7.31 (m, 3 H), 7.25(m, 2 H), 4.82 (d, 1 H), 3.32 (m, 4 H), 3.18 (s, 1 H), 3.11 (m, 2 H), 1.16 (t, 1 H). ¹³C-NMR (100 MHz, CDCl₃): δ(ppm) = 176.4, 174.7, 140.1, 139.8, 137.8, 137.4 127.6, 127.5, 127.2, 126.9, 125.0, 123.94, 123.92, 123.7, 79.5, 78.6, 60.0, 50.5, 47.4, 46.5, 44.9, 41.3. HPLC-MS(ESI⁺): m/z = 344.00 (calcd. 344.12 for C₂₂H₁₈NO₃⁺).

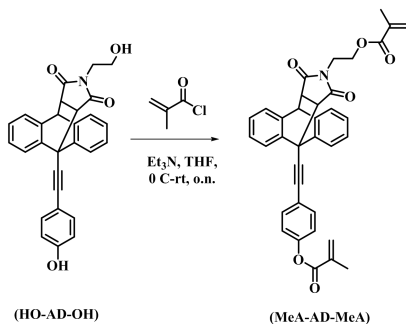
**9-(4-Hydroxyphenyl)ethynylantracene
9,10-Diels-Alder adduct (OH-AD-OH)**

N-(2-hydroxyethyl)maleimide



9-Ethynylantracene N-(2-hydroxyethyl)maleimide 9,10-Diels-Alder adduct (HO-AD-H) (180 mg, 0.524 mmol), 4-bromophenol (150 mg, 0.867 mmol), Pd(PPh₃)₂Cl₂ (18 mg, 0.026 mmol), and CuI (5 mg, 0.026 mmol) were dissolved in dry THF (1.5 mL) and degassed. To this solution was added dry diisopropylamine (1.5 mL) whereupon the solution turned black. The whole was stirred at 50 °C under Ar for 4 h. Afterwards, the solution was cooled down, diluted with THF, and filtered to remove the HBr salt. Subsequent removal of the solvent in vacuo and column chromatography (silica, cyclohexane : EtOAc = 1 : 1) yielded 9-(4-hydroxyphenyl)ethynylantracene N-(2-hydroxyethyl)maleimide 9,10-Diels-Alder adduct (HO-AD-OH) (yield: 54%) as off-white solid. ¹H-NMR (400 MHz, (CD₃)₂SO): δ(ppm) = 9.93 (s, 1H), 7.76 (d,1H), 7.55 (m, 4H), 7.27 (m, 5H), 6.87 (d, 2H), 4.84 (m, 1H), 4.62 (m, 1H) 3.33 (m, 2H), 3.01 (t, 2H), 2.56 (m, 2H). HPLC-MS(ESI⁺) : m/z = 436.17 (calcd. 436.15 for C₂₈H₂₂NO₄⁺).

9-(4-Hydroxyphenyl)ethynylantracene **N-(2-hydroxyethyl)maleimide**
9,10-Diels-Alder adduct dimethacrylate (MeA-AD-MeA)



9,10-Diels-Alder adduct (HO-AD-OH) (20 mg, 0.046 mmol) and Et₃N (13 μL, 0.096 mmol) were dissolved in dry THF (0.5 mL) under Ar and the solution was then cooled with an ice bath. Subsequently, methacryloyl chloride (9.3 μL, 0.096 mmol) was added and the final solution was left to stir over night at rt. Subsequently, the reaction mixture was passed through a plug of silica and all volatiles were removed in vacuo to yield pure 9-(4-hydroxyphenyl)ethynylantracene N-(2-hydroxyethyl)maleimide 9,10-Diels-Alder adduct dimethacrylate (MeA-AD-MeA) (yield: 95%) as colorless wax that was stored at -30 °C in a Schlenk flask under Ar and could not be characterized further due to its instable nature. HPLC-MS(ESI⁺): m/z = 572.17 (calcd. 572.20 for C₃₆H₃₀NO₆⁺).

PNIPAm network films with DA adduct

N-isopropyl acrylamide (1000 mg, 8.84 mmol) tetraethylene glycol dimethacrylate (53 μL, 0.175 mmol), 9-(4-hydroxyphenyl)ethynylantracene N-(2-hydroxyethyl)maleimide 9,10-Diels-Alder adduct dimethacrylate (1.010 mg, 1.767 μmol), and AIBN (3.63 mg, 0.022 mmol) were dissolved in dioxane (1 mL) in a vial and degassed by bubbling Ar through the solution for 30 s. Slight heating in a water bath was necessary to dissolve the NIPAAm completely. Then, the whole mixture was transferred into a Teflon mold, covered with a glass slide, and polymerized in an oven at 65 °C under slight N₂ flow for 24 h. Afterwards, residual, non-evaporated dioxane was removed for 1 d *in vacuo*.

PNIPAm cylinders

This synthesis was carried out analogously to the general procedure with the difference that no mechanophore crosslinker was used and the amount of TEGDMA was increased to compensate for the lack of mechanophore crosslinker. The solution was polymerized in a Teflon mold consisting of multiple cylinder-shaped gaps with $d \times h$ of the gap being 3 mm \times 3 mm. Due to shrinkage during polymerization, non-uniform cylinders were obtained and hence the top was flattened by cutting away *ca.* 1 mm of height with a razorblade.

Swelling of the networks with water

Controlled swelling of the PNIPAm networks was carried out by weighing the vacuum-dried samples and then adding a specific amount of water to the sample with a microliter syringe to reach the desired d_s . The samples were then weighed after 1 d to determine the final d_s . The degree of swelling d_s of PNIPAm networks was calculated according to

$$d_s = 100 \cdot \frac{m_{sw} - m_d}{m_d}$$

where m_{sw} is the mass of the swollen sample and m_d the mass of the completely dry material respectively. Equilibrium swelling of the samples was reached after 1 d of immersion in excess water and confirmed by the lack of weight-change of the sample.

References

- 1 B S Thompson, M V Gandhi and S Kasiviswanathan, *Mater. Des.* **1992**, 13 (1): 3-9
- 2 Q. Li (ed), *Intelligent Stimuli-Responsive Materials: From Well-Defined Nanostructures to Applications*, **2013**, John Wiley & Sons, Inc., Hoboken, NJ, USA.
- 3 M. W. Urban (ed), *Stimuli-Responsive Materials: From Molecules to Nature Mimicking Materials Design*, **2016**, Royal Society of Chemistry, Burlington House, London, UK
- 4 a) C. R. Hickenboth, J. S. Moore, S. R. White, et al., *Nature* **2007**, 446, 423; b) M. M. Caruso, D.A. Davis, Q. Shen, et al., *Chem. Rev.* DOI: 10.1021/cr9001353
- 5 a) M. M. Caruso, D. A. Davis, Q. Shen, S. A. Odom, N. R. Sottos, S. R. White and J. S. Moore, *Chem. Rev.*, **2009**, 109, 5755–5798; b) Z. S. Kean and S. L. Craig, *Polymer*, **2012**, 53, 1035–1048; c) J. N. Brantley, K. M. Wiggins and C. W. Bielawski, *Polym. Int.*, **2013**, 62, 2–12; d) R. Groote, R. T. M. Jakobs and R. P. Sijbesma, *Polym. Chem.*, **2013**, 4, 4846–4859; e) J. Li, C. Nagamani and J. S. Moore, *Acc. Chem. Res.*, **2015**, 48, 2181–2190.
- 6 a) D. R. T. Roberts, S. J. Holder, *J. Mater. Chem.* **2011**, 21, 8256–8268; b) A. Pucci, G. Ruggeri, *J. Mater. Chem.* **2011**, 21, 8282–8291; c) J. Eyckmans, T. Boudou, X. Yu, C. S. Chen, *Dev. Cell* **2011**, 21, 35–47; d) Y. Jiang, *Mater. Sci. Eng. C* **2014**, 45, 682–689; e) M. J. Jacobs, K. Blank, *Chem. Sci.* **2014**, 5, 1680–1697;
- 7 a) D. A. Davis, A. Hamilton, J. Yang, L. D. Cremar, D. Van Gough, S. L. Potisek, M. T. Ong, P. V. Braun, T. J. Martínez, S. R. White, J. S. Moore, N. R. Sottos, *Nature* **2009**, 459, 68-72; b) C. K. Lee, D. A. Davis, S. R. White, J. S. Moore, N. R. Sottos, P. V. Braun, *J. Am. Chem. Soc.* **2010**, 132, 16107-16111 c) C.K. Lee, B.A. Beiermann, M.N. Silberstein, J. Wang, J.S. Moore, N.R. Sottos, P.V. Braun, *Macromolecules*, **2013**, 46, 3746-3752; d) C.M. Degen, P.A. May, J.S. Moore, S.R. White, N.R. Sottos, *Macromolecules*, **2013**, 46, 8917-8921.
- 8 a) Y. Chen, A. J. H. Spiering, S. Karthikeyan, G. W. M. Peters, E. W. Meijer, R.P. Sijbesma, *Nat. Chem.*, **2012**, 4(7): 559-562; b) Y. Chen, R.P. Sijbesma, *Macromolecules*, **2014**, 47(12): 3797-3805; c) J. M. Clough, A. Balan, T. L. J. Van Daal, R.P. Sijbesma, *Angew. Chem. Int. Ed.*, **2015**, 55(4): 1445–1449;
- 9 a) E. Ducrot, Y. Chen, M. J. H. Bulters, R.P. Sijbesma, C. Creton, *Science*, 2014, 344, 186-189; b) J. M. Clough, C. Creton, S. L. Craig, R. P. Sijbesma, *Adv. Funct. Mater.*, **2016**, 26(48): 9063–9074.
- 10 S. K. Surampudi, H. R. Patel, G. Nagarjuna and D. Venkataraman, *Chem. Commun.*, **2013**, 49, 7519–7521.
- 11 K. Imato, A. Irie, T. Kosuge, T. Ohishi, M. Nishihara, A. Takahara and H. Otsuka, *Angew. Chem., Int. Ed.*, **2015**, 54, 6168–6172.
- 12 Z. S. Kean, G. R. Gossweiler, T. B. Kouznetsova, G. B. Hewage and S. L. Craig, *Chem. Commun.*, **2015**, 51, 9157–9160.
- 13 a) Y. Sagara and T. Kato, *Nat. Chem.*, **2009**, 1, 605–610; b) A. Pucci and G. Ruggeri, *J. Mater. Chem.*, **2011**, 21, 8282–8291; c) Z. Chi, X. Zhang, B. Xu, X. Zhou, C. Ma, Y. Zhang, S. Liu and J. Xu, *Chem. Soc. Rev.*, **2012**, 41, 3878–3896.
- 14 a) S. S. M. Konda, J. N. Brantley, B. T. Varghese, K. M. Wiggins, C. W. Bielawski and D. E. Makarov, *J. Am. Chem. Soc.*, **2013**, 135, 12722–12729; b) G. R. Gossweiler, G. B. Hewage, G. Soriano, Q. Wang, G. W. Welshofer, X. Zhao and S. L. Craig, *ACS Macro Lett.*, **2014**, 3, 216–219; c) J. Li, T. Shiraki, B. Hu, R. A. E. Wright, B. Zhao and J. S. Moore, *J. Am. Chem. Soc.*, **2014**, 136, 15925–15928; d) D. C. Church, G. I. Peterson and A. J. Boydston, *ACS Macro Lett.*, **2014**, 3, 648–651.
- 15 C. K. Lee, B. A. Beiermann, M. N. Silberstein, J. Wang, J. S. Moore, N. R. Sottos, and P. V. Braun, *Macromolecules* **2013**, 46, 3746–3752

- 16 R. Göstl, R. P. Sijbesma, *Chem. Sci.* **2016**, 7: 370–375.
- 17 K.N. Plunkett, X. Zhu, J.S. Moore, D.E. Leckband, *Langmuir*, **2006**, 22: 4259–4266.
- 18 R. Göstl, L. C. A. van Breemen, J. P. A. Heuts, and R. P. Sijbesma, Optical sensing of covalent bond scission for the observation of stress dissipation in hydrogels, [unpublished work].
- 19 J. A. Syrett, G. Mantovani, W. R. S. Barton, D. Price and D. M. Haddleton, *Polym. Chem.*, **2010**, 1, 102-106.
- 20 Y. Yu, K. Hearon, T. S. Wilson and D. J. Maitland, *Smart Mater Struct.* **2011**, 20(8): 085010
- 21 N. Lakhera, K. E. Smith, C. P. Frick, *J. Appl. Polym. Sci.* **2013**, 1913–1921
- 22 W. Luo, W. Liu, *Polym. Test.* **2007**, 26, 413–418
- 23 a) E. J. Kramer, *J. Polym. Sci. Polym. Phys.* **1975**, 13, 509-525; b) H.G.H. van Melick, L.E. Govaert, H.E.H. Meijer, *Polymer* 2003, 44, 2493–2502
- 24 A. S. Argon and M. I. Bessonov, *Polym. Eng. Sci.*, **1977**, 17(3), 174-182
- 25 K. Kendall, *Proc. R. Soc. Lond. A*, **1978**, 361: 245-263
- 26 Y. Higo, F. Oka, S. Kimoto, T. Sanagawa, and Y. Matsushima, *Soils Found*, **2011**, 51(1), 95-111
- 27 a) D. Raabe, D. M. F. Roters, *Acta Mater.*, **2007**, 55, 4567-4583; b) Z. Wang, L. Qi, G. Wang, H. Li, M. S. Dargusch, *Mech. Mater.*, **2016**, 102, 90-96; c) K. Sridharan, K. Elangovan, *J Pharm Sci*, **2015**, JCHPS special issue 9, 130-136
- 28 D. A. Davis, A. Hamilton, J. Yang, L. D. Cremer, D. Van Gough, S. L. Potisek, M. T. Ong, P. V. Braun, T. J. Martinez, S. R. White, J. R. Moore, N. R. Sottos, *Nature*, **2009**, 459, 68-72
- 29 a) P. K. Dutta, *Behavior of materials at cold regions temperatures*, **1988**, US Army Corps of Engineers, Special Report 88-9; b) Y. Duan, A. Saigal, R. Greif, *Polym. Eng. Sci.*, 2003, 43(1), 112-124
- 30 M. G. Müller, I. Georgakoudi, Q. Zhang, J. Wu, and M. S. Feld, *Appl. Opt.* **2001**, 40: 4633-4646
- 31 Q. Zhang, M. G. Müller, J. Wu, and M. S. Feld, *Opt. Lett.* **2000**, 25: 1451-1453; A. J. Durkin, S. Jaikumar, and R. Richards-Kortum, *Appl. Spectrosc.* **1993**, 47: 2114-2121
- 32 M. Keijzer, R. R. Richards-Kortum, S. L. Jacques, and M. S. Feld, *Appl. Opt.* **1989**, 28: 4286-4292

Chapter IV

Study on mechanochemistry of *N*-heterocyclic salts polymeric materials

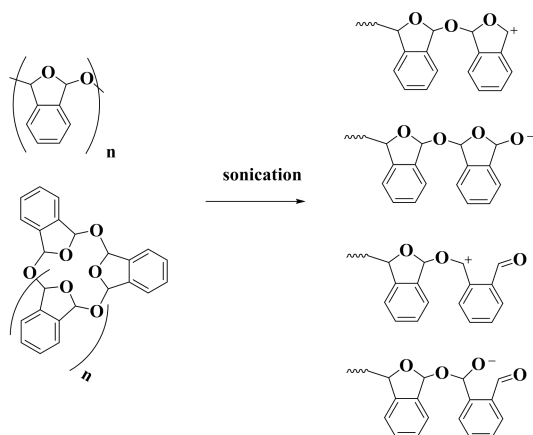
ABSTRACT

A trial on developing mechanically induced heterolytic scission in polymer chemistry was launched in this chapter. Three candidates polymeric materials including bis(phenyl)fluorene-centered polymer (bPF-*c*-PMA), imidazolium-centered polyTHF (Imi-*c*-pTHF), and *N*-benzyl pyridinium system were prepared and synthesized. Both bPF-*c*-PMA and Imi-*c*-pTHF did not undergo the targeted heterolytic bond scission under sonication. As for the *N*-benzyl pyridinium system, grinding of the network did not produce active initiation sites as thermally activation of the network, exhibiting that the grinding is not enough for the activation of the initiator.

4.1 Introduction to mechanically induced heterolytic bond cleavage

Polymeric materials exhibit an extraordinary range of responses to mechanical tension, varying from simple conformational changes to bond stretching and deformation, and finally to bond cleavage when sufficient mechanical energy is absorbed. Although molecular dynamics work from Frank's group¹ demonstrates that mechanical stress can cause not only a simple homolytic bond breakage but also heterolytic bond scission, historically polymer mechanochemistry mainly focuses on polymer degradation via homolytic scission reactions². Up to date, most of the literature on polymer mechanochemistry reports homolytic bond scission of mechanophore-containing polymers under mechanical force, including ultrasonication-induced elongational force³, tensile stress⁴, compression tension⁵, and elongational tension from force spectroscopy⁶, while only few systems undergo heterolytic scission which will be discussed in following sentences. One of the few exceptions is the generation of a low yield of ionic products via mechanically induced heterolytic bond scission from the mechanical fracture of a range of polymers (polyethylene, polytetrafluoroethylene, polypropylene, poly(vinylidene fluoride)) in the presence of tetracyanoethylene (TCNE) as electron acceptor.⁷ Recent polymer mechanochemistry has focused on the use of weak units that break preferentially to other bonds in the polymer chain, so called mechanophores. Recently, there have been two synthetic polymers with designed mechanophores that undergo heterolytic scission: one is a report on a polymer with triarylsulfonium salt as mechanophore that produces phenyl cation through heterolytic bond scission⁸; the second system concerns poly(phthalaldehyde) including both linear and cyclic polymers (Scheme 4.1)⁹, which can generate mechanoions, with two reports that investigate the kinetics and the influence of molecular weights on the mechanochemical process. Compared to polymers undergoing homolytic scission, polymers undergoing mechanically induced heterolytic bond scission are limited both in number and applications; more efforts should be paid to seeking such kind of functional materials and making them useful for applications.

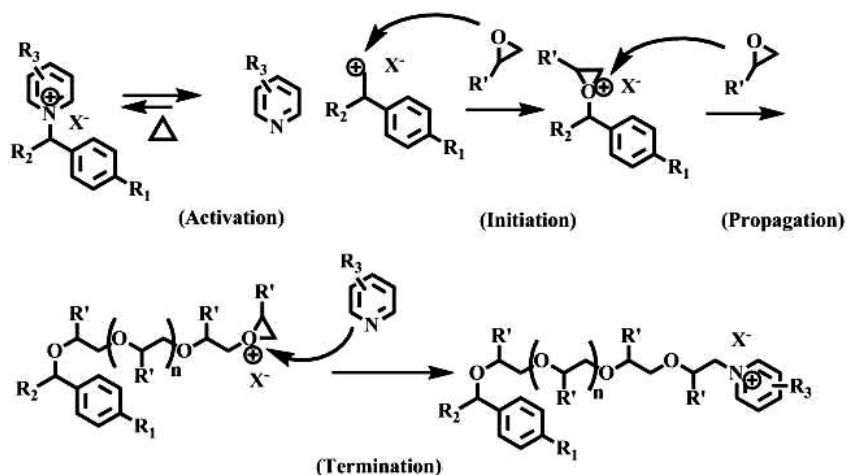
Potential mechanophores that give heterolytic bond scission include compounds that decompose to give stable cations. The current chapter reports on the investigation of such building blocks, including neutral bis(phenyl)fluorene, and cationic imidazolium and pyridinium salts. The formation of triphenylmethanium from bis(phenyl)fluorene is favored because of delocalisation of the positive charge in the conjugated cation.



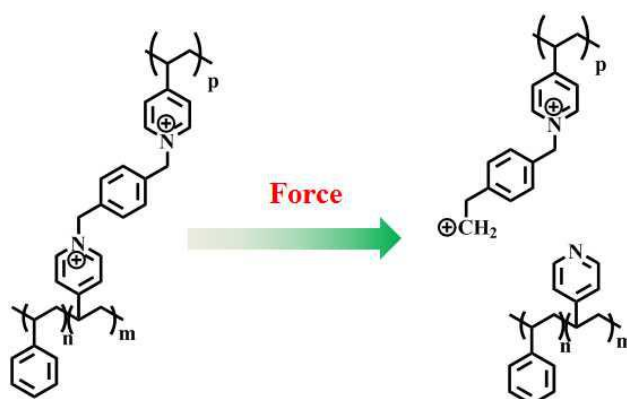
Scheme 4.1. Mechanically induced heterolytic scission of poly (phthalaldehyde)

N-heterocyclic salts constitute a large family of compounds that are widely used as antimicrobials¹⁰, in catalysis¹¹, as solvents¹² *etc.* The neutral precursors of the *N*-heterocyclic compounds are usually organic bases such as amines, pyridine, imidazole or other *N*-heterocyclic compounds. These compounds are usually, although not always, proton acceptors and play multifaceted roles in many applications, particularly in catalysis because of their mild basicity or nucleophilicity and good solubility in organic solvents. Among ammonium salts, *N*-benzyl pyridinium salts are of specific interest for mechanochemistry because they have been shown to act as thermally latent initiators to initiate the cationic polymerization of various monomers, such as epoxides¹³ by decomposition into a benzyl cation as the initiator and a pyridine as the terminator for the polymerization. An analogous mechanochemical activation mechanism would create the possibility to make mechanically activated polymerization initiators.

Scheme 4.2 illustrates the mechanism of thermal initiation of epoxide polymerization by *N*-benzyl pyridinium salts which, at high temperature undergo a heterolytic bond scission to form benzylic cations. Since *N*-benzyl pyridinium salts undergo a thermally heterolytic bond scission, a proposal to test whether *N*-benzyl pyridinium-based polymer networks can be activated mechanically is schematically shown in Scheme 4.3 and will be investigated experimentally in this chapter.



Scheme 4.2. Schematic illustration of mechanism for thermopolymerization of epoxides with pyridinium salts



Scheme 4.3. Proposal for the mechanically induced heterolytic bond scission of benzylpyridinium-based polymer network

The current chapter reports on the investigation of imidazolium and pyridinium mechanophores: their mechanochemical activation and their potential use as latent polymerization initiators. First, imidazolium-centered linear polyTHF was prepared and subjected to sonication in solution. The product was characterized with NMR and MALDI-TOF. Second, benzyl pyridinium was introduced into a network and was mechanically activated by grinding for initiation of the ring opening polymerization of epoxides. Additionally, a bis(phenyl)fluorene-based

mechanophore was also studied by sonication.

4.2 Sonication of imidazolium-centered linear polyTHF

4.2.1 Synthesis

Linear imidazolium-centered polyTHF (Imi-*c*-pTHF) was synthesized via cationic polymerization of THF and termination by sodium imidazolate. In Figure 4.1, ¹H NMR and MALDI-TOF MS analysis results of the polymer are shown. In the NMR spectrum, the ratio of the integral values of each characteristic signal above 4.0 ppm in ¹H NMR spectrum is a: b: c = 1: 2: 4, which can be assigned to the imidazolium protons and CH₂ protons next to the imidazolium center. Comparison of the MALDI-TOF mass spectra of Imi-*c*-pTHF (Figure 4.1(c)) and pTHF-OH (Figure 4.1(b)), the molecular weight of Imi-*c*-pTHF is nearly twice of that of the pure pTHF-OH obtained via termination of the polymerization with water. Both the NMR and MALDI-TOF MS results suggest that the termination of the polymerization of THF with sodium imidazolyl formed imidazolium-centered polyTHF (Imi-*c*-pTHF).

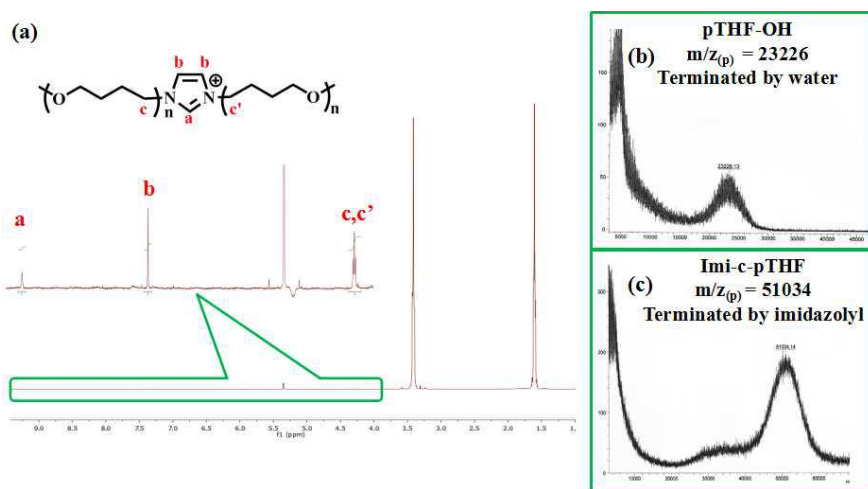


Figure 4.1. (a) ¹H NMR spectrum of Imi-*c*-pTHF obtained via cationic polymerization of THF and termination with sodium imidazolyl; (b) and (c) MALDI-TOF MS spectra of polyTHF terminated by water and imidazolium, respectively.

The polymerization was terminated with sodium imidazolyl formed by deprotonation of imidazole with NaH. Without NaH, the termination with imidazole can only form imidazolyl-ended polyTHF, which was also found experimentally; the

obtained product terminated with imidazole had a similar molecular weight as the product terminated with water.¹⁴ To terminate the polymerization, NaH is necessary for the formation of Imi-*c*-pTHF. The obtained Imi-*c*-pTHF has a molecular weight of 51 kDa by MALDI -TOF MS analysis.

4.2.2 Chain scission in Imi-*c*-pTHF with sonication

Chain scission in Imi-*c*-pTHF was investigated by sonication in toluene solution. Prior to and during sonication, methane was bubbled through the solution as blanket gas¹⁵. The double-jacketed glass sonication vessel was cooled down to (5.0 ± 0.5) °C by a water cooling circulation system from a thermostat-controlled bath. After thermal equilibration for 15 min, sonication was initiated, and continued for 60 min with 30% of the maximum amplitude (225 W). The solvent was removed in vacuum and subsequently the product was analyzed by MALDI-TOF MS and ¹H NMR (Figure 4.2). After sonication, new ¹H NMR signals in the range of 5.5-6.5 ppm appeared, while the intensity of signals from imidazolium and the protons close to imidazolium in the polymer chain decreased. The peak maximum in MALDI-TOF moved from the initial molecular weight of 51 kDa to nearly half this value at 25.3 Da, indicating chemical bond cleavage during the sonication.

It is difficult to get detailed information about the generated product only with ¹H NMR spectroscopy and MALDI-TOF, so further characterization with Diffusion-Ordered Spectroscopy (DOSY) was performed. In the DOSY spectrum of a solution that was sonicated for 1 h (Figure 4.3), new signals appear in the range of 5.5-6.5 ppm corresponding to products with a lower diffusion constant than the pTHF peaks above 6.8 ppm. This indicates that these signals derive from low-molecular-weight fragments, while their chemical shift suggest that the signals come from protons attached to sp² hybridized carbon atoms. A scission pathway that is in line with these observations is shown in Scheme 4.4, in which bond scission takes place close to the center with a preference for the weaker ether bonds. The ether bond breaks and generates a hydroxyl group and a C-C double bond via hydrogen abstraction. Scission could, however, also take place in other chemical bonds, and there are still some polymer chains which had not undergone any scission left in the system. As a result, the product after sonication is a mixture, and it is evident that imidazolium is not a good mechanophore.

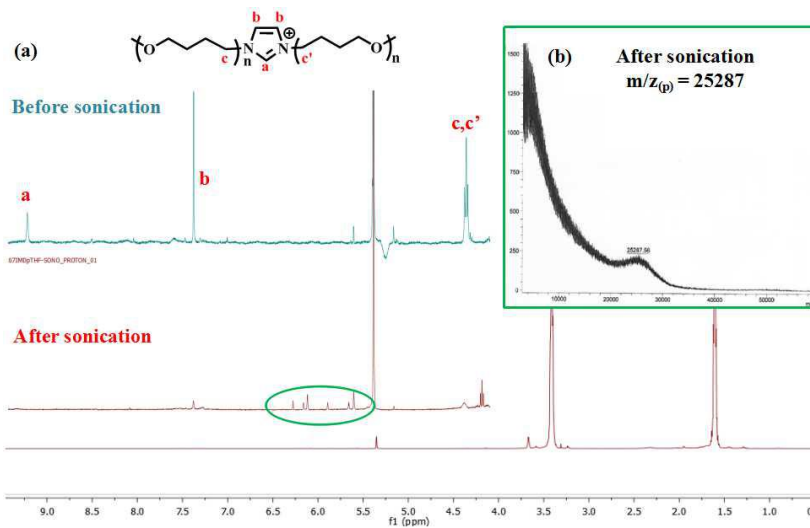


Figure 4.2. (a) ^1H NMR spectra of Imi-*c*-pTHF before and after sonication; (b) MALDI-TOF MS spectrum of Imi-*c*-pTHF after sonication.

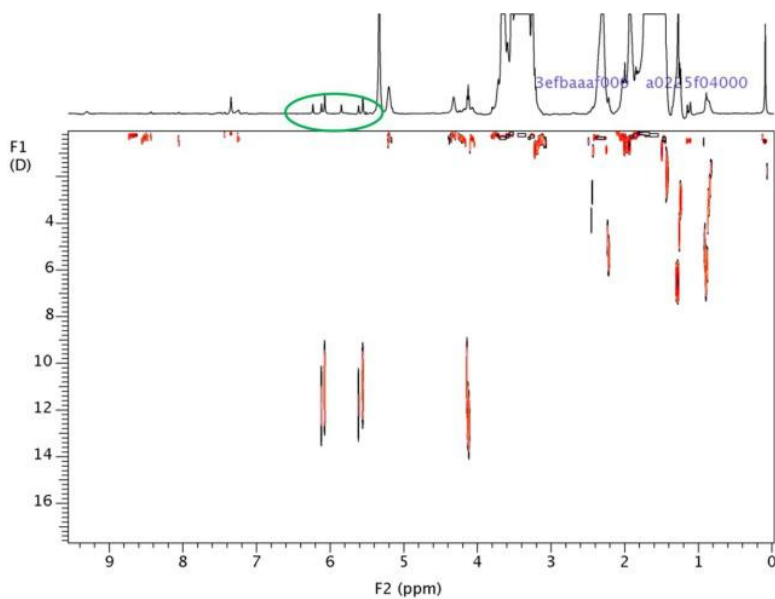
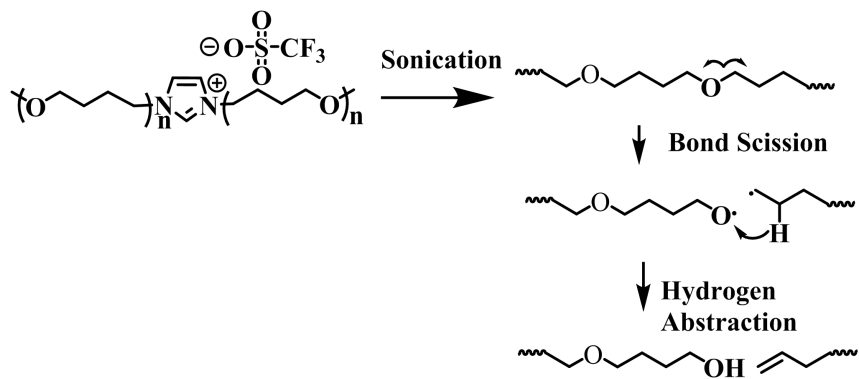


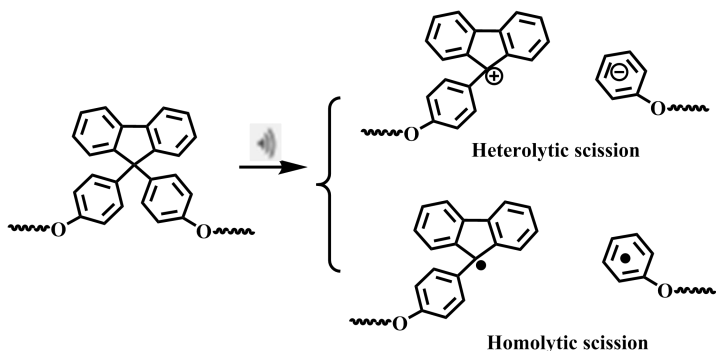
Figure 4.3. Two-dimensional DOSY spectrum of Imi-*c*-pTHF after sonication.



Scheme 4.4. Schematic of the suggested bond scission in ether bond along the polymer chain.

4.3 Study on mechanochemistry of linear bis(phenyl)fluorene-centered poly(methyl acrylate)

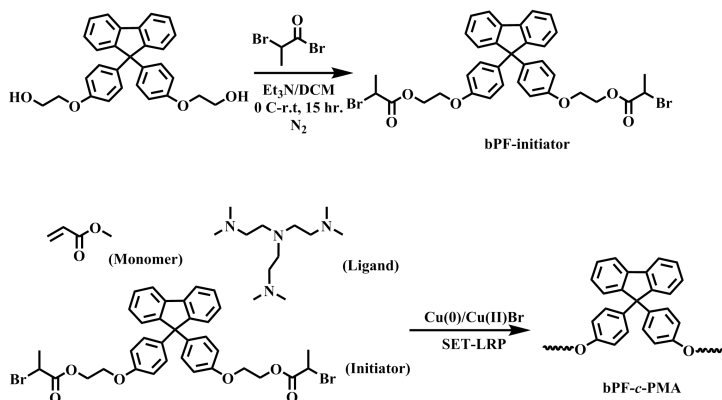
Triphenylmethanium is a stable carbocation because the conjugated three phenyl groups strongly stabilize the charge. A bulky substituent will promote formation of methanium, via heterolytic scission of this unit. Inspired by this concept, a bis(phenyl)fluorene-based mechanophore was designed and the possible scission of bis(phenyl)fluorene-centered polymer chain is schematically shown in Scheme 4.5. Because the triphenylmethyl radical is also stabilized, homolytic scission is a potential competing mechanism for mechanoactivation of bis(phenyl)fluorene.



Scheme 4.5. Schematic of the proposed heterolytic scission of bis(phenyl)fluorene-centered polymers.

4.3.1 Synthesis

Following the procedure in Scheme 4.6, the bifunctional initiator (bPF-initiator) was prepared by direct esterification of 2,2'-(((9H-fluorene-9,9-diyl)bis(4,1-phenylene))bis(oxy))bis(ethan-1-ol) with 2-bromopropionyl bromide. With the obtained initiator, single-electron transfer living radical polymerization (SET-LRP) was performed to obtain the bis(phenyl)fluorene-centered poly(methyl acrylate) (bPF-*c*-PMA). Copper wire was used as the copper(0) source, and CuBr₂ as the copper(II) source, Me₆TREN as ligand, and methyl acrylate as the monomer. By varying the polymerization time, linear bPF-*c*-PMA chains were obtained with molecular weights of 25, 43, 59 and 71 kDa. Figure 4.4(a) shows the ¹H NMR spectrum of the prepared initiator. All the signals from the spectrum can be assigned to the protons of the bPF-initiator, clearly suggesting that the initiator is pure enough except some solvent residue from the chromatography. Proton NMR and gel permeation chromatography (GPC) were employed to characterize the products. The ¹H NMR in Figure 4.4(b) gives a reasonable explanation of the structure of the product with a molecular weight of 71 kDa (bPF-*c*-PMA-71K), and GPC results in Figure 4.5(a) demonstrates the distribution of molecular weight of all obtained polymers. For the molecular weights, they are relatively higher than theoretic value calculated according to the feed ratio of the initiator to the monomer, which is because of the bimolecular termination and clearly explained by the small peak side by the main peak within the GPC curve. All the distributions are narrow with a PDI <1.10.



Scheme 4.6. Preparation of the bis(phenyl)fluorene-based initiator and bis(phenyl)fluorene-centered polymer through SET-LRP.

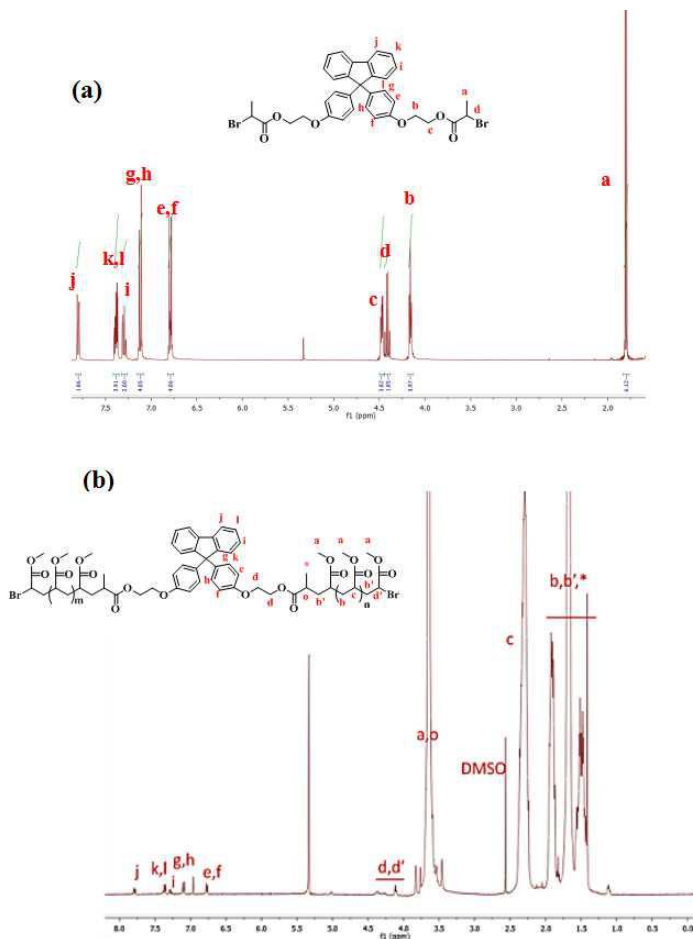


Figure 4.4. ^1H NMR spectrum of a) the obtained initiator (bPF-initiator) and b) the prepared polymer (bPF-*c*-PMA-71K).

4.3.2 Chain scission in bPF-*c*-PMA with sonication

The bPF-*c*-PMA chains prepared with narrow molecular weight distributions were sonicated in toluene at a concentration of 10 mg/mL. Samples were taken to follow the kinetics of bond scission with GPC, as shown in Figure 4.5. The polymer with a molecular weight of 25 kDa did not exhibit any mechanoactivation upon sonication for 3 h (Figure 4.5(b)) while for bPF-*c*-PMA-43K, only a small amount of polymer chains underwent bond scission, as is demonstrated in Figure 4.5(c). However, the GPC traces of bPF-*c*-PMA-59K and bPF-*c*-PMA-71K (Figure 4.5(d) and (e),

respectively) show that new peaks emerged with a molecular weight around half value of the main peak, while the decomposition of bPF-*c*-PMA-71K is much faster than that of bPF-*c*-PMA-59K.

Figure 4.5(f) also shows the sonication-induced chain scission of PMA with a molecular weight of 69 kDa. Although the molecular weight (the degree of polymerization as well) of PMA-69K is almost the same as bPF-*c*-PMA-71K, the mechanoactivity is much less than that of bPF-*c*-PMA-71K, further supported by the kinetics in Figure 4.6. Because of the existence of high molecular weight polymer chains from bimolecular termination which can be seen from the small peak in higher molecular weight region in GPC curves, the conversion rate is referred by the generation rate of the sonication-induced product. The sonication-induced chain scission of bPF-*c*-PMA-71K appears to be a zero-order reaction while the sonication-induced chain scission of PMA-69K is more like a first-order reaction. Generally, the mechanoactivation of bPF-*c*-PMA-71K is much faster than that of PMA-69K, suggesting that bis(phenyl)fluorene as mechanophore improves the mechanoactivity upon sonication.

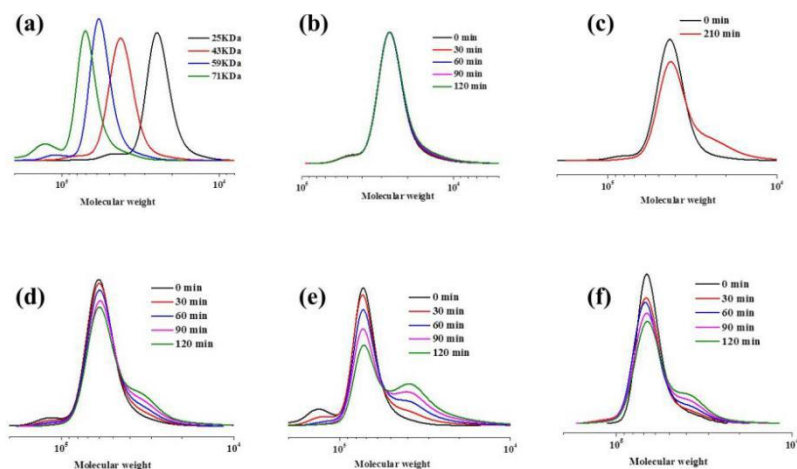


Figure 4.5. Molecular weight distribution of a) bis(phenyl)fluorene-centered PMA (bPF-*c*-PMA) with different molecular weights obtained by SET-LRP; b) sonication product of bPF-*c*-PMA-25K; c) sonication product of bPF-*c*-PMA-43K; d) sonication product of bPF-*c*-PMA-59K; e) sonication product of bPF-*c*-PMA-71K; f) sonication product of PMA-69K

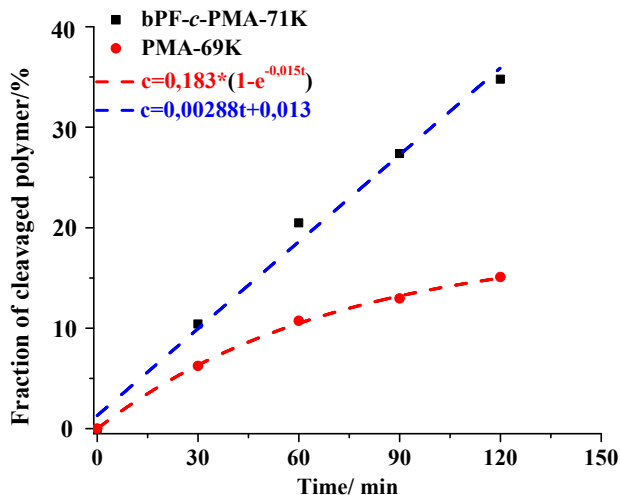


Figure 4.6. Plotting and fitting of conversion vs. time in sonication-induced chain scission of bPF-c-PMA-71K and PMA-69K

To investigate the mechanism of chain scission, the product with lower molecular weight was isolated by recycling GPC and then further characterized with ^1H NMR (Figure 4.7). The aromatic region of the spectrum of the polymer is identical to that of the small molecule initiator except for a peak at 7.0 ppm from an impurity which might be from decomposed inhibitor as labeled with an asterisk in Figure 4.7(b). Between 4.00 - 4.50 ppm, the peaks from protons b, c, and d shift to higher-field and have become broader in the polymer. Comparison of the spectra of the isolated sonication product with the initial polymer showed no change, suggesting that bond scission did not take place at the bis(phenyl)fluorene unit. However, halving of the molecular weight of the initial polymer shows that the mechanophore indeed increases the mechanoactivity of the polymer chain during sonication, and it can be inferred that chain scission must have taken place close to the bis(phenyl)fluorene unit. Good candidates for the location of bond scission are the ether bonds connected to bis(phenyl)fluorene or the ester bonds of the initiator unit.

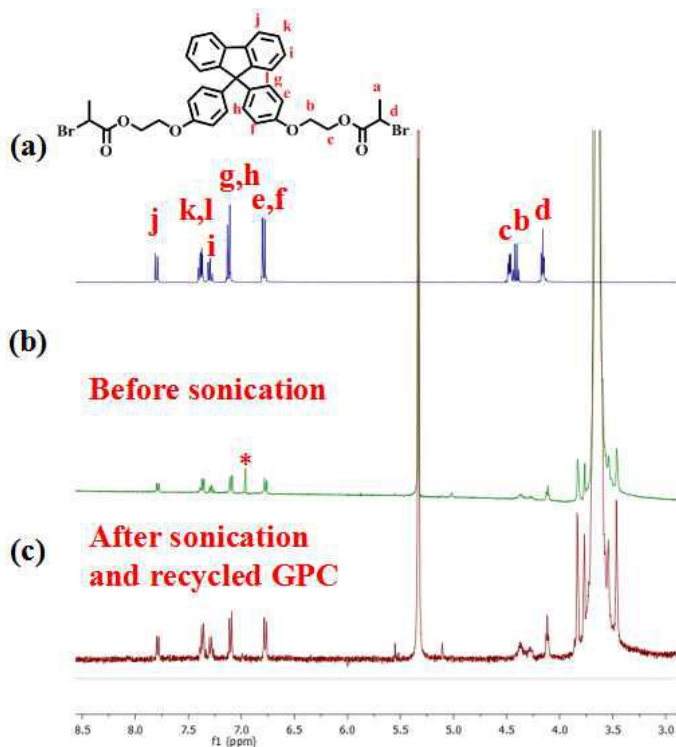
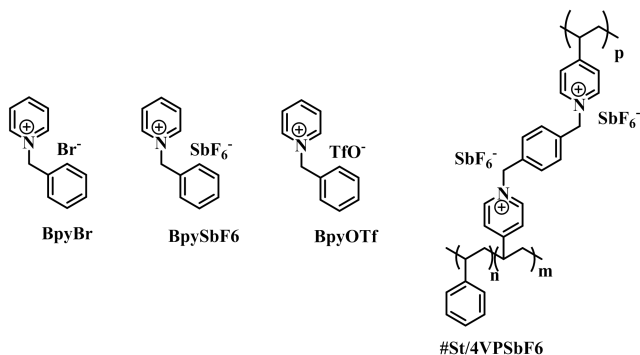


Figure 4.7. ^1H NMR spectra of the initiator, the prepared polymer before and after sonication for 3 h

4.4 Study on mechanochemistry of an *N*-benzyl pyridinium-based network

4.4.1 Synthesis

For the study of mechanochemical activation of benzyl pyridinium initiators, low molecular weight model compounds *N*-benzyl pyridinium with different counterions (BbyBr, BpyOTf and BpySbF₆, Scheme 4.7) and crosslinked benzylpyridinium (#St/4VPSbF₆, Scheme 4.7) compounds were synthesized. The model pyridinium compound BpySbF₆ was obtained via direct counterion exchange from BpyBr; BpyOTf, however, could not be obtained by counterion exchange with silver trifluoromethanesulfonate (AgOTf), a method reported in literature. BpyOTf was therefore synthesized via direct reaction of benzyl triflate with pyridine.



Scheme 4.7. Structures of the pyridinium's and crosslinked benzylpyridinium network.

The pyridinium network was synthesized from the copolymer poly(St-*co*-4VP) with ~10% of 4VP which was obtained by radical polymerization, crosslinked with α,α' -dibromo-*p*-xylene. Iodomethane was used to convert all non-reacted pyridine groups to pyridinium groups because any remaining pyridine groups in the polymer will act as terminator for the cationic ring opening polymerization of epoxides. For the counterion exchange, a large excess of silver hexafluoroantimonate (AgSbF_6) was added to a suspension of the network in toluene and kept stirring for 24 h, followed by filtration and washing with toluene and water to ensure complete conversion of all iodide ions to insoluble silver iodide. Figure 4.8 (a) shows the full spectra of products of each step and Figure 4.8 (b), (c) and (d) give the zoom in views of the differences. The benzylation of 4-vinylpyridine units in PS-*co*-P4VP converts pyridine to pyridinium, which is supported by the emergence of a band at 1633 cm^{-1} in its IR spectrum (Figure 4.8(b)). This band is also found in the products of the following steps. In the IR spectrum of the product after reaction with an excess of iodomethane, a weak band is present at 732 cm^{-1} indicating methylation, suggesting the pyridine was not completely converted to pyridinium in the previous step and the methylation with iodomethane is necessary. Ion exchange of the iodide and bromide with hexafluoroantimonate led to the appearance of bands at 657 cm^{-1} and 1115 cm^{-1} in the final product, while the band of iodide at 732 cm^{-1} disappeared, indicating complete exchange of the counterion.

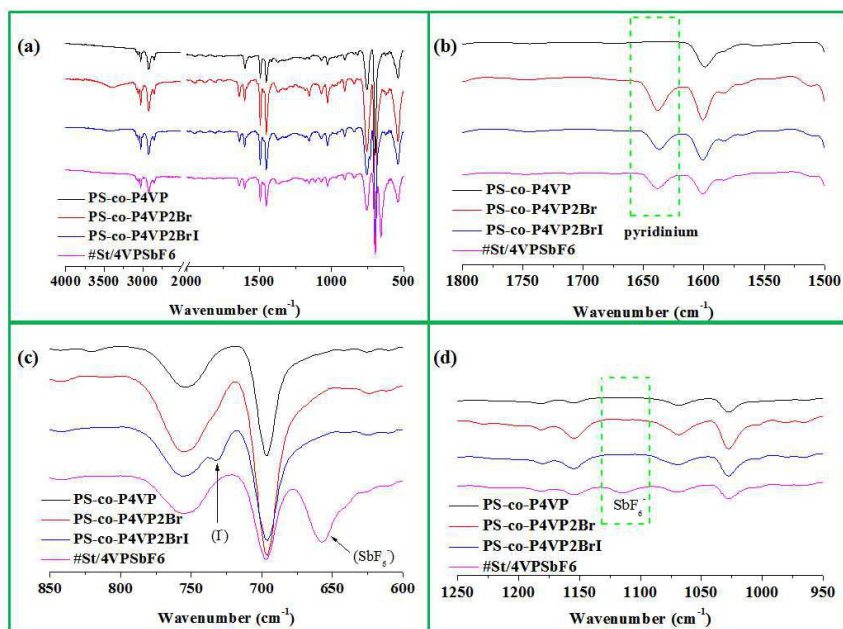


Figure 4.8. FT-IR spectra of the product towards the benzylpyridinium network step by step

4.4.2 Cationic ring opening polymerization of epoxide initiated with model pyridinium initiator

Phenyl glycidyl ether (GPE) was polymerized with the latent pyridinium initiators either in a sample pan with DSC instrument or in a normal reactor using the composition listed in Table 4.1. The GPC traces of the reaction mixtures without workup are shown in Figure 4.9 and their NMR spectra are shown in Figure 4.10. The ^1H NMR spectra of the products in Figure 4.10(b) and Figure 4.10(e) are the same as the spectrum of the monomer itself ((Figure 4.10(a)), indicating that BpyBr and BpyOTf are inactive for the polymerization. Their inactivity can be explained by their low solubility in GPE and in BpyBr potentially from the nucleophilicity of the bromide ions, which react with the benzyl cations formed in the thermal activation to form inactive benzyl bromide.

In contrast with BpyBr and BpyOTf, BpySbF₆ did lead to polymerization of GPE upon heating up to 120 °C for 2 h. In the presence of 2 wt% of this latent initiator, a 85.2% conversion to polymer was observed, while, the conversion was lower when

4 wt% of of BpySbF6 was used, as can be seen in the GPC traces in Figure 4.9 and by the monomer signals in the ¹H NMR spectrum in Figure 4.10(d). The lower conversion of sample III could be attributed to the larger amount of pyridine generated from the excess of BpySbF6 which terminates the polymerization.

Table 4.1 Composition of GPE Polymerization reaction mixtures with benzyipyridinium salts as initiator¹

Sample	GPE	BpyBr	BpySbF6	BpySbF6	BpyOTf	PSbF6 ³	AgBr	Polym. ⁴
I	98	2	0	0	0	0	0	-
II	98	0	2	0	0	0	0	✓
III	96	0	0	4	0	0	0	✓
IV ²	98	0	0	0	2	0	0	-
V	98	0	0	0	0	8	0	✓
VI ²	96	0	0	0	0	5	1	✓

1. all in mg, performed in the DSC instrument, with heating rate of 5 K min⁻¹, up to 225 °C, and cooling rate of 10 K min⁻¹, down to room temperature.

2. performed in normal reactor for 2 h.

3. PSbF6 = Poly (St-co-4VPSbF6)

4. - = no polymerization, ✓ = polymerization

The ¹H NMR spectrum of reaction V in Figure 4.10 (f) provides evidence that at higher temperatures copolymer initiator Poly(St-co-4VPSbF6) is an active initiator for the polymerization. The high molecular weight of the product obtained with sample V in GPC traces can be explained by the fact that the GPE chains are grafted to the polymeric initiator backbone. The polymer product obtained in the presence of AgBr (Figure 4.10 (g)) shows that the influence of AgBr on the polymerization is minor.

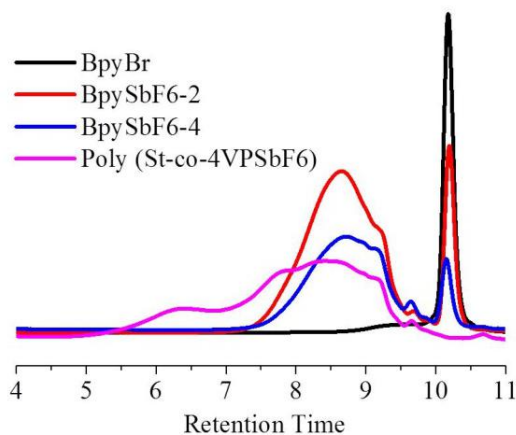


Figure 4.9. GPC traces for polymerization products initiated with pyridinium initiators

4.4.3 Kinetics

Polymerization kinetics of BpySbF6 and poly(*St-co-4VPSbF6*) as initiator at 150 °C were compared by determining conversions with ¹H NMR spectroscopy. The conversion *vs.* time in Figure 4.11 demonstrates that the activity of the macromolecular initiator is much higher than the small molecular initiator. After polymerization for 1 h, the conversion was 84.3 % with poly(*St-co-4VPSbF6*) and 45.0 % with BpySbF6, respectively. The high activity of macromolecular initiator can be attributed to its solubility promoted by the polystyrene backbone. Fitting conversion *vs.* time at low reaction times shows a linear relationship. According to the fitting results, the apparent reaction rate constant (*k*, the slope of the linear fitting) are 0.032 s⁻¹ and 0.012 s⁻¹ for poly(*St-co-4VPSbF6*) and BpySbF6, respectively. It is supposed that the activation and the propagation for both initiators should be same for the activation energy of C-N(pyridinium) is always the same, and the activation of the monomer for ring opening also does not change, therefore the difference of the kinetics for two initiators should come from the deactivation. Deactivation is a bimolecular reaction. If initiated with BpySbF6, the terminator is pyridine while if initiated with poly(*St-co-4VPSbF6*), the terminator is a long polymer chain, significantly slowing the deactivation rate.

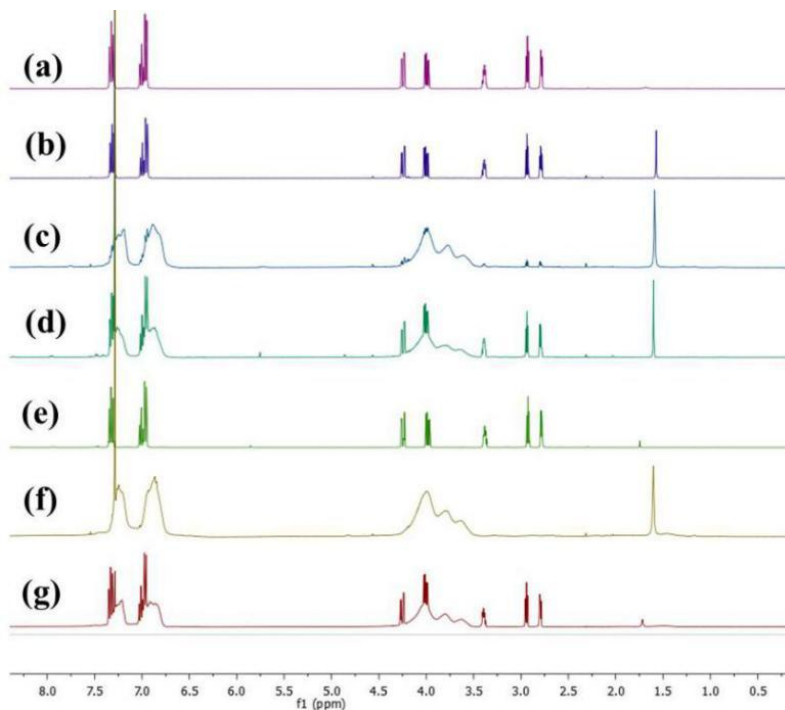


Figure 4.10. ^1H NMR spectra of (a) GPE, monomer and the polymerization product initiated by (b) BpyBr, 2 mg (sample I); (c) BpySbF₆, 2 mg (sample II); (d) BpySbF₆, 4 mg (sample III); (e) BpyOTf, 2 mg (sample IV); (f) Poly (St-co-4VPSbF₆), 8 mg (sample V); (g) 5 mg of Poly (St-co-4VPSbF₆) with 1 mg of AgBr (sample VI) with DSC.

4.4.4 Temperature-dependent reactivity of BpySbF₆ for polymerization

Polymerization of GPE at different temperatures was performed to study the influence of temperature on the reactivity of BpySbF₆ and determine the lowest temperature to activate initiation of polymerization. As shown in Table 4.2, after polymerization for 2 h at 80 °C, the conversion is about 5.6 %, which is in the tolerance range of ^1H NMR, so it can be concluded that the temperature limit for the activation of BpySbF₆ is close to 80 °C. Since at low conversions, the conversion is proportional to time; therefore, assuming the conversion at $t = 0$ is 0 %, then with the conversions at $t = 2$ h (all the conversions are in the linear region), the apparent rate constant can be calculated, and the results are shown in Table 4.2. With the apparent rate constant 100, 120 and 150 °C, the apparent activation energy (E_A) and frequency factor (A) can be calculated according to the Arrhenius equation: $E_A = 56.8$ kJ/mol, $A = 11.8$ s⁻¹, respectively. Based on k_{100} and k_{120} , it is calculated that E_A

= 58.6 kJ/mol and $A = 12.3 \text{ s}^{-1}$, while based on k_{120} and k_{150} , it is $E_A = 54.9 \text{ kJ/mol}$ and $A = 11.2 \text{ s}^{-1}$, but the differences are negligible, therefore the final values are obtained as the mean of two values.

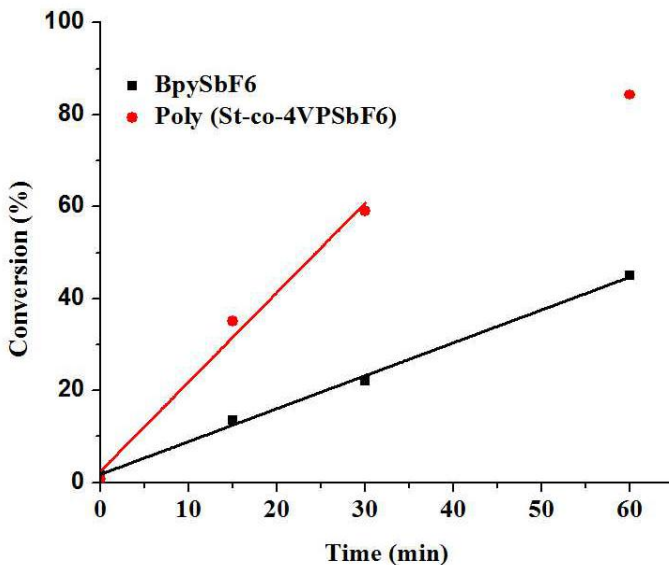


Figure 4.11. Conversion of monomer vs. time for polymerization with two pyridinium initiators (with same molar of pyridinium units) at 150 °C and their linear fitting at low conversion region

Table 4.2 Conversions and apparent rate constant of polymerization initiated with BpySbF6 at different temperatures

Temperature/ ^o C	80	100	120	150
Conversion ¹ /%	5.6	10.0	26.0	59.1 ²
$k^3/(\text{s}^{-1})$	0.000783	0.00124	0.00362	0.0119

1. Conversion for 2 h. polymerization, determined with ¹H NMR.
2. Conversion for 1 h polymerization
3. Apparent rate constant

4.4.5 Thermally initiated polymerization and mechanically induced polymerization with *N*-benzyl pyridinium-based network

Polymerization of GPE, initiated with the prepared network, was performed thermally in a normal tube reactor at 120 °C for 2 h. The solid was isolated, washed with acetone for three times and dried in vacuum. FT-IR measurements of the products are shown in Figure 4.12. In the 1036-1190 cm^{-1} region shown in the green dashed rectangle in Figure 4.12, the absorption of the product after polymerization is the same as the absorption of the poly (glycidyl phenyl ether) (shown as PolyGPE in the Figure), and totally different from the absorption of both the monomer GPE and the network itself, and also the same situation at 887 cm^{-1} and 810 cm^{-1} , suggesting thermo-polymerization took place within #St/4VPSbF6 and the polymer grows from the network.

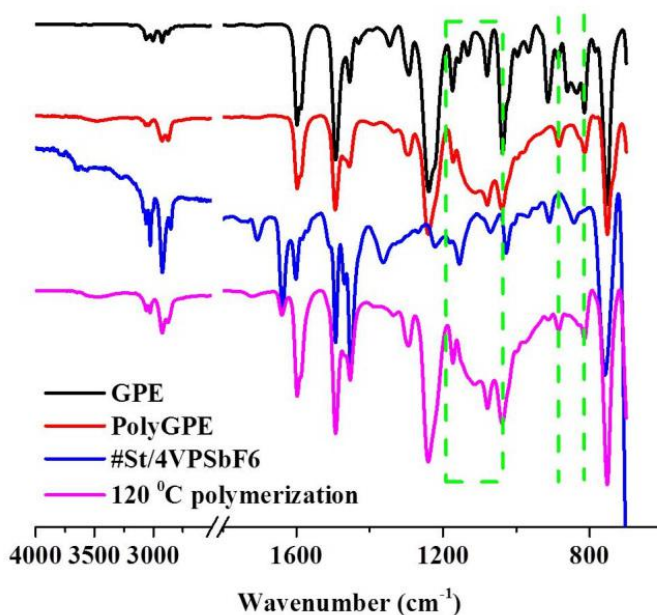


Figure 4.12. FT-IR spectra of GPE monomer, polyGPE, #St/4VPSbF6 and polymerization product with #St/4VPSbF6 as initiator at 120 °C

The successful thermopolymerization of GPE with #St/4VPSbF6 is evidence that #St/4VPSbF6 is active enough to initiate the polymerization. Mechanochemical activation of the polymerization was tested by mechanical grinding. After the same

workup, FT-IR of the product shows no bands of polyGPE (Figure 4.13). These results with #St/4VPSbF6 as initiator indicates that this polymer is not mechanically active. Mechanical grinding has been shown to activate mechanochemical reactions¹⁶, but in #St/4VPSbF6, activation is apparently insufficient to form appreciable amounts of polymer. The lack of activity might be due to the low activity of the monomer at room temperature, or the relative fast deactivation of benzyl cation with pyridine. The presence of moisture may also have affected the activity. Because grinding was performed in open air, atmospheric water may have acted as nucleophile and terminate polymerization.

4.5 Conclusions

The imidazolium-centered polyTHF (Imi-*c*-pTHF) was prepared via cationic polymerization of THF and termination with sodium imidazolidate. When the prepared Imi-*c*-pTHF was sonicated in toluene, it underwent scission randomly along the polymer chain, suggesting imidazolium is not a good mechanophore. So is the bis(phenyl)fluorene as mechanophore for the bis(phenyl)fluorene-centered polymer also did not undergo targeted bond scission to generate the cation as expected.

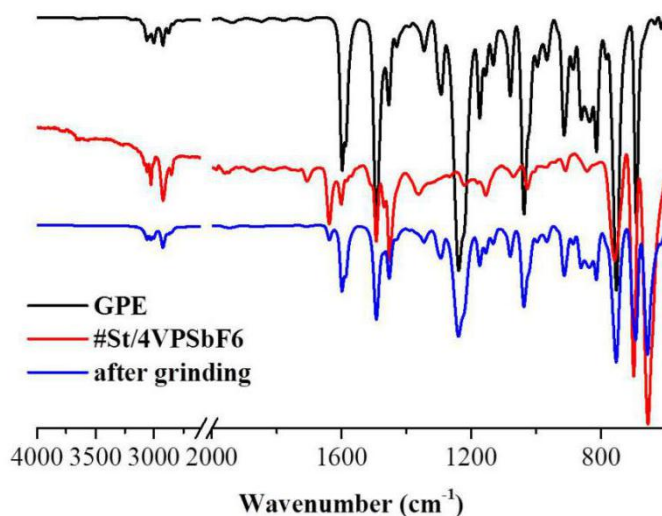


Figure 4.13. FT-IR spectra of GPE monomer, #St/4VPSbF6 and product after grinding with #St/4VPSbF6

In the benzyl pyridinium systems, both small molecular pyridinium BpySbF₆ and large molecular pyridinium Poly (St-co-4VPSbF₆) can be well activated thermally to initiate the cationic ring opening polymerization of glycidyl phenyl ether (GPE), but the pyridinium salt with bromide as counterion, BbyBr, is inactive, because the nucleophilicity of bromide results in the inactivation of the initiator. Additionally, the solubility has a large effect on the activity of the initiators. As a result, Poly (St-co-4VPSbF₆) is more active than BpySbF₆ because of its better solubility in solution. For thermopolymerization of GPE by BpySbF₆ in the temperature range of 100-150, the apparent activation energy (E_A) is = 57 kJ/mol. The pyridinium network, #St/4VPSbF₆, with SbF₆⁻ as counterion, was thermally activated to initiate the polymerization, but unfortunately it was mechanically inactive for polymerization in a grinding experiment.

4.6 Experimental

4.6.1 Materials and instrumentation

Unless otherwise specified, reagent and solvents were purchased from Sigma-Aldrich, Merck, or Acros and used without further purification. Dry THF was freshly taken from an MBRAUN Solvent Purification System (MB SPS-800), deuterated solvents were obtained from Cambridge Isotopes Laboratories. Toluene was dried over 4 Å molecular sieves for at least 12 h. prior to use.

NMR spectra were recorded on a 400 MHz (100 MHz for ¹³C) Varian Mercury VX spectrometer at room temperature using residual protonated solvent signals as internal standards (¹H: $\delta(\text{CDCl}_3) = 7.26$ ppm, $\delta(\text{CD}_2\text{Cl}_2) = 5.32$ ppm, $\delta((\text{CD}_3)_2\text{SO}) = 2.50$ ppm; ¹³C: $\delta(\text{CDCl}_3) = 77.16$ ppm, $\delta(\text{CD}_2\text{Cl}_2) = 53.84$ ppm, $\delta((\text{CD}_3)_2\text{SO}) = 39.52$ ppm).

Matrix assisted laser desorption/ionisation time-of-flight mass spectrometry (MALDI-TOF MS) was performed on a Autoflex Speed MALDI-MS instrument (Bruker, Bremen, Germany) equipped with a 355 nm Nd:YAG smartbeam laser. MALDI-TOF MS experiments were performed by spotting samples on a MTP 384 target ground steel plate using an α -cyano-4-hydroxycinnamic acid (CHCA) (Fluka, Switzerland) matrix. Samples were 1:1 premixed with CHCA in 50/50 acetonitrile/water supplemented with 0.1% v/v trifluoroacetic acid (TFA). Mass spectra were acquired in reflector positive ion mode by summing spectra from 500 selected laser shots. The MS spectra were calibrated with cesium triiodide of known masses.

Gel permeation chromatography (GPC) was carried out on a Shimadzu Prominence-i LC-2030C 3D system equipped with refractive index and UV/vis detectors (Shimadzu RID-10A and Shimadzu SPD-M10A photodiode array detector respectively) using Polymer Laboratories PL Gel 5 μm MIXED-C and MIXED-D columns. THF or CHCl_3 was used as eluent.

All infrared measurements were performed in ATR mode on a Perkin Elmer FT-IR Spectrum Two apparatus.

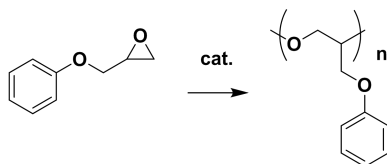
Differential scanning calorimetry (DSC) experiments were performed in hermetic T-zero aluminum sample pans using a TA Instruments Q2000 – 1037 DSC equipped with a RCS90 cooling accessory.

Sonication experiments were performed with a Sonic Vibra-Cell VC750 setup using a Sonics titanium alloy (Ti-6Al-4V) ultrasound probe (630-0220) at 20 kHz. The sonication experiments were performed at 30% power and 5 ± 0.5 °C.

4.6.2 Sonication experiments

To a home-made 10 mL double-jacketed glass sonication vessel was added a solution of Imi-*c*-pTHF in toluene (7 mL, concentration 10 mg/mL). The reaction vessel was placed under an inert methane atmosphere and cooled to (5.0 ± 0.5) °C with water from a recirculation thermostat bath. The reaction mixture was kept at this temperature for 15 minutes during which it was saturated with methane by bubbling through. The content of molecular oxygen is assumed to be below 1 ppm. Following the saturation period, sonication was initiated. Sonication was carried out using a Sonics VC750 sonication set-up (maximum power 750 W) operating at 20 kHz and 30% of the maximum amplitude (225 W). A continuous sonication protocol was used for all the tests in this work. The sample was taken after an hour sonication, and solvent was removed in vacuum. The residue product was used for MALDI-Tof MS, GPC, and NMR characterization.

4.6.3 General procedure for epoxide polymerization with pyridinium salts as initiators



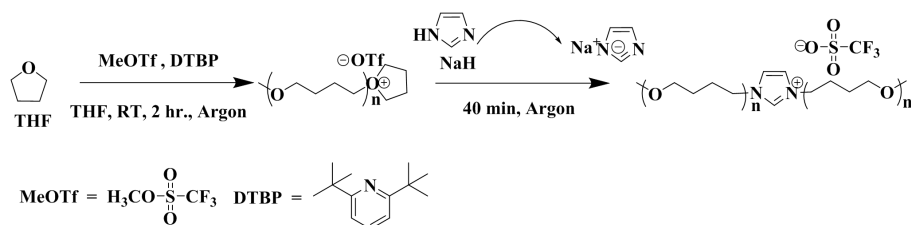
Scheme 4.8. General procedure for epoxide polymerization

Polymerization in normal reactor. Phenyl glycidyl ether (GPE) and the pyridinium initiator were mixed together in a tube reactor and degassed with N₂ by bubbling through for 2 mins., and then the tube reactor was sealed, allowed to warm to targeted polymerization temperatures for certain periods, respectively. After polymerization, the products were utilized for characterization without further purification.

Polymerization with DSC aid. About 9 mg of the mixture of GPE and pyridinium initiators was loaded in DSC pans, and then sealed with lids. Polymerizations were performed with heating rate of 5 K min⁻¹, up to 225 °C, and then cooled to room temperature with cooling rate of 10 K min⁻¹. Without further purification, the samples were either applied to ¹H NMR characterization or to GPC characterization.

4.6.4 Synthetic procedures and characterization

Imidazolium-centered poly(THF) (Imi-*c*-pTHF).

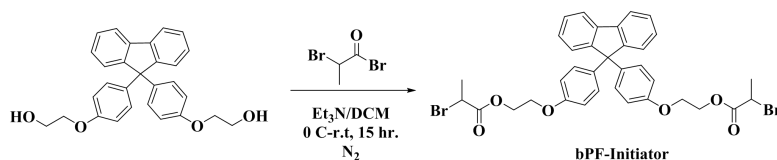


Scheme 4.9. Synthesis of Imi-*c*-pTHF via cationic polymerization of THF

Imi-*c*-pTHF was synthesized via cationic polymerization of THF. All the glassware and magnetic stirring bars were dried in 120 °C oven prior to reaction and THF used for polymerization was directly obtained from solvent purification system. Under Ar

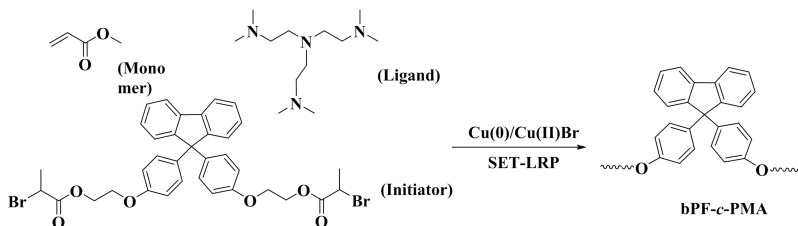
atmosphere, 50 μ L of ditert-butylpyridine (DTBP) was added to 50 mL of dry THF in Schlenk flask. Subsequently, methyl trifluoromethanesulfonate (MeOTf, 50 μ L) was added to the reaction mixture to initiate the cationic polymerization. At the same time, in a separate round bottom flask, the end capper imidazolyl was prepared by addition of imidazole (10 mg) to sodium hydride (NaH, 15 mg) suspension in dry THF under Ar atmosphere. After 2 h, the prepared imidazolyl was transferred into the Schlenk flask to terminate the polymerization and the reaction was kept stirring for another 40 min. Furthermore, several drops of methanol were added and the solvent was removed in vacuum till there was about 15 mL left, and then the viscous oily residue was poured into 100 mL water to get the crude product as precipitate and stirred in water for hours. Afterwards, the water was decanted, and the solid polymer was dissolved in diethyl ether, dried over magnesium sulphate, filtered over filter paper, and cooled down in freezer overnight. The polymer product was obtained by filtration and washed with cold diethyl ether.

(((9H-fluorene-9,9-diyl)bis(4,1-phenylene))bis(oxy))bis(ethane-2,1-diyl)bis(2-bromopropanoate) (bPF-initiator)

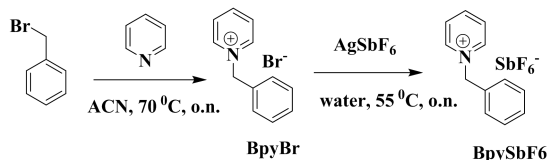


2,2'-(((9H-fluorene-9,9-diyl)bis(4,1-phenylene))bis(oxy))bis(ethan-1-ol) (1.3156 g, 3 mmol) dissolved in 30 mL anhydrous dichloromethane in a 100 ml flask, and the mixture was kept in ice bath for 15 min under stirring. Triethylamine (1.8215 g, 18 mmol) was added to the flask, to which further added 2-bromopropionyl bromide (2.5905 g, 12 mmol) dropwisely with the drop funnel. After 2-bromopropionyl bromide was finished to add, the reaction mixture was moved to room temperature, and kept stirring for another 15 h under nitrogen atmosphere. The solution was washed with water and sat. NaHCO₃ (aq.) respectively for twice. The organic layer was dried with MgSO₄ and condensed. The residue dissolved in acetone, and precipitated from water twice, and went through a column with heptane/DCM (1:4) as eluent to reach the pure initiator (bPF-initiator). 1.5292 g, yield: 72%. ¹H NMR (CDCl₃, 400 MHz, ppm): 7.79 (ddd, 2H), 7.38 (m, 4H), 7.29 (t, 2H), 7.12 (m, 4H), 6.79 (m, 4H), 4.47 (ddd, 4H), 4.41 (m, 4H), 4.16 (m, 2H), 1.79 (dd, 6H).

Bis(phenyl)fluorene-centered poly(methyl acrylate) (bPF-c-PMA).



The obtained initiator, bPF-initiator (35.4 mg, 0.05 mmol), Me₆TREN (2 μ l, 8,00 μ mol), methyl acrylate (3.2 mL, 35.00 mmol), and CuBr₂ (0.56 mg, 2,50 μ mol) were dissolved in DMSO (3.2 mL) in a Schlenk flask and degassed by 3 consecutive freeze-pump-thaw cycles. During that time, copper wire (0.5 cm) was activated in conc. HCl, subsequently washed with water and acetone, and dried. Under argon atmosphere, the activated copper wire was then added to the solution and the polymerization was allowed to run at room temperature for different periods. Then, the viscous solution was diluted with THF, passed through a plug of basic Al₂O₃, and after concentration in vacuo, added dropwise to stirred, ice-cold MeOH. MeOH was decanted and the viscous polymer redissolved in THF whereupon after concentration in vacuo it was again precipitated dropwise in fresh MeOH. After repeating the precipitation process 3 times, the polymer was dried in vacuo and received as a ductile white solid. M_n (GPC): 71 kDa, 59 kDa, 43 kDa and 25 kDa.



Scheme 4.10. Synthetic route towards BpyBr and BpySbF₆.

1-Benzylpyridinium bromide (BpyBr).

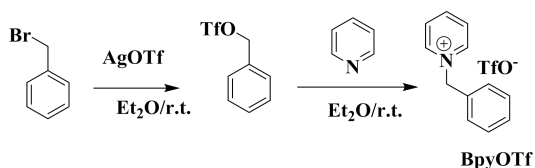
Pyridine (79.1 mg, 1 mmol) and benzyl bromide (188 mg, 1.1 mmol) were dissolved in acetonitrile, and then the solution was heated up to 70 °C and kept overnight. The product was obtained by precipitation from diethyl ether, and it is pure enough for use after dried in vacuum without further purification. 235.1 mg, yield 94%. ¹H NMR (DMSO-*d*₆, 400 MHz, ppm): 9.25 (d, 2H), 8.65 (t, 1H), 8.20 (t, 2H), 7.55 (m, 2H), 7.44 (m, 3H), 5.91 (s, 2H); ¹³C NMR (DMSO-*d*₆, 400 MHz, ppm): 146.48,

145.30, 134.76, 129.85, 129.71, 129.27, 128.96, 63.64; MALDI-TOF : $[M-Br]^+$, 170.27.

1-Benzylpyridinium hexafluoroantimonate (BpySbF₆).

BpyBr (250.1 mg, 1 mmol) and silver hexafluoroantimonate (AgSbF₆, 429.5 mg, 1.25 mmol) were dissolved in water, and allowed to react at 55 °C overnight. The precipitate solid was washed with diethyl ether and dried in vacuum to yield the titled compound. 349.2 mg, yield 86%. ¹H NMR (DMSO-*d*₆, 400 MHz, ppm): 9.19 (d, 2H), 8.63 (t, 1H), 8.18 (t, 2H), 7.52 (d, 2H), 7.45 (m, 3H), 5.85 (s, 2H); ¹³C NMR (DMSO-*d*₆, 400 MHz, ppm): 146.47, 145.28, 134.70, 129.87, 129.73, 129.21, 128.96, 63.84; MALDI-TOF : $[M-SbF_6]^+$, 170.23

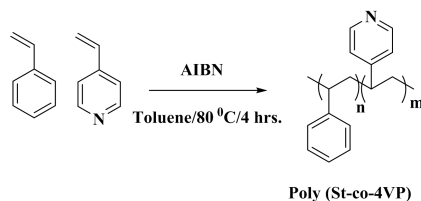
1-Benzylpyridinium Trifluoromethanesulfonate (BpyOTf).



Scheme 4.11. Synthesis of BpyOTf.

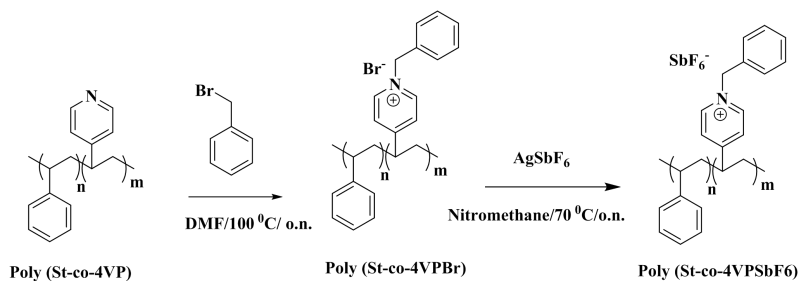
To a solution of benzyl bromide (0.855 g, 5 mmol) in anhydrous diethyl ether (10 mL) was added silver trifluoromethanesulfonate (1.2847 g, 5 mmol). Immediately a yellow precipitate was formed. After half hour, the organic solution was isolated by filtration, and then a solution of pyridine (0.395g, 5 mmol) in anhydrous diethyl ether (5 mL) was added to the isolated solution. The mixture was kept stirring for another half hour and formed a white precipitate. The crude solid product was isolated, dissolved in acetone, precipitated again from diethyl ether, repeated the precipitation procedure three times, and dried in vacuum to yield the titled compound. 1.3 g, yield 82% ¹H NMR (DMSO-*d*₆, 400 MHz, ppm): 9.20 (d, 2H), 8.63 (t, 1H), 8.19 (t, 2H), 7.53 (d, 2H), 7.45 (m, 3H), 5.86 (s, 2H); ¹³C NMR (DMSO-*d*₆, 400 MHz, ppm): 146.48, 145.29, 134.71, 129.87, 129.73, 129.22, 128.97, 63.84; ¹⁹F NMR (DMSO-*d*₆, 400 MHz, ppm): -77.74; MALDI-TOF : $[M-TfO]^+$, 170.23

Poly (styrene-*co*-vinylpyridine) (Poly (St-*co*-4VP)).



Scheme 4.12. Synthesis of Poly (St-*co*-4VP).

AIBN was recrystallized twice from ethanol, styrene and 4-vinylpyridine were distilled under reduced pressure, the solvent, toluene was dried over 4 Å molecular sieves, and the flask and stirring bar were dried in 120 °C oven prior to use. Styrene (3957.7 mg, 38 mmol) and 4-vinylpyridine (210.3 mg, 2 mmol) were dissolved in 45 mL of toluene, degassed with argon for 1 h, and then heated up to 80 °C. AIBN (32.8 mg, 0.2 mmol) in toluene solution was added subsequently after degassed for 20 min. Then the reaction was stirred for another 4 h. at 80 °C under Ar atmosphere. After the reaction finished, the mixture was poured into n-heptane and the polymer precipitated out as solid. The crude product was then dissolved in toluene again, precipitated from methanol, filtered with filter paper and washed with n-heptane to yield Poly (St-*co*-4VP) as white powder. Mw = 2.4 kDa (determined with GPC in CHCl₃), St/4VP = 9:1 (determined with ¹H NMR).



Scheme 4.13. Synthetic route towards to Poly (St-*co*-4VPSbF₆).

Poly (styrene-*co*-(1-benzyl-4-vinylpyridinium bromide)) (Poly (St-*co*-4VPBr)).

Poly (St-*co*-4VP) (208.4 mg, 0.2 mmol in 4-vinylpyridine units) and benzyl bromide (42.7 mg, 0.25 mmol) were dissolved in 5 mL DMF, heated up to 100 °C, and kept

The counterion exchange from halide to hexafluoroantimonate was performed following the procedure to synthesize Poly (St-*co*-4VPSbF6) and the network #St/4VPSbF6 was obtained after dried in vacuum.

References

- 1 D. Aktah and I. Frank, *J. Am. Chem. Soc.* **2002**, 124, 3402-3406
- 2 A. L. Black, J. M. Lenhardt and S. L. Craig, *J. Mater. Chem.*, **2011**, 21, 1655-1663
- 3 Z. S. Kean, G. R. Gossweiler, T. B. Kouznetsova, G. B. Hewage and S. L. Craig *Chem. Commun.*, **2015**, 51, 9157-9160
- 4 Z. Wang, Z. Ma, Y. Wang, Z. Xu, Y. Luo, Y. Wei, X. Jia, *Adv. Mater.* **2015**, 27, 6469-6474
- 5 M. B. Larsen and A. J. Boydston, *J Am Chem Soc*, **2013**, 135, 8189-8192
- 6 J. Wang, T. B. Kouznetsova, Z. S. Kean, L. Fan, B. D. Mar, T. J. Martínez, and S. L. Craig *J. Am. Chem. Soc.*, **2014**, 136 (43), 15162-15165
- 7 a) M. Sakaguchi, H. Kinpara, Y. Hori, S. Shimada, H. Kashiwabara *Polymer* **1984**, 25(7): 944-946; b) M. Sakaguchi, H. Kinpara, Y. Hori, H. Kashiwabara, *Polymer Communications (Guildford)* **1985** 26(5): 142-144; c) M. Sakaguchi, H. Kinpara, Y. Hori, S. Shimada, H. Kashiwabara *J. Polym. Sci. Part B Polym. Phys.* **1987** 25(7): 1431-1437; d) M. Sakaguchi, H. Kinpara, Y. Hori, S. Shimada, H. Kashiwabara *J. Polym. Sci. Part B Polym. Phys.* **1988** 26(6): 1307-1312; e) M. Sakaguchi, H. Kinpara, Y. Hori, S. Shimada, H. Kashiwabara *Macromolecules* **1989** 22(3): 1277-1280; f) M. Sakaguchi, S. Shimada, H. Kashiwabara *Macromolecules*, **1990**, 23 (23): 5038-5040; g) M. Sakaguchi, M. Makino, T. Ohura, and T. Iwata *J. Phys. Chem. A*, **2012**, 116 (40) : 9872-9877
- 8 T. Shiraki, C. E. Diesendruck and J. S. Moore *Faraday Discuss.*, **2014**, 170, 385-394
- 9 a) C. E. Diesendruck, G. I. Peterson, H. J. Kulik, J. A. Kaitz, B. D. Mar, P. A. May, S. R. White, T. J. Martínez, A. J. Boydston & J. S. Moore *Nature Chemistry* **2014**, 6, 623-628; b) G. I. Peterson, A. J. Boydston *Macromol. Rapid Commun.* **2014**, 35, 1611-1614
- 10 Y. Xue, H. Xiao, Y. Zhang, *Int. J. Mol. Sci.* **2015**, 16, 3626-3655
- 11 M. S. Kim, K. W. Lee, T. Endo, and S. B. Lee, *Macromolecules*, **2004**, 37 (15): 5830-5834
- 12 S. Zhang, X. Lu, Q. Zhou, X. Li, X. Zhang and S. Li, ISBN: 978-0-444-53427-9, *Ionic Liquids: Physicochemical Properties*
- 13 Y. Yagci and T. Endo, *Polymer Synthesis/Polymer Catalysis: Advances in Polymer Science*, **1997**, 127: 59-86
- 14 A. Balan, *Mechanochemical Scission Transition Metal-Ligand Bonds Coordination Polymers*, **2015**, PhD thesis
- 15 R. Groote, R. T. M. Jakobs, R. P. Sijbesma, *ACS Macro Lett.* **2012**, 1: 1012-1015;
- 16 K. Ishizuki, H. Oka, D. Aoki, R. Goseki, H. Otsuka, *Chem. Eur. J.* **2018**, 24: 3170-3173.

Chapter V

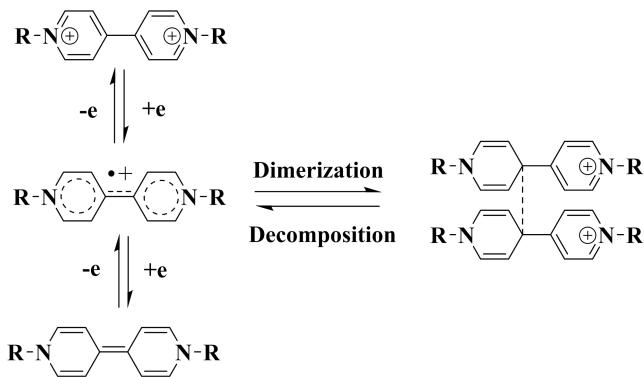
Electrochemistry of mono and bifunctional viologen derivatives

ABSTRACT

A family of viologens and bis(viologen)s were prepared and studied with cyclic voltammetry. The compounds showed differences of the formal potentials of two reduction steps which were around 0.43 and 0.56 V for viologens and bis(viologen)s, respectively. The difference suggests dimerization takes place in bis(viologen)s, which is further supported with temperature-dependent ESR measurements. After incorporation of a polymeric bis(viologen) into hydrogel networks, the reduction of bis(viologen) was successful, the limitation of the characterization, however, prevented us to get more information on mechanically induced switching of spin states of the reduced diamagnetic bis(viologen).

5.1 Introduction

Since 1933, when Michaelis¹ first gave the name of viologen to the family of 1,1'-disubstituted 4,4'-bipyridinium dications, there have been successive waves of interest in this class of compounds. Viologens², which can undergo two reversible, one-electron reductions to a radical cation and a neutral form,³ respectively (Scheme 5.1), have attracted a lot of interest recently because they can be used in various applications, such as (photo)electrochromic materials⁴, host-guest chemistry⁵, anion receptors⁶, solar cell or fuel batteries⁷, redox pairs⁸, herbicides⁹, *etc.* In polar environments, the product of the first reduction of viologens, the radical cations, can form face-to-face dimers/pimers by stacking at low temperature in relatively high concentration, while the dimers can also dissociate reversibly with an equilibrium constant for the methylviologen radical cation in aqueous solution at 25 °C in the range of 380-840 M⁻¹.¹⁰ Kosower *et. al.*¹¹ reported that the dissociation constant for methylviologen is 2.6×10⁻³ M (385 M⁻¹ for equilibrium constant) at 1 mol/L salt concentration, corresponding to a ΔG of -14.7 kJ/mol, which is consistent with the reported values from Evans¹² for various viologens: ΔG^0 ranges from -10.6 to -16.37 kJ/mol. The free radical cations obtained from the first reduction of viologens are paramagnetic because of the unpaired electron within the rings, giving a significant Electron Spin Resonance (ESR) signal while the diamagnetic dimers/pimers are ESR silent.



Scheme 5.1. Reduction of viologens, the corresponding dication, radical cation and neutral form of viologens, and the inter-/intramolecular dimerization of the radical cation

When two viologen units are connected by a bridge to give a bis(viologen), the effective molarity of viologen units is high; as a result, upon reduction, the viologen

units dimerise regardless of concentration. The intramolecular equilibrium between the dimers/pimers and the free radical cations is concentration-independent, but changes with temperature. Atherton *et. al.*¹³ studied the redox reactions of three bis(viologen)s with different bridges, reaching the conclusion that the redox reactions of bis(viologen)s with a number of types of oxidants and reductants conform well to Marcus theory; and Passon *et. al.*¹⁴ studied the effect of the electrolyte anion on redox properties of (bis)(viologen)s, suggesting the influence is more pronounced for the highly charged *tetra*-cationic bis-viologen species. Bis(viologen)s have been employed in multiple applications. Their use in host-guest systems was studied by Yuan *et. al.*¹⁵ and Madasamy *et. al.*¹⁶ with cucurbituril and calixarene, respectively, and the application in photocatalysis was studied by Hiraishi *et. al.*¹⁷ with bis(viologen)-linked ruthenium complexes, who suggested that a two-step electron transfer from the photoexcited state of ruthenium complexes to bis(viologen) may occur.

The spin states of reduced bis(viologen)s can be switched by host-guest interaction with cucurbit[7]uril and a tighter-binding guest, and the process is reversible (Figure 5.1).¹⁸ The successful switch from diamagnetic diradical dimer to stable paramagnetic diradical form by host-guest interaction indicates that the bridge bonding of two viologen units is weak enough to be reverted with small force, such as mechanical strain. Here, we suggest to combine elements of mechanoresponsivity and electroresponsivity in these materials. By incorporation of bis(viologen)s into a cross-linked network we aim to obtain a hydrogel which undergoes highly interesting nonlinear behavior resulting from coupling of volume transitions with diffusion of redox reactants.

Cyclic voltammetry (CV) is a straightforward way for the determination of the redox potentials of viologens. In electrochemistry, the Nernst equation (**Eq. 5.1**) is usually used to determine the formal potential ($E^{0'}$) and standard potential (E^0) for the investigated redox reaction based on the chemical activities of substrates, which at low activities can be replaced with its concentration (**Eq. 5.2**). At the potential in a cyclic voltammogram where the concentration of the reduced form ([Red]) is equal to the concentration of the oxidized form ([Ox]), $E^{0'} = E^0$ for a reversible process. For a reversible redox couple in CV measurements, the equimolar concentrations of reduced and oxidized species occur at the midpoint between the anodic and cathodic waves, therefore E^0 can easily be determined using the anodic (E_{pa}) and cathodic (E_{pc}) peak potentials according to **Eq. 5.3**.

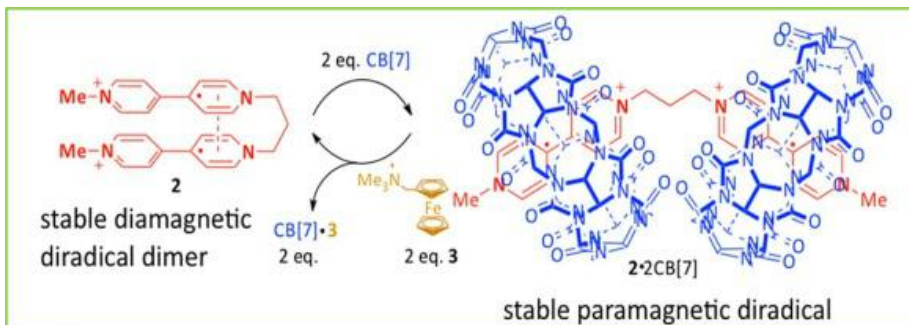


Figure 5.1. Schematic illustration of the reversible switch of reduced bis(viologen) between diamagnetic diradical dimer and paramagnetic diradical form by cucurbit[7]uril (CB[7]) with host-guest interaction. Reprinted with permission from ref. [18]

$$E^{0'} = E^0 - \frac{RT}{nF} \ln \frac{\alpha_{\text{Red}}}{\alpha_{\text{Ox}}} \quad (\text{Eq. 5.1})$$

$$E^{0'} = E^0 - \frac{RT}{nF} \ln \frac{[\text{Red}]}{[\text{Ox}]} \quad (\text{Eq. 5.2})$$

wherein R is the universal gas constant, T is the temperature in Kelvin, n is the number of moles of electrons transferred in the redox reaction, F is the Faraday constant, α_{Red} and α_{Ox} are the chemical activities of reduced and oxidized form, respectively, and $[\text{Red}]$ and $[\text{Ox}]$ are the concentrations of the reduced and oxidized form, respectively.

$$E^0 = \frac{E_{\text{pa}} + E_{\text{pc}}}{2} \quad (\text{Eq. 5.3})$$

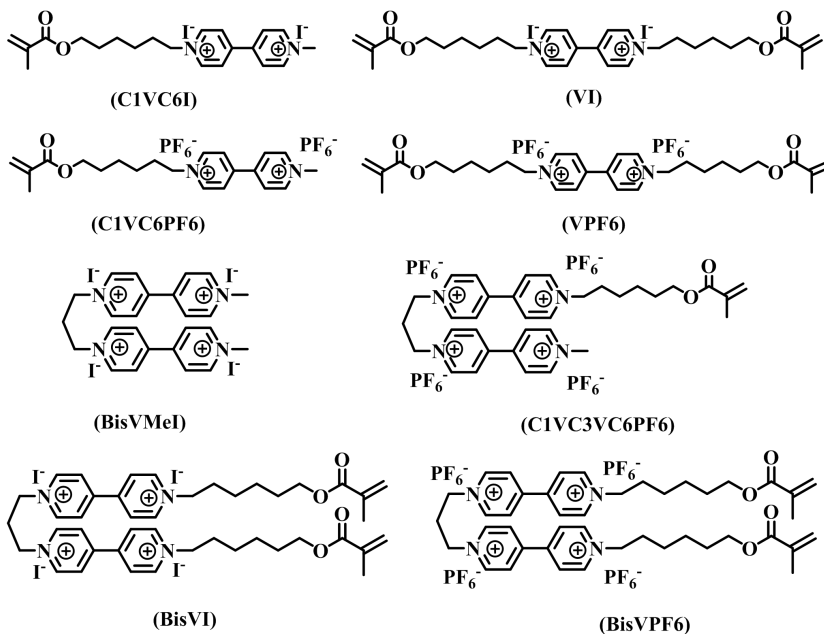
wherein anodic (E_{pa}) and cathodic (E_{pc}) are the potentials of anodic and cathodic peaks, respectively.

In this Chapter, several (a)symmetric viologens and/or bis(viologen)s (abbreviated to (bis)(viologen)s) with different counterions were synthesized, and the Gibbs free energy and the reversibility of the redox reaction, the equilibrium constant of the dimerization of radical cations for the bis(viologen)s, and the comproportionation constants for all (bis)(viologen)s were investigated with CV, and the

temperature-dependent dimerization of (bis)(viologen)s were studied with ESR. The incorporation of polymeric bis(viologen)s into a network is reported, and attempts to shift the dimerization equilibrium of the radical cation of bis(viologen) cross-linkers with mechanical force are discussed.

5.2 Electrochemistry of viologen and its derivatives

To study the electrochemical properties of viologens and bis(viologen)s, a series of compounds was prepared : asymmetric viologen C1VC6I and C1VC6PF6, symmetric viologen C6VC6I and C6VC6PF6, asymmetric bis(viologen) C1VC3VC6PF6, symmetric bis(viologen) BisVI and BisVVPF6, and BisVMel as reference. The structure of the synthesized (bis)(viologen)s is showed in Scheme 5.2.



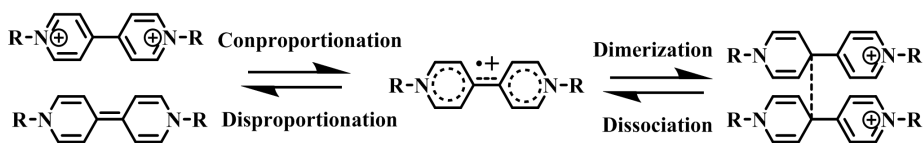
Scheme 5.2. The structures of synthetic viologens and bis(viologen)s

Electrochemical measurements (cyclic voltammetry (CV)) were performed with 0.1 M NBu_4PF_6 in anhydrous acetonitrile as electrolyte solution at 5×10^{-4} mol/L for viologens or 2.5×10^{-4} mol/L for bis(viologen)s. The ferrocene/ferrocenium redox couple was used as internal reference. Potentials and currents after normalization

with ferrocene/ferrocenium internal reference are listed in Table 5.1 and 5.2. According to **Eq. 5.3**, the formal potential ($E^{0'}$) (or standard potential (E^0), because the CV measurements were performed at low concentration, $E^{0'}$ can be replaced by E^0 in this work) of each reduction of every compound are listed in Table 5.1 and 5.2: reduction of dications to radical cations, takes place at formal potentials around -0.8 V and -0.7 V for viologens and bis(viologen)s, respectively; while reduction of radical cations to neutral molecules, occurs at potentials around -1.25 V for all (bis)(viologen)s. According to **Eq. 5.4**, the differences of the formal potentials of two reductions for each compound have been determined and are listed in Table 5.2: the values of ΔE are around 0.43 V and 0.56 V for viologens and bis(viologen)s, respectively. The stability of the radical cations with respect to disproportionation (Seen Scheme 5.3) is expressed by their comproportionation constants (k_{comp}), which were calculated according to **Eq. 5.4**, in which R is the universal gas constant, T is the temperature in Kelvin, F is the Faraday constant, and k_{comp} is the comproportionation constant.

$$\Delta E = E_1^{0'} - E_2^{0'} = \frac{RT}{F} \ln k_{comp} \quad (\text{Eq. 5.4})$$

Table 5.1 shows that the values of k_{comp} are quite large with values in the order of 10^7 and 10^9 for viologens and bis(viologen)s, respectively, suggesting that little disproportionation occurs in both systems and that the radical cations obtained from bis(viologen)s are more stable against disproportionation than those from viologens.



Scheme 5.3. The possible conversion of the radical cation from (bis)(viologen)s

The stability of the radical cations of bis(viologen)s is influenced significantly by the intramolecular stacking dimerization. Intramolecular dimerization of bis(viologen)s stabilizes the bis(radical cation) relative to the neutral state and the bis(dication), reflected in a lowering of the formal reduction potential of bis(viologen)s and a higher comproportionation constant than for viologens. For viologens, at the experimental concentration 5×10^{-4} mol/L, dimerization of the

radical cation is negligible, while for bis(viologen)s, the local concentration is much higher than the bulk concentration, and intramolecular dimerization is favored, leading to a lower reduction potential.

The energy diagram of BisVI (Scheme 5.4) can be used to provide the Gibbs free energy for dimerization if the free energy of the open form of the bis(radical cation) is known. This energy can be calculated under the assumption that the change in electrostatic repulsion for two consecutive reduction steps of the bis(viologens) are the same. The difference in total free energy change upon full reduction of the viologen and the bis(viologen) is 9.4 kJ/mol, and therefore the bis(radical cation) is calculated to be 4.7 kJ/mol less stable than the the mono(radical cation) according to **Eq. 5.5**:

$$\begin{aligned}\Delta G_{er}^0 &= \frac{1}{2}(\Delta_r G_{mi}^0 - \Delta_r G_{bi}^0) \\ \Delta_r G_{mi}^0 &= \Delta_r G_{mi-1}^0 + \Delta_r G_{mi-2}^0 \\ \Delta_r G_{bi}^0 &= \Delta_r G_{bi-1}^0 + \Delta_r G_{bi-2}^0\end{aligned}\quad (\text{Eq. 5.5})$$

Wherein the subtitle *er* refers to electrostatic repulsion, *r* refers to redox reaction, *m* refers to viologens, *b* refers to bis(viologen)s, *i* refers to *ith* (bis)(viologen), 1 refers to the first reduction, and 2 refers to the second reduction.

Subsequently, based on the calculated Gibbs free energy of the first reduction for viologens, the Gibbs free energy for the dimerization was estimated according to **Eq. 5.6**:

$$\Delta G_{b-d}^0 = \Delta_r G_{b-1}^0 - \Delta_r G_{b-2}^0 = \Delta_r G_{b-1}^0 - (\overline{\Delta_r G_{m-1}^0} + \Delta G_{er}^0) \quad (\text{Eq. 5.6})$$

Wherein the subtitle *b* refers to bis(viologen)s, *d* refers to dimerization, *r* refers to redox reaction, *m* refers to viologens, *er* refers to electrostatic repulsion, 1 refers to the first reduction, and 2 refers to the second reduction.

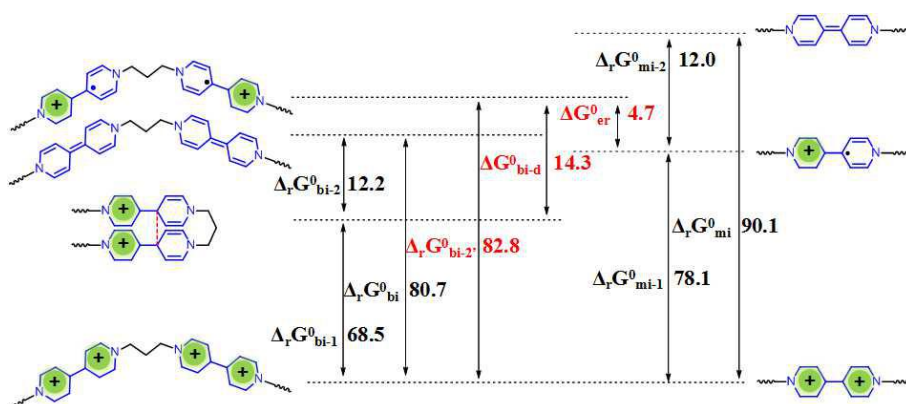
Equilibrium constants were calculated according to **Eq. 5.7** and **Eq. 5.8**:

$$\Delta G^0 = -RT \ln K_{\text{dim}} \quad (\text{Eq. 5.7})$$

$$K_{\text{dim}} = e^{\frac{-\Delta G^0}{RT}} \quad (\text{Eq. 5.8})$$

Wherein R is the universal gas constant, T is the temperature in Kelvin, K_{dim} is the dimerization equilibrium constant, ΔG^0 is the standard free Gibbs energy of the equilibrium.

It can be seen in Table 5.3 that the estimated equilibrium constants for bis(viologen)s in this work are 200-400 in acetonitrile solution based on experimental results and estimated calculations. The dimerization equilibrium constants in non-aqueous solution for bis(viologen)s have rarely been reported. Bucher and co-workers¹⁹ reported the estimated equilibrium constants for two ferrocene-based bis(viologen)s at 1248, and 2756 in DMF solution based on a similar calculation.



Scheme 5.4. The energy diagram of typical bis(viologen) (BisVI) and viologen (VI) and their reduced forms: the values in the scheme are given as kJ/mol, black (obtained from CV results) and red (obtained based calculation).

Table 5.1 The electrochemical properties of various (bis)(viologen)s in acetonitrile (part 1)

	Dication to radical cation							$\Delta_r G^0_1/$
	E_{c1}/V	E_{a1}/V	$E^{0'}_1/V$	$\Delta E_{p1}/mV$	$I_{pc1}/\mu A$	$I_{pa1}/\mu A$	$ I_{pa1}/I_{pc1} $	(kJ/mol)
C1VC6I	-0.7812	-0.8520	-0.8166	70.8	4.2397	-3.9841	0.94	78.8
C1VC6PF6	-0.7788	-0.8521	-0.8155	73.3	5.9557	-6.4571	1.11	78.7
VI	-0.7739	-0.8447	-0.8093	70.8	3.4171	-3.1573	0.92	78.1
VPF6	-0.7751	-0.8435	-0.8093	68.4	4.4030	-4.7466	1.08	78.1
C1VC3VC6PF6	-0.6921	-0.7360	-0.7141	43.9	5.4352	-5.4657	1.00	68.9
BisVI	-0.6872	-0.7336	-0.7104	46.4	4.2082	-3.6293	0.86	68.5
BisVPF6	-0.6994	-0.7483	-0.7239	48.9	5.4596	-5.2986	0.97	69.8
BisVMeI	-0.7092	-0.7361	-0.7227	26.9	6.0212	-5.7303	0.95	69.7

Table 5.2 The linear fitting of the function of $I \sim v^{1/2}$ (part 1)

	$I_{pc1} (A) \sim v^{1/2} ((Vs^{-1})^{1/2})$				$I_{pa1} (A) \sim v^{1/2} ((Vs^{-1})^{1/2})$			
	$B \times 10^5$	$h \times 10^7$	R^2	$D \times 10^{12}/(cm^2s^{-1})$	$B \times 10^5$	$h \times 10^7$	R^2	$D \times 10^{12}/(cm^2s^{-1})$
C1VC6PF6	2.0957	-9.8534	0.998	12.3	-2.2327	9.1861	0.997	14.0
VPF6	1.3834	0.7592	0.999	5.36	-1.4845	-0.8761	>0.999	6.18
C1VC3VC6PF6	1.8004	-1.8117	>0.999	9.09	-1.7470	-0.0517	>0.999	8.56
BisVPF6	1.7673	-1.2148	>0.999	8.76	-1.6549	-0.8116	>0.999	7.68

Table 5.1 The electrochemical properties of various (bis)(viologen)s in acetonitrile (part 2)

	Radical cation to neutral form							$\Delta_r G^{0_2}/$ (kJ/mol)	$\Delta E/V$	k_{comp}
	E_{c2}/V	E_{a2}/V	E^{0_2}/V	$\Delta E_{p2}/mV$	$I_{pc2}/\mu A$	$I_{pa2}/\mu A$	$ I_{pa2}/I_{pc2} $			
C1VC6I	-1.2109	-1.2841	-1.2475	73.2	4.7815	-4.5411	0.95	12.0	0.4309	1.92×10^7
C1VC6PF6	-1.2061	-1.2793	-1.2427	73.2	5.8273	-6.0805	1.04	12.0	0.4273	1.67×10^7
VI	-1.2084	-1.2792	-1.2438	70.8	3.4711	-3.4432	0.99	12.0	0.4345	2.21×10^7
VPF6	-1.2097	-1.2830	-1.2464	73.3	4.4466	-4.4684	1.00	12.0	0.4371	2.45×10^7
C1VC3VC6PF6	-1.2560	-1.3000	-1.2780	44.0	4.9250	-5.1811	1.05	12.3	0.5640	3.42×10^9
BisVI	-1.2463	-1.2903	-1.2683	44.0	3.5855	-3.2872	0.92	12.2	0.5579	2.70×10^9
BisVPF6	-1.2609	-1.3049	-1.2829	44.0	4.7906	-5.0692	1.06	12.4	0.5591	2.83×10^9
BisVMeI	-1.2634	-1.3049	-1.2842	41.5	5.5176	-5.8428	1.06	12.4	0.5615	3.10×10^9

Table 5.2 The linear fitting of the function of $I \sim v^{1/2}$ (part 2)

	$I_{pc1} (A) \sim v^{1/2} ((Vs^{-1})^{1/2})$				$I_{pa1} (A) \sim v^{1/2} ((Vs^{-1})^{1/2})$			
	$B \times 10^5$	$h \times 10^7$	R^2	$D \times 10^{12}/(cm^2s^{-1})$	$B \times 10^5$	$h \times 10^7$	R^2	$D \times 10^{12}/(cm^2s^{-1})$
C1VC6PF6	1.9613	-6.2070	0.992	10.7	-2.0495	5.9859	0.993	11.8
VPF6	1.3180	2.6954	>0.999	4.87	-1.3592	-2.1482	>0.999	5.18
C1VC3VC6PF6	1.5248	1.5626	>0.999	6.52	-1.5429	-3.0495	>0.999	6.67
BisVPF6	1.3596	4.6876	>0.999	5.18	-1.5118	-2.5219	>0.999	6.41

Table 5.3 The estimated dimerization equilibrium constants of bis(viologen)s

	$\Delta_r G^{0_1}/$	$\Delta_r G^{0_2}/$	$\Delta_r G^0/$	$\Delta G^{0_{b-d}}/$	K_{dim}
	(kJ/mol)	(kJ/mol)	(kJ/mol)	(kJ/mol)	
C1VC3VC6PF6	68.9	12.3	81.2	-14.2	307
BisVI	68.5	12.2	80.7	-14.6	361
BisVPF6	69.8	12.4	82.2	-13.3	214
BisVMeI	69.7	12.4	82.1	-13.4	223

In electrochemical systems, CV curves can provide information on the reversibility of the reaction with $|I_{pa}/I_{pc}|$, the differences of the cathodic and anodic peak potentials, and the relation between the peak current I_p vs. the square root of the scan rate $v^{1/2}$. According to **Eq. 5.9**, the differences of the cathodic and anodic peak potentials for each redox reaction are determined and listed in Table 5.1 and 5.2. It can be seen that for viologens, the differences are around 70 mV, suggesting a one electron reduction occurs. For the multielectron reduction in bis(viologen)s, the differences are around 45 mV. However, the difference for the first reduction of bisVMeI is only 27 mV, suggesting that the reversibility of the first reduction for bisVMeI is much better than others. All the differences are relatively small, so it can be concluded that both reductions for all (bis)(viologen)s are reversible, and it is further evident by $|I_{pa}/I_{pc}|$ and the linear relation between I_p vs. $v^{1/2}$. All values of $|I_{pa}/I_{pc}|$ are close to 1, and the linear fitting of I_p vs. $v^{1/2}$ is excellent with R^2 larger than 0.99. Furthermore, the peak potentials do not change, also suggesting the good reversibility of the redox reaction.

$$\Delta E_p = E_{pc} - E_{pa} \quad (\text{Eq. 5.9})$$

wherein E_{pc} is the cathodic peak potential, E_{pa} is the the anodic peak potential.

From theory, it is expected that for the reversible reaction under conditions of semi-infinite planar diffusion, the peak current of reversible reactions will depend on the square root of the scan rate (**Eq. 5.10**). From the slope of a linear plot of peak

current vs. the square root of the scan rate, the diffusion coefficient can be determined with **Eq. 5.11**. For the current measurements, the scan rate was varied from 10 to 400 mVs⁻¹. The calculated diffusion constants are listed in Table 5.2. The diffusion constants of four (bis)(viologen)s with PF₆⁻ as counterion are around 10⁻¹² cm²s⁻¹. The diffusion constants of the asymmetric bisviologens are larger than that of the symmetric ones. For the symmetric ones, the long aliphatic tails slow down the diffusion. In the viologen systems because the molecule itself is relatively small, the influence becomes more profound, and the diffusion constant of C1VC6PF6 is double of that of C6VC6PF6 while in bis(viologen) systems, the diffusion constant of C1VC3VC6PF6 is only a bit larger than that of BisVPPF6.

$$I_p = 2.69 \times 10^5 n^{3/2} AD^{1/2} c \nu^{1/2} \quad (\text{Eq. 5.10})$$

$$D = \left(\frac{B}{2.69 \times 10^5 n^{3/2} A c} \right)^2 \quad (\text{Eq. 5.11})$$

wherein I_p is the peak current, n is the number of the electrons transferred in the reaction, A is the area of the electrode, D is the diffusion constant, c is the total concentration of the redox substrates, ν is the scan rate, and B is the slope of the linear function of between I_p vs. $\nu^{1/2}$.

5.3 ESR dimerization studies of (bis)(viologen)s

The peak potential differences of the two reduction steps for bis(viologen)s in CV are larger than for viologens, as described in section 5.2. The difference is attributed to the dimerization of the radical cation; however, more evidence is needed to prove the dimerization. Dimerization of the radical cation was studied with ESR at different temperatures.

The radical cations usually give significant ESR signals, while the dimers/pimers are ESR silent, and the fast equilibrium of the dissociation and dimerization can also give a broad signal in ESR spectra. As shown in Figure 5.2, at low temperature, both BisVI and BisVMeI showed obvious broad signals. The difference is that BisVI also showed some slight hyperfine signals while BisVMeI did not. With increasing temperature, the hyperfine signals from both bis(viologen)s became stronger, and the broad signals became unclear compared with the those at relatively low temperature. For the hyperfine structures of both ESR spectra, there are perfect 27 lines, consistent with the results from literature²⁰.

For BisVI, the hyperfine splitting is already obvious at low temperature, and the hyperfine structure in the spectra clearly demonstrates the presence of unpaired electrons. When temperature increases, the equilibrium between the dimers/pimers and the diradical forms moves to the direction of radical cations (Scheme 5.5), and the signals became stronger. Reference compound BisVMel, only showed a broad signal at low temperatures, suggesting that most of the radical cations are dimerized, while at 80 °C, the hyperfine structure emerged, suggesting that the dissociation of the dimers/pimers started. Dimers/pimers formed from BisVMel are more stable than those formed from BisVI, which might be attributed to the long aliphatic tails that provide more flexibility to BisVI.

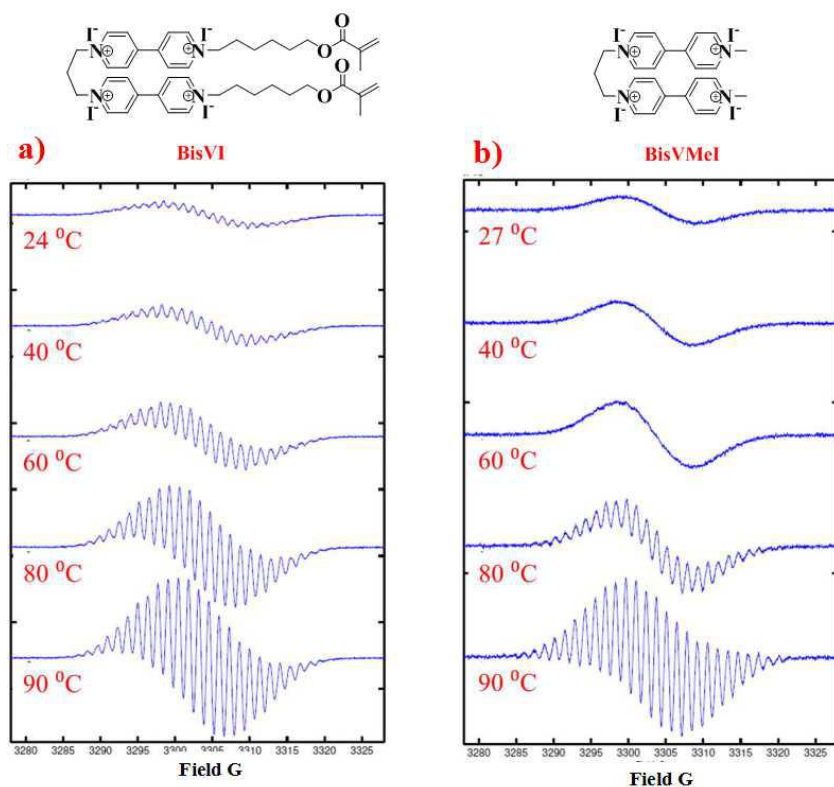
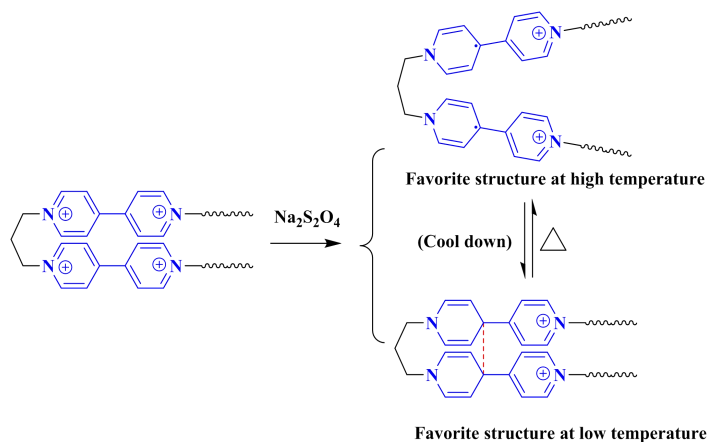


Figure 5.2. The temperature-dependence of ESR signals in DMSO: a) BisVI, and b) BisVMel



Scheme 5.5. The equilibrium of the dimerization and dissociation of the radical cation form of bis(viologen)s

5.4 Mechanical activation of diamagnetic bis(viologen)

Polymeric BisVI as crosslinker was polymerized with 2-hydroxyethyl methacrylate (HEMA) as monomer, phenylbis(2,4,6-trimethylbenzoyl)phosphine oxide (PI) as photoinitiator, poly(ethylene glycol) diacrylate (PEGDA, $M_n = 700$ Da) as co-crosslinker to obtain film networks. The films are slightly yellowish with bis(viologen) while without bis(viologen), the film is colorless, as can be seen in Figure 5.3, and with addition of reductant, sodium dithionite, within minutes, the network with bis(viologen) became purple while the network without bis(viologen) remained colorless.

The networks after reduction with sodium dithionite were kept in pH 9.6 aqueous buffer solution under N_2 atmosphere. As can be seen in Figure 5.3, before and after reduction, the UV-vis absorption of the networks changed differently: the absorption of the network without bis(viologen) did not change while with bis(viologen), before reduction, the absorption was zero, but after reduction, the absorption reached a maximum at around 850 nm. The network with bis(viologen) after reduction was further placed between two glass plates and compressed with two metal clamps in order to induce opening of the dimers by straining the network (Seen Figure 5.4). The UV-vis absorption of the compressed film did not show any clear changes. A possible explanation is that the open and closed forms of reduced bis(viologen) changes very little at very low concentration,²¹ and especially when the efficiency of the mechanically induced switch between two forms is low, detection of the

open-formed isomer is not possible with UV-*vis*. Further trials were performed with ESR, however, because the reduced forms are very sensitive to oxygen, these measurements were not successful.

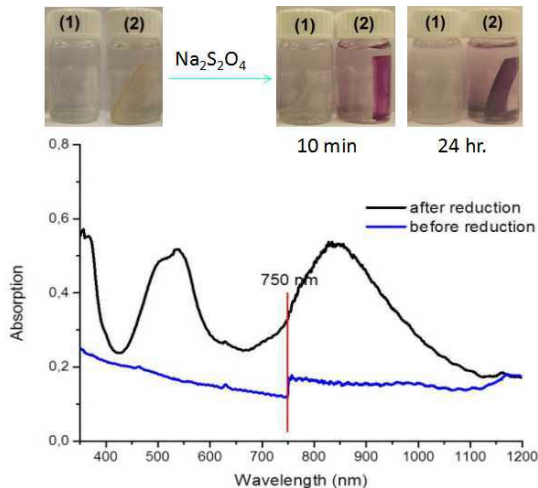


Figure 5.3. The images of prepared film networks without (1) and with (2) BisVI before and after reduction and the corresponding UV-*vis* absorption spectra of the network with BisVI before and after reduction

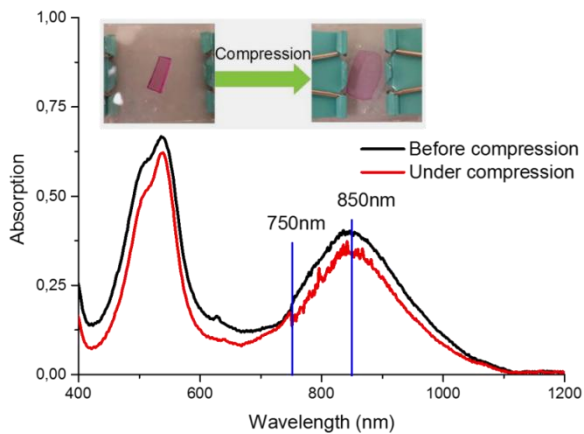


Figure 5.4. The normalized UV-*vis* absorption spectra of the film network with BisVI before and under compression

5.5 Conclusion

A Cyclic voltammetry study on viologen and its derivatives demonstrates that the (bis)(viologen)s have reversible redox reactions, and differences of the formal potentials of two reductions are around 0.43 V and 0.56 V for viologen and bis(viologen)s, respectively. The comproportionation constants are quite large in the order of 10^7 and 10^9 for viologens and bis(viologen)s, respectively, suggesting that little disproportionation take places in both systems, and the radical cations in bis(viologen)s systems are much more stable than those in viologens systems. The estimated dimerization equilibrium constants in acetonitrile are in the range of 200-400. The diffusion constants of the asymmetric (bis)(viologen)s with one aliphatic tail are larger than that of symmetric ones with two tails for the long aliphatic tails slow down the diffusion. The temperature-dependent ESR measurements support dimerization in bis(viologen)s and indicates a very fast equilibrium between open and closed forms. A polymeric bis(viologen) was incorporated into hydrogel networks, and was reduced successfully, but the limitation of the characterization prevented us from drawing further conclusions on mechanoactivation of reduced diamagnetic bis(viologen)s.

5.6 Experimental

5.6.1 Materials and instrumentation

Unless otherwise specified, reagent and solvents were purchased from Sigma-Aldrich, Merck, or Acros and used without further purification. Dry THF was freshly taken from an MBRAUN Solvent Purification System (MB SPS-800), deuterated solvents were obtained from Cambridge Isotopes Laboratories.

NMR spectra were recorded on a 400 MHz (100 MHz for ^{13}C) Varian Mercury VX spectrometer at room temperature using residual protonated solvent signals as internal standards (^1H : $\delta(\text{CDCl}_3) = 7.26$ ppm, $\delta(\text{CD}_2\text{Cl}_2) = 5.32$ ppm, $\delta((\text{CD}_3)_2\text{SO}) = 2.50$ ppm; ^{13}C : $\delta(\text{CDCl}_3) = 77.16$ ppm, $\delta(\text{CD}_2\text{Cl}_2) = 53.84$ ppm, $\delta((\text{CD}_3)_2\text{SO}) = 39.52$ ppm).

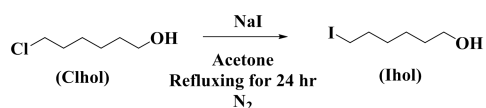
Matrix assisted laser desorption/ionisation time-of-flight mass spectrometry (MALDI-TOF MS) was performed on a Autoflex Speed MALDI-MS instrument (Bruker, Bremen, Germany) equipped with a 355 nm Nd:YAG smartbeam laser. MALDI-TOF MS experiments were performed by spotting samples on a MTP 384 target ground steel plate using an α -cyano-4-hydroxycinnamic acid (CHCA) (Fluka,

Switzerland) matrix. Samples were 1:1 premixed with CHCA in 50/50 acetonitrile/water supplemented with 0.1% v/v trifluoroacetic acid (TFA). Mass spectra were acquired in reflector positive ion mode by summing spectra from 500 selected laser shots. The MS spectra were calibrated with cesium triiodide of known masses.

Electrochemical measurements (cyclic voltammetry) were performed under an inert atmosphere with an Eco Chemie Autolab PGSTAT 30 potentiostat/galvanostat using a three-electrode microcell with a Pt working electrode, A platinum working electrode (2 mm in diameter), a silver counter electrode and a silver wire coated with silver chloride (Ag/AgCl) quasi-reference electrode. The reference electrode was calibrated against ferrocene/ferrocenium as an external standard.

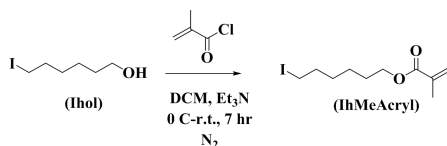
5.6.2 Synthetic procedure and characterization

6-iodohexan-1-ol (Ihol)



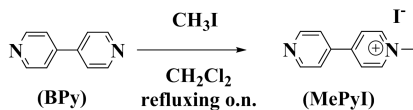
To a 3-necked round-bottomed flask with a magnetic stirring bar, the mixture of 6-chlorohexanol (Clhol, 10.93 g, 0.08 mol) and sodium iodide (35.97 g, 0.24 mol) in 70 mL acetone were added and refluxed under nitrogen atmosphere for 24 hrs. The mixture was filtered to remove the excess sodium iodide and the generated sodium chloride. For the filtrate, the solvent was evaporated giving the raw product. The raw solid product was dissolved in dichloromethane, filtered and the solvent was evaporated. This dissolving-filtration-evaporation process was repeated twice. The resulting oil was dissolved in a 1:1 mixture of diethyl ether/hexane and then filtered again. The solution was washed with water and brine. The organic layer was dried with MgSO₄, filtered and the solvent evaporated in vacuum giving a red liquid (yield: 74.6%). ¹H NMR (CDCl₃, 400 MHz, ppm): 3.58 (t, 2H), 3.15(t, 2H), 2.15 (s, 1H), 1.79 (m, 2H), 1.53 (m, 2H), 1.37 (m, 4H); ¹³C NMR (CDCl₃, 400 MHz, ppm): 62.72, 33.41, 32.45, 30.26, 24.72, 7.15.

6-iodohexyl methacrylate (IhMeAcryl)



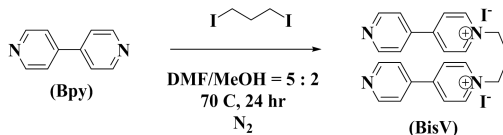
Ihol (4.56 g, 0.020 mol) was placed in a 3-necked round flask with a magnetic stirring bar and dissolved in 35 mL dichloromethane, to which, triethylamine (7 mL, 0.050 mol) was added and stirring in an ice bath for several minutes. When the solution cooled down, methacryloyl chloride (3.5 mL, 0.036 mol) was added dropwise within 10 mins. at 0 °C under nitrogen atmosphere. After the methacryloyl chloride was completely added in the reaction system, the reaction mixture was removed to the room temperature and kept stirring for 7 hr. After reaction, the generated triethylammonium chloride was removed by filtration. The filtrate was washed by water, saturated NaHCO₃ aqueous solution, 2 mol/L cold NaOH aqueous solution, and NaCl solution sequentially. The organic layer was dried with MgSO₄, filtered and the solvent evaporated in vacuo giving the raw product. The raw product was dissolved in acetone, isolated from water, and then dissolved in acetone again. The solution was dried with MgSO₄, filtered and the solvent was evaporated giving the final product (yield: 78.6%). ¹H NMR (CDCl₃, 400 MHz, ppm): 6.06 (s, 1H), 5.52 (s, 1H), 4.11 (t, 2H), 3.16 (t, 2H), 1.91 (t, 3H), 1.81 (m, 2H), 1.66 (m, 2H), 1.40 (m, 4H); ¹³C NMR (CDCl₃, 400 MHz, ppm): 167.44, 136.44, 125.25, 64.52, 33.31, 30.12, 28.44, 24.99, 18.34, 6.83.

1-methyl-[4,4'-bipyridin]-1-ium iodide (MePyI)



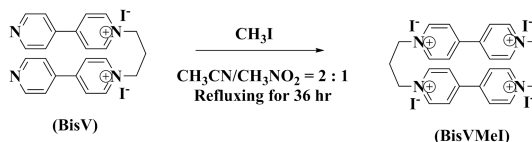
Following the modified literature procedure²²: Methyl iodide (0.8 mL, 12 mmol, 1.2 equiv.) was added to a solution of 4,4'-bipyridyl (1.562 g, 10 mmol) in dichloromethane and the reaction mixture was kept refluxing overnight. The produced yellow precipitate was isolated by filtration and subsequently purified by recrystallization from methanol, washed with diethyl ether three times, dried in vacuum to yield the targeted compound. (yield: 92%). ¹H NMR (DMSO-*d*₆, 400 MHz, ppm): 9.12 (d, 2H), 8.85, (d, 2H), 8.60 (d, 2H), 8.02 (d, 2H), 4.36 (s, 3H).

1',1''-(propane-1,3-diyl)bis([4,4'-bipyridin]-1-ium) iodide (BisVI)



According to the literature procedure¹⁷, BisV was prepared by *N*-alkylation of 4,4'-bipyridyl. In a 3-necked round-bottomed flask with a magnetic stirring bar, 4,4'-bipyridyl (Bpy, 2.46 g, 0.015 mol) was dissolved in 10 mL of DMF/methanol (v/v = 5:2) mixture, to which, 1,3-diiodopropane (1.33 g, 0.005 mol) was added dropwise. Then a reflux condenser was fitted to the flask, and the reaction was heated to 70 °C under nitrogen atmosphere and kept stirring at 70 °C for 24 hr. Toluene was then added to the solution, and the solvents were removed by filtration. The resulting solid was washed with acetone and chloroform, after which the solid was dried in vacuum. After drying, the solid was hot filtrated again using 95% ethanol and then dried to get the targeted compound (yield: 67.5%). ¹H NMR (DMSO-*d*₆, 400 MHz, ppm): 9.106 (d, 4H), 8.80 (d, 4H), 8.54 (d, 4H), 7.95 (d, 4 H), 4.73 (t, 4H), 2.68 (t, 2H); ¹³C NMR (DMSO-*d*₆, 400 MHz, ppm): 153.06, 151.55, 146.06, 141.20, 125.92, 122.35, 57.65, 31.95. MALDI-TOF: 481.10, [M-I]⁺.

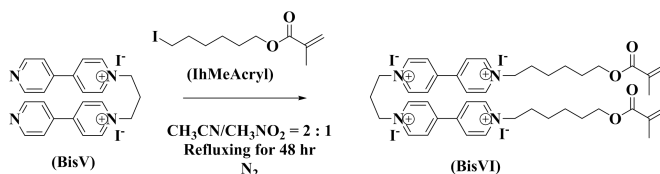
1,1''-(propane-1,3-diyl) bis((1-methyl)-[4,4'-bipyridine]-1,1'-diium) iodide (BisVMeI)



BisVMeI was prepared following a modified literature procedure¹⁴, 0.6083 g of BisV (1 mmol) was added to a 50 mL round-bottomed flask charged with a stir bar fit with a reflux condenser, and dissolved in 15 mL of mixture of acetonitrile/nitromethane (v/v = 2:1). Then, 0.35 mL of methyl iodide (5 mmol, 2.5 equiv.) was added to the solution and the reaction was kept refluxing for 36 h. Then, most of the solvent was removed under a vacuum, and then crude product was obtained by predication from diethyl ether. The solid was washed with diethyl ether three times and acetone once to remove any unreacted starting material and dried in vacuum to afford the red-colored salt. (yield: 71.2%). ¹H NMR (DMSO-*d*₆, 400

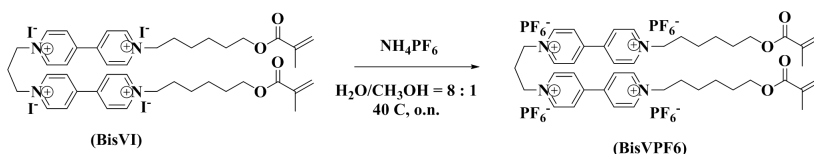
MHz, ppm): 9.45 (d, 2H), 9.32 (d, 2H), 8.89 (d, 2H), 8.81 (d, 2H), 4.88 (t, 4H), 4.46 (s, 6H), 2.81 (p, 2H); ¹³C NMR (DMSO-*d*₆, 400 MHz, ppm): 149.23, 148.34, 147.20, 146.56, 127.10, 126.53, 58.02, 48.61, 32.03.

1,1''-(propane-1,3-diyl)bis(1-(6-(methacryloyloxy)hexyl)-[4,4'-bipyridine]-1,1'-diium) iodide (BisVI)



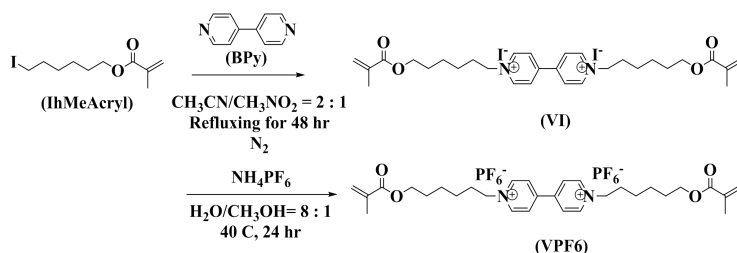
In a 3-necked flask with a reflux condenser, BisV (0.61 g, 1 mM) and IhMeAcryl (0.77 g, 2.5 mM) was added to 15 mL of mixture of acetonitrile/nitromethane (v/v = 2:1) under N₂ atmosphere. The reaction was refluxing for 48 hr. After the reaction mixture cooled down, it was poured into a mixture of hexane/ethyl acetate (v/v = 1:1). The solid was isolated by filtration, and then washed by 1:1 hexane/ethyl acetate three times, giving the raw product without further purification (yield: 65.8%). ¹H NMR (DMSO-*d*₆, 400 MHz, ppm): 9.44 (dd, 8H), 8.89 (d, 4H), 8.83 (d, 4H), 6.01 (s, 2 H), 5.58 (s, 2H), 4.86 (t, 4H), 4.71 (t, 4H), 4.11 (t, 4H), 2.80 (dt, 2H), 2.02 (p, 4H), 1.88 (t, 6H), 1.64 (m, 4H), 1.39 (m, 8H); ¹³C NMR (DMSO-*d*₆, 400 MHz, ppm): 167.25, 149.29, 148.80, 146.54, 146.32, 136.49, 127.10, 126.11, 64.52, 61.38, 58.12, 32.01, 31.13, 28.31, 25.25, 18.49.

1',1'''-(propane-1,3-diyl)bis(1-(6-(methacryloyloxy)hexyl)-[4,4'-bipyridine]-1,1'-diium) hexafluorophosphate(V) (BisVPPF6)



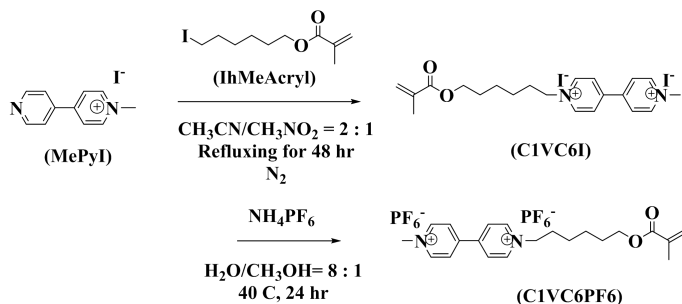
In a 3-necked flask, BisVI (1.2 g, 1 mM) was dissolved in 90 mL of mixture of water/methanol (v/v = 8:1) at 45 °C, to which, NH₄PF₆ (0.978 g, 6 mM) aqueous solution was added to the flask. The reaction was kept stirring at 40 °C overnight. The produced solid was isolated by filtration. And then it was dissolved in acetone. The raw product was obtained by precipitation from water and then from the mixture

of diethyl ether/hexane (v/v = 1:1) respectively. Then it was washed by hexane three times to give the final product (yield: 80.2%). ¹H NMR (DMSO-*d*₆, 400 MHz, ppm): 9.37 (m, 8H), 8.83 (m, 4H), 8.76 (m, 4H), 5.99 (s, 2H), 5.65 (s, 2H), 4.80 (t, 4H), 4.68 (t, 4H), 4.08 (t, 4H), 2.74 (dt, 2H), 1.99 (p, 4H), 1.85 (t, 6H), 1.62 (m, 4H), 1.37 (m, 8H); ¹³C NMR (DMSO-*d*₆, 400 MHz, ppm): 167.015, 149.37, 148.79, 146.55, 146.31, 136.40, 126.98, 126.03, 64.52, 61.41, 58.09, 32.03, 31.07, 28.25, 25.40, 18.45; FT-IR (cm⁻¹): 3081, 1715, 1642, 1173, 816, 554; UV-*vis* : λ_{max} = 261 nm in acetonitrile, ε_{max} = 45 500 L·mol⁻¹ cm⁻¹; MALDI-TOF: [M-PF6]⁺, 1127.36.



1,1'-bis(6-(methacryloyloxy)hexyl)-[4,4'-bipyridine]-1,1'-diium iodide (VI) was synthesized following the procedure to synthesize BisVI by changing the feeding ratio of the start materials. ¹H NMR (DMSO-*d*₆, 400 MHz, ppm): 9.37 (d, 4H), 8.77 (d, 4H), 5.99 (s, 2H), 5.66 (s, 2H), 4.68 (t, 4H), 4.08 (t, 4H), 1.98 (m, 4H), 1.85 (s, 3H), 1.62 (m, 4H), 1.36 (m, 8H); ¹³C NMR (DMSO-*d*₆, 400 MHz, ppm): 167.03, 149.07, 146.23, 136.45, 127.04, 126.07, 64.56, 61.34, 31.05, 28.30, 25.52, 25.30, 18.48; ¹³C NMR (DMSO-*d*₆, 400 MHz, ppm): MALDI-TOF: 494.40, [M-2I+e]⁺.

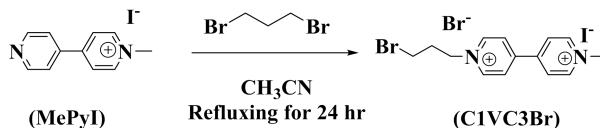
1,1'-bis(6-(methacryloyloxy)hexyl)-[4,4'-bipyridine]-1,1'-diium hexafluorophosphate(V) (V) was synthesized following the procedure to synthesize BisV by changing the feeding ratio of the start materials. ¹H NMR (DMSO-*d*₆, 400 MHz, ppm): 9.36 (d, 4H), 8.75 (d, 4H), 5.99 (s, 2H), 5.66 (s, 2H), 4.66 (t, 4H), 4.08 (t, 4H), 1.98 (m, 4H), 1.85 (s, 3H), 1.62 (m, 4H), 1.36 (m, 8H); ¹³C NMR (DMSO-*d*₆, 400 MHz, ppm): 167.03, 149.03, 146.23, 136.42, 127.05, 126.08, 64.57, 61.23, 31.05, 28.31, 25.52, 25.31, 18.49; MALDI-TOF: 494.39, [M-2PF6+e]⁺.



1-(6-(methacryloyloxy)hexyl)-1'-methyl-[4,4'-bipyridine]-1,1'-dium iodide (C1VC6I) was synthesized following the procedure to synthesize BisVI by changing the feeding ratio of the start materials. ^1H NMR (DMSO- d_6 , 400 MHz, ppm): 9.37 (d, 2H), 9.27 (d, 2H), 8.75 (m, 4H), 5.99 (s, 1H), 5.65 (s, 1H), 4.67 (t, 2H), 4.42 (s, 3H), 4.08 (t, 2H), 1.98 (m, 2H), 1.85 (s, 3H), 1.61 (m, 2H), 1.36 (m, 4H); ^{13}C NMR (DMSO- d_6 , 400 MHz, ppm): 167.02, 151.48, 148.81, 146.64, 141.32, 136.42, 126.56, 125.41, 122.32, 64.59, 61.30, 48.30, 31.06, 28.30, 25.51, 25.31, 18.49. MALDI-TOF: 340.29, $[\text{M}-2\text{I}+\text{e}]^+$.

1-(6-(methacryloyloxy)hexyl)-1'-methyl-[4,4'-bipyridine]-1,1'-dium hexafluorophosphate(V) (C1VC6PF6) was synthesized following the procedure to synthesize BisVFPF6 by changing the feeding ratio of the start materials. ^1H NMR (DMSO- d_6 , 400 MHz, ppm): 9.36 (d, 2H), 9.27 (d, 2H), 8.75 (dd, 4H), 6.01 (s, 1H), 5.67 (s, 1H), 4.68 (t, 2H), 4.43 (s, 3H), 4.10 (t, 2H), 1.99 (p, 2H), 1.87 (t, 3H), 1.64 (m, 2H), 1.38 (m, 4H); ^{13}C NMR (DMSO- d_6 , 400 MHz, ppm): 167.03, 149.05, 148.66, 147.10, 146.24, 136.43, 126.99, 126.53, 126.07, 64.57, 61.33, 48.52, 31.06, 28.30, 25.51, 25.31, 18.48. MALDI-TOF: 485.21, $[\text{M}-\text{PF}_6]^+$.

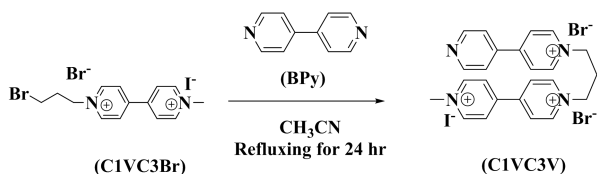
1-(3-bromopropyl)-1'-methyl-[4,4'-bipyridine]-1,1'-dium bromide iodide (C1VC3Br)



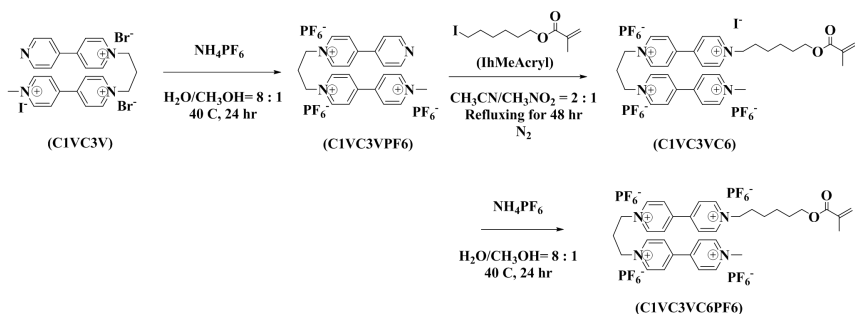
MePyI (2.98 g, 10 mmol) and 1,3-dibromopropane (20.20 g, 100 mmol) were dissolved in 50 mL of acetonitrile, and refluxed for 24 hr. After the mixture cooled down, crude product was obtained by filtration and washed with diethyl ether for

three times. The solid product was then recrystallized from ethanol to reach the pure product. ^1H NMR (DMSO- d_6 , 400 MHz, ppm): 9.46 (d, 2H), 9.33 (d, 2H), 8.88 (d, 2H), 8.79 (d, 2H), 4.84 (t, 2H), 4.45 (s, 3H), 3.61 (t, 2H), 2.57 (m, 2H); ^{13}C NMR (DMSO- d_6 , 400 MHz, ppm): 148.86, 146.87, 126.79, 60.11, 48.51, 33.56, 30.59. MALDI-TOF: 292.09, $[\text{M}-\text{Br}-\text{I}+\text{e}]^+$.

1-(3-([4,4'-bipyridin]-1-ium-1-yl)propyl)-1'-methyl-[4,4'-bipyridine]-1,1'-diium dibromide iodide (C1VC3V)



C1VC3Br (1.5 g, 3mmol) and BPy (4.68 g, 30 mmol) were dissolved in 20 mL of acetonitrile, and refluxed for 24 hr. After the mixture cooled down, crude product was obtained by filtration and washed with acetonitrile twice. The final product was obtained by recrystallization from ethanol. ^1H NMR (DMSO- d_6 , 400 MHz, ppm): 9.29 (m, 6H), 8.79 (m, 8H), 8.05 (d, 2H), 4.77 (m, 4H), 4.42 (s, 3H), 2.70 (q, 2H).



1-(3-([4,4'-bipyridine]-1-ium-1-yl)propyl)-1'-methyl-[4,4'-bipyridine]-1,1'-diium hexafluorophosphate(V) (C1VC3VPF6) was synthesized following the procedure to synthesize BisVPF6 by changing the feeding ratio of the start materials. ^1H NMR (DMSO- d_6 , 400 MHz, ppm): 9.30 (m, 6H), 8.86 (m, 4H), 8.73 (m, 4H), 8.05 (d, 2H), 4.77 (m, 4H), 4.43 (s, 3H), 2.73 (q, 2H).

1-(6-(methacryloyloxy)hexyl)-1'-(3-(1'-methyl-[4,4'-bipyridin]-1,1'-diium-1-yl)propyl)-[4,4'-bipyridine]-1,1'-diium tris(hexafluorophosphate(V)) iodide (C1VC3VC6) was synthesized following the procedure to synthesize BisVI by changing the feeding ratio of the start materials.

1-(6-(methacryloyloxy)hexyl)-1'-(3-(1'-methyl-[4,4'-bipyridin]-1,1'-diium-1-yl)propyl)-[4,4'-bipyridine]-1,1'-diium hexafluorophosphate(V) (C1VC3VC6PF6) was synthesized following the procedure to synthesize BisVPPF6 by changing the feeding ratio of the start materials. ¹H NMR (DMSO-*d*₆, 400 MHz, ppm): 9.36 (m, 6H), 9.29 (d, 2H), 8.83 (m, 4H), 8.76 (m, 4H), 5.99 (s, 1H), 5.66 (s, 1H), 4.79 (m, 4H), 4.68 (m, 2H), 4.43 (s, 3H), 4.08 (t, 2H), 2.73 (m, 2H), 1.99 (m, 2H), 1.85 (s, 3H), 1.62 (m, 2H), 1.38 (m, 4H); ¹³C NMR (DMSO-*d*₆, 400 MHz, ppm): 167.04, 152.34, 151.48, 148.99, 148.62, 147.08, 146.61, 146.23, 141.32, 136.42, 127.02, 126.56, 126.09, 125.41, 122.32, 64.59, 61.30, 48.56, 48.04, 31.06, 28.30, 25.51, 25.31, 18.49; MALDI-TOF: 973.23, [M-PF6]⁺.

Film network

The film networks were prepared with a general procedure. To prepare different films, the addition of the crosslinker changed according to component of the targeted films. The 2-hydroxyethyl methacrylate (HEMA, 98.2wt% or 97.8wt%), BisVI (0 or 0.5wt%), and poly(ethylene glycol) diacrylate (PEGDA, Mn = 700 Da, 1.3wt% or 1.2wt%) were mixed together and stirred with a magnetic stirring bar under N₂ bubbling for half an hour, then under yellow light, phenylbis(2,4,6-trimethylbenzoyl)phosphine oxide (0.5wt%) was added and stirred for another 1 minute, and then 450 mg of the solution was transferred to a Teflon mold, covered with a glass slide, exposed to 256 nm wavelength light with N₂ flow for 15 minutes. Afterwards, the film networks were obtained by soaking in pH 9.6 aqueous buffer solution (0.045 M NaHCO₃/0.0091 M NaOH buffer).

References

- 1 L. Michaelis and E. S. Hill, *J. Gen. Physiol.*, **1933**, 16:859-873
- 2 P. M. S. Monk, *The Viologens*; John Wiley and Sons: New York, **1998**
- 3 C. L. Bird, A. T. Kuhn, *Chem. Soc. Rev.*, **1981**, 10: 49-82
- 4 a) J. Lanzo, M. De Benedittis, B. C. De Simone, D. Imbardelli, P. Formoso, S. Manfredi and G. Chidichimo, *J. Mater. Chem.*, **2007**, 17: 1412-1415; b) M. Grätzel, *Nature* **2001**, 409: 575-576
- 5 a) Y. Takashima, Y. Yuting, M. Otsubo, H. Yamaguchi and A. Harada, *Beilstein J. Org. Chem.* **2012**, 8: 1594-1600; b) F. E. Oddy, S. Brovelli, M. T. Stone, E. J. F. Klotz, F. Ciaciali and H. L. Anderson, *J. Mater. Chem.*, **2009**, 19: 2846-2852; c) M. Juetten, A. Buck, A.H. Winter, *Chem. Commun.*, **2015**, 51: 5516-5519; d) J. W. Park, N. H. Choi, and J. H. Kim *J. Phys. Chem.*, **1996**, 100 (2): 769-774
- 6 a) L. Chen, H. Wang, D. Zhang, Y. Zhou, Z. Li, *Angew. Chem. Int. Ed.* **2015**, 54: 4028-4031; b) R. Kannappan, C. Bucher, E. Saint-Aman, J. Moutet, A. Milet, M. Oltean, E. Metay, S. Pellet-Rostaing, M. Lemaire and C. Chaix, *New J. Chem.*, **2010**, 34: 1373-1386
- 7 a) A. Chira, B. Bucur, M. Radulescu, T. Galaon, G. Radu, *Int. J. Electrochem. Sci.*, **2014**, 9: 4493-4511; b) X. Liu, M. Hao, M. Feng, L. Zhang, Y. Zhao, X. Du, G. Wang, *Applied Energy*, **2013**, 106: 176-183; c) Y. Matsuo, K. Kanaizuka, K. Matsuo, Y. Zhong, T. Nakae, and E. Nakamura, *J. Am. Chem. Soc.* **2008**, 130: 5016-5017
- 8 Z. Wang and N. V. Tsarevsky, *Polym. Chem.*, **2016**, 7: 4402-4410, b) B. Gadgil, E. Dmitrieva, P. Damlin, T. Aaritalo, C. Kvarnstrom, *J Solid State Electrochem* **2015**, 19:77-83.
- 9 C. L. Bird and A. T. Kuhn, *Chem. Soc. Rev.*, **1981**, 10(1): 49
- 10 a) D. G. Whitten, *Acc. Chem. Res.* **1980**, 13: 83-90; b) D. Meisel, W. A. Mulac, M. S. Metheson, *J. Phys. Chem.* **1981**, 85: 179-187; c) J. F. Stargardt, F. M. Hawkrigde, *Anal. Chim. Acta* **1983**, 146: 1-8; d) J. G. Gaudiello, P. K. Ghosh, C. C. Jones, *J. Am. Chem. Soc.* **1985**, 107: 3027-3032; e) O. Johansen, J. W. Loder, W. W.-H. Mau, J. Rabani, W. H. F. Sasse, *Langmuir* **1992**, 8: 2577-2581.
- 11 E. M. Kosower and J. L. Cotter, *J. Am. Chem. Soc.*, **1964**, 86: 5524-5527.
- 12 A. G. Evans, J. C. Evans, and M. W. Baker, *J. Chem. Soc. Perkin 2*, **1977**, 1787-1789.
- 13 S. J. Atherton, K. Tsukahara, and R. G. Wilkins, *J. Am. Chem. Soc.* **1986**, 108: 3380-3385.
- 14 M. Passon, A. Ruff, P. Schuler, B. Speiser, W. Leis, *J Solid State Electrochem* **2015**, 19: 85-101
- 15 L. Yuan, R. Wang, and D. H. Macartney, *J. Org. Chem.* **2007**, 72: 4539-4542
- 16 K. Madasamy, S. Gopi, M. S. Kumaran, S. Radhakrishnan, D. Velayutham, P. M. Mareeswaran, and M. Kathiresan, *Chemistry Select* **2017**, 2: 1175-1182
- 17 T. Hiraishi, T. Kamachi, I. Okura, *J. Photochem. Photobiol. A* **1998**, 116: 119-125
- 18 A.T. Buck, J.T. Paletta, S. Khindurangala, C.L. Beck, A.H. Winter, *J. Am. Chem. Soc.* **2013**, 135, (29): 10594-10597.
- 19 A. Iordache, M. Oltean, A. Milet, F. Thomas, B. Baptiste, E. Saint-Aman, and C. Bucher, *J. Am. Chem. Soc.* **2012**, 134: 2653-2671
- 20 a) M. Lapkowski, G. Biah, *J. Electroanal. Chem.* **1993**, 362: 249-256; b) C. S. Johnson Jr., H. S. M. Gutowsky, *J. Chem. Phys.*, **1963**, 39: 58-62
- 21 M. R. Geraskina, A.T. Buck, and A. H. Winter, *J. Org. Chem.* **2014**, 79: 7723-7727
- 22 Y. S. Park, E. J. Lee, Y. S. Chun, Y. D. Yoon, and K. B. Yoon, *J. Am. Chem. Soc.* **2002**, 124: 7123-7135

Summary

Productive Bond Scission Processes in Polymer Mechanochemistry

Mechanochemistry, defined as the fourth sub-discipline of chemistry based on the different modes of supplying energy to promote chemical reactions alongside the thermochemistry, photochemistry and electrochemistry, studies those reactions which are activated by direct absorption of external mechanical energy, usually observed in milling or grinding of crystals, metals, and alloys, and stretching of single chemical bonds in single molecule force spectroscopy. Previous work in our group demonstrates that mechanical force can produce light by reacting with dioxetane-based polymers and improve the catalytic properties of latent catalysts. Based on previous work, this project continued on mechanically induced homolytic bond scission with dioxetane- and π -extended anthracene adduct-based mechanoresponsive systems, and further developed to do a pioneering trial on mechanically induced heterolytic bond scission with *N*-heterocyclic salts-based polymeric materials and mechanically induced switch of electron spin states.

In **chapter II**, the study of the effect of strain rates was performed with PHMA-based network films with a glass transition temperature close to room temperature. The results from the tensile tests demonstrates that the mechanical properties including tensile strength, strain energy, and glass transition temperature are highly strain rate dependent, and the trend with the change of the strain rate suggests a transition between the strain rates 0.1 to 1 s^{-1} , although the failure strain is less strain rate dependent. The recorded light intensity is also strain rate dependent: the intensity of generated light increases with increasing the strain rate. The mechanical behavior at a strain rate of 0.1 s^{-1} combines properties of rubber and glass, and the total intensity of generated light at this strain rate is the highest. Light emission is also strain rate dependent: at low strain rates, most of the light was generated close to the final crack with a short strain interval just before failure while, at high strain rates, the light was generated throughout the whole film with a wider strain interval.

Based on dr. R Gostl's work on π -extended anthracene adduct-based mechanochemistry, in **chapter III**, the compressive force was employed to activate the retro Diels-Alder reaction. The generated fluorescent anthracene unit by compression can be well used to map the deformation of materials, and demonstrates that the compressive deformation is highly localized in the area close to the center of the sample. It is also concluded that swelling also influence the mechanoactivation because the T_g is significantly lowered by the presence of water. However, much of the observed fluorescence is lost when scattering of the compressed sample is suppressed by adding a solvent with matching refractive index. Therefore we conclude that mechanoactivation takes place at the surface layer of the samples and the generated fluorescence is strongly enhanced by scattering and reflection, which occurs commonly in turbid media.

Up to date, most of researches on mechanochemistry has focused on homolytic bond scission reactions, and few heterolytic bond scission have been reported. A pioneering trial on searching mechanically induced heterolytic bond cleavage was launched in **chapter IV**. An imidazolium-centered linear polyTHF and a linear bis(phenyl)fluorene-centered PMA were synthesized by living/controlled polymerization, and sonication was employed to study the mechanochemical scission, the results, however, did not show the expected type of bond scission. Furthermore, benzylpyridinium was incorporated into network, and grinding was employed and tried to activate the heterolysis to generate the initiator sites for ring-opening polymerization. With thermoactivation, the inert precursor was activated and showed initiation properties both in linear polymer and crosslinked network, it, however, could not be activated mechanically by grinding, demonstrating that grinding as the external mechanical force is not enough for the activation of the benzylpyridinium-based crosslinked network for initiation of polymerization of epoxides.

Inspired by a work from Winter's group that host-guest interaction can switch the spin states of reduced bis(viologen)s, in **chapter V**, a family of viologens and bis(viologen)s were prepared and cyclic voltammetry technique was employed to

study the electrochemical properties of all (bis)(viologen)s: the differences of the formal potentials of two reductions are around 0.43 and 0.56 V for viologens and bis(viologen)s, respectively. Temperature-dependent ESR measurements support dimerization in reduced bis(viologen)s in polar solvents and indicates a very fast equilibrium between open and closed forms. Polymeric bis(viologen) was incorporated into hydrogel networks and reduced successfully, but the limitation of the characterization prevented this project from going further and reaching the further conclusions on mechanoactivation of reduced bis(viologen)s.

This work shows that mechanically induced homolytic bond scission, to some extent, is easy to reach, there is, however, a long way to go on the study of mechanically induced heterolytic bond scission and its use in mechanochemistry for practical applications.

Curriculum Vitae



Bao Li was born on 6th September 1987 at Sanyuan county, Shaanxi Province, P. R. China and grew up in his birthplace. After graduated from Beicheng Middle School in 2003 at Sanyuan, he went to Zhejiang Province and began his study in Chemical Engineering and Technology at Zhejiang University. During his undergraduate study, he took part in the “ZEDC” Chemical Process Design Competition with another 4 group members and won a 2nd Prize in the Eastern China. In his final year, he joined in Prof. Wenjun Wang’s group and completed a research project on study of olefin/acrylate block copolymer. In 2010, he went to Shanghai Jiaotong University where, after two and half years in Prof. Xuesong Jiang’s group, he received his Master Degree in 2013. During his master study, he worked on development of novel efficient photoinitiators for Dry Films in industrial application in collaboration with Hitachi Chemical, and on preparation of multi-responsive microgel of hPEA for selective absorption of organic dye. Afterwards he began his PhD research on mechanochemistry in Macromolecular and Organic Chemistry group at Eindhoven University of Technology under the supervision of Prof. Rint Sijbesma.

List of Publications

- **Bao Li**, Xuesong Jiang, Jie Yin, Multi-responsive microgel of hyperbranched poly (ether amine) (hPEA-mGel) for the selective adsorption and separation of hydrophilic fluorescein dyes, *J. Mater. Chem.*, **2012**, 22, 17976-17983
- Xianwen Lou, **Bao Li**, Bas F. M. de Waal, Jurgen Schill, Matthew B. Baker, Ralf A. A. Bovee, Joost L.J. van Dongen, Lech-Gustav Milroy and E.W. Meijer, Fragmentation of organic ions bearing fixed multiple charges observed in MALDI MS, *J. Mass Spectrom.*, **2017**, DOI: 10.1002/jms.4035
- Yasuharu Murakami, Makoto Kaji, Jie Yin, Xuesong Jiang, **Bao Li**, Photosensitive resin composition, photosensitive element employing it, Resist pattern forming method, process for manufacturing printed circuit board, Patent No. 5799799
- Jia Huo, Li Wang, Elisabeth Irran, Haojie Yu, Jingming Gao, Dengsen Fan, **Bao Li**, et al., Hollow Ferrocenyl Coordination Polymer Microspheres with Micropores in Shells Prepared by Ostwald Ripening, *Angew. Chem. Int. Ed.*, **2010**, 49, 1-6

Acknowledgement

It was on 9th February, the Chinese New Year Eve of 2013, that I took the last interview with Prof. Rint Sijbesma, and at the end of that interview, I received Rint's offer as a PhD candidate in his group, which marked a new phase of my life. In the following several months, the preparation for the overseas study at Technical University Eindhoven (TU/e), the Netherlands, was made with the assistance of Rint, Joke Rediker and HR Office of the Department of Chemical Engineering and Chemistry, TU/e. Not until 3rd June, 2013 was it that I started my journey to the Netherlands, 19 hours later, I landed at Schiphol International Airport, and it was around 07:30 a.m., 4th June, from then on, a new chapter of my life begun in the Netherlands.

Now, the long journey of my PhD study will arrive at its end. At this moment, every scene during these years in the Netherlands comes to my mind, I find that I really need to thank a lot of kind people, and without their help, my life in the Netherlands would have not been so smooth, colorful, and valuable. First of all, I would like to thank my promotor, Prof. Rint Sijbesma. I want to express my sincere thanks and profound respect to you for offering me this opportunity to work on this pioneering and meaningful project as a PhD student in your group. Your broad scientific views and constructive suggestions could always light up my world when I got lost in the confusions and frustrations; and your kind consideration about my health and daily life also reduced my loneliness and helpless when I lived in the Netherlands alone. Particularly, in the past year, although I was not in the Netherlands, your advice, encouragement, and efforts on my PhD thesis supported me, I really appreciate all you have done for me. It was my great pleasure and privilege to get your supervision and be a member of your research group.

I would like to sincerely express my thanks to Prof. dr. J. H. van Esch, Prof. dr. A. P. H. J. Schenning, Prof. dr. N. A. J. M. Sommerdijk, dr. ir. J. P. A. Heuts for kindly agreeing to be a part of defence committee and kind comments on my thesis. Moreover, I also want to thank dr. ir. J. P. A. Heuts again for being my co-promoter, the discussion with you helped me a lot on deeply understanding the mechanical experiments. I would also like to thank Prof. dr. ir. E. J. M. Hensen as well for agreeing to preside over my defense ceremony as the chairman.

I am grateful to Dr. Jessica Clough, Dr. Delei Chen, and Prof. Yulan Chen who was a postDoc in Sijbesma's group, for providing your kind help when I constructed the Chapter II. Jessica, you are an excellent scientist and a kind British lady who is always ready to offer your help to your friends; Delei, thank you very much for your

expertise on MATLAB analysis; and Yulan, thank you again for the scientific and non-scientific discussion with you. Only with the assistance of all you could I successfully finish Chapter II.

I would also like to thank Dr. Robert Göstl for your contribution on Chapter III. You developed the π -extended anthracene mechanophore, and based on your preliminary work, the third chapter could be a successful and meaningful piece. When I performed the experiments and wrote the third chapter, the discussion with you also created a lot of smart ideas and answered my questions. Moreover, I would like to thank you, Dr. Edward J. Reijerse, from Max-Planck-Institut fuer Chemische Energiekonversion for your kind contribution on ESR measurements to perform the Chapter V. Herein I want to express my gratitude to you for your kind help.

On 13th December, 2017, I terminated my resident permit in the Netherlands and flew back to China, because my contract had already been terminated and I did not have any additional income to support my living in the Netherlands. After I arriving back in China, I needed a place to continue writing my thesis. Prof. Yulan Chen and Prof. Xuesong Jiang who supervised my master thesis were happy to provide me a seat to finish my writing. I am really grateful that I could get support from both of you although I finally went to Jiang's group in Shanghai Jiaotong University. Furthermore, I also want to thank both of you for your enthusiasm, patience and encouragement when I was prone to losing my faith to finish my PhD. The overseas calls from both of you did change my mind and made me energetic and faithful on my PhD thesis. I thank both of you for your kind help and support.

My thanks also go to several MST staff members: Ralf Bovee, Xianwen Lou, and Joost van Dongen for your help and support in the analytic Lab; Joke Rediker, Marjo van Hoof and Martina Jiricka for taking care of everything administrative, especially Martina for what you did to help me return to Eindhoven, the Netherlands; Hans Damen for ordering chemicals; my officemates, Berry Bögels, Marko Mihajlovic and Ellen Schmitz for your nice personality and kindness, and with you guys, the office life brought much excitement to my research in the Netherlands. Without a group of friendly colleagues could my life in the Netherlands not be so smooth. I really want to express my thanks to all of you: Hans, you have a nice personality, thank you very much; Jody, you are an enthusiastic and knowledgeable scientist and a big China fan, welcome to China again in the future, and thank you for your special postcard from Lisbon; Marcos, you are always optimistic, and your Spanish style was really a nice additives influencing your friends significantly and lightening the tough days at work, and thank you for your sangria; Xiao 蒙, 嬉嬉闹闹了四年, 却又不失体面, 希望以后生活越来越好; Tom and Eveline, both of

you have professional skills and innovative and creative ability, thank you, Tom for the discussion with you and Eveline for your invitation for your birthday party; Yanwu 周, 一个中国好男人, 既有家庭责任心, 又有科学专业素养, 希望尽快飞鸿腾达; Samaneh, you have a lovely family, thank you for your invitation for the group-dinner at your home. I would also like to thank Erik, Subham, and new comers Annelore, Huiyi, Patricia, and Jie, especially Jie 刘, 谢谢收留我的东西 and Huiyi 张, 一直关心我的论文和答辩。

当然, 生活总少不了几个江湖损友: LLL, 你那什么都在乎什么都不在乎的人生态度, 我喜欢, 仗剑去国, 一壶浊酒笑苍天; 大魔王 Yang, 你那什么都不在乎的人生态度需要改改, 做事情啊, 需要踏踏实实的哦。饭友们也是不能相忘于江湖的: 春亮 Li, 同是李家人, 段子腔少点多点不碍事, 但是不要总放在嘴巴上哦; 浩 Liu, 非常感谢刚到荷兰时候的江湖救急; 一流 Liu, 希望你们一家和和美, 你的科研生活蒸蒸日上; 德雷 Chen, 该去跑步瘦身了, 别忘了女朋友哦; 当然还有 SMK 和 SFD 的小伙伴。与同住 Hemelrijken 舍友们的过往也时常记忆在脑: 将军 Zhou, 希望真拿个将军头衔吧, 说不定还可以去部队上和你喝酒哦; 聪聪 Wang, 同命相怜, 希望你早点答辩; 曲曲儿, 东北那嘎达的爷们, 豪爽好客好朋友。荷兰一行好多年, 认识很多人, 一些匆匆而过, 成了永远的过客; 一些也许在未来还会相遇, 总之, 感谢大家的一路相伴, 且行且珍惜。

Lastly, I want to say without the steadfast support of my family, I could not go so far and obtain such success because I know that no matter how far away I go, all of you will always be there. I would like to say thank you very much for your love and support, 尤其是父亲, 虽然您已经不在, 但是, 从小您的谆谆教诲会永远影响着我, 叩首; 谢谢母亲, 虽然您不善言语, 但是您的关心和爱护, 我心中谨记; 最后谢谢小妹, 如果没有一直照顾着家, 我也不会安心外出游学, 谢谢你! 还有潘老师和惠叔一直的支持和关怀, 谢谢你们!

大恩不多谢, 尽在一壶酒! 干杯, cheer up!

Bao
2019.01.01